LOAD SHEDDING SCHEME FOR ISLANDED DISTRIBUTION NETWORK WITH FLEXIBLE LOAD SELECTION AND POWER CHANGES

JA'FAR SAIFEDDIN ABDELHAFIZ JALLAD

FACULTY OF ENGINEERING
UNIVERSITY OF MALAYA
KUALA LUMPUR

2018

LOAD SHEDDING SCHEME FOR ISLANDED DISTRIBUTION NETWORK WITH FLEXIBLE LOAD SELECTION AND POWER CHANGES

JA'FAR SAIFEDDIN ABDELHAFIZ JALLAD

THESIS SUBMITTED IN FULFILMENT OF THE REQUIREMENTS FOR THE DEGREE OF DOCTOR OF PHILOSOPHY

FACULTY OF ENGINEERING
UNIVERSITY OF MALAYA
KUALA LUMPUR

2018

UNIVERSITY OF MALAYA

ORIGINAL LITERARY WORK DECLARATION

Name of Candidate: **JA'FAR JALLAD**

Registration/Matric No: **KHA140056**

Name of Degree: **Doctor of Philosophy**

Title of Project Paper/Research Report/Dissertation/Thesis ("this Work"):

LOAD SHEDDING SCHEME FOR ISLANDED DISTRIBUTION NETWORK WITH FLEXIBLE LOAD SELECTION AND POWER CHANGES

Field of Study: **Power System**

I do solemnly and sincerely declare that:

(1) I am the sole author/writer of this Work;
(2) This Work is original;
(3) Any use of any work in which copyright exists was done by way of fair dealing and for permitted purposes and any excerpt or extract from, or reference to or reproduction of any copyright work has been disclosed expressly and sufficiently and the title of the Work and its authorship have been acknowledged in this Work;
(4) I do not have any actual knowledge nor do I ought reasonably to know that the making of this work constitutes an infringement of any copyright work;
(5) I hereby assign all and every rights in the copyright to this Work to the University of Malaya ("UM"), who henceforth shall be owner of the copyright in this Work and that any reproduction or use in any form or by any means whatsoever is prohibited without the written consent of UM having been first had and obtained;
(6) I am fully aware that if in the course of making this Work I have infringed any copyright whether intentionally or otherwise, I may be subject to legal action or any other action as may be determined by UM.

Candidate's Signature Date:

Subscribed and solemnly declared before,

Witness's Signature Date:

Name:

Designation:

LOAD SHEDDING SCHEME FOR ISLANDED DISTRIBUTION NETWORK WITH FLEXIBLE LOAD SELECTION AND POWER CHANGES

ABSTRACT

Islanding is one of the most important issue in modern distribution networks. Islanding condition usually results in a large excursion of a distribution network's frequency and voltage due to the imbalance between generation and load demand. In this case, the distributed generation (DG) units need to operate at a maximum output power to reduce a power deficit in the islanding operation of the distribution network. When the output power of the DG units fails to compensate for the imbalance of power, load shedding can be used to maintain the power system's stability via the curtailment of partial loads in some parts of the system. The main aim of this research is to address two important aspects; increasing the reliability of the system by maximizing the remaining load by improving the voltage bus after the application of load shedding in the planning mode, and detecting and estimating a new power deficit during the UFLS process in the operation mode with flexible load selection. In order to realize the first aspect, a combination of particle swarm optimization (PSO) algorithm and firefly algorithm (FA) can be used to maximize the amount of remaining load and the voltage stability index (SI) in the distribution network. A metaheuristic algorithm in the UFLS scheme can be used to select the best load combination in real time. Taking into account the time execution, the artificial neural network (ANN) model was constructed based on the daily load plots. The second aspect involve monitoring the overshooting signal of the second frequency derivative of the center of inertia so that we can detect new power deficits during the load shedding process. An equivalent system inertia constant needs to be estimated in order to quantify the new power deficit. In this method, the calculated total load shed amount is to be shed properly using binary PSO optimization for the selection of the best load combination. The capabilities of the proposed methods can be assessed

using the IEEE 33 - bus radial distribution system with different types of DGs, and a part of Malaysia's distribution network was selected to validate the proposed methods in MATLAB and PSCAD/EMTDC X4 4.3.1.0. The simulation results confirmed that the proposed hybrid algorithm, in the context of the planning load shedding scheme, is able to stabilize the voltage and frequency of an islanded distribution network with the maximum remaining load while improving the voltage buses. The proposed UFLS scheme-I in operation mode is also capable of recovering the network frequency within allowed limits (47.5-52.5 Hz). Furthermore, during the sudden changing power during the shedding process, the proposed UFLS scheme-II can still recover the frequency by shedding the required loads within (0.2 seconds) without overshooting the frequency.

Keywords: Under frequency load shedding (UFLS), Frequency regulation, Particle swarm optimization, Firefly algorithm, Distribution generator (DG).

SKIM PENANGGAL BEBAN UNTUK RANGKAIAN PEMBAHAGIAN DENGAN PILIHAN BEBAN YANG FLEXIBLE DAN PERUBAHAN KUASA

ABSTRAK

Pembentukan pulau merupakan salah satu isu yang paling penting dalam rangkaian pembahagian moden. Keadaan pulau biasanya menyebabkan perubahan drastik frekuensi di rangkaian pembahagian, voltan akibat ketidakseimbangan antara generasi dan permintaan beban. Dalam kes ini, unit pengeluaran generasi (DG) yang diagihkan perlu beroperasi pada kuasa keluaran maksimum untuk mengurangkan defisit kuasa dalam pengendalian rangkaian pembahagian pulau. Penumpuan beban adalah teknik biasa yang digunakan apabila kuasa keluaran unit DG gagal untuk mengimbangi ketidakseimbangan kuasa. Ini adalah untuk mengekalkan kestabilan sistem kuasa dengan mengurangkan beban separa dalam beberapa sistem pembahagian. Tujuan utama penyelidikan ini adalah untuk menangani dua aspek penting, iaitu yang pertama adalah meningkatkan sistem kebolehpercayaan dengan memaksimumkan beban yang tinggal dengan meningkatkan voltan bas selepas memohon penanggal beban dalam mod perancangan. Yang terakhir mengesan dan menganggarkan defisit kuasa baru semasa proses UFLS dalam mod operasi dengan pemilihan beban fleksibel. Untuk mencapai aspek pertama, algoritma 'particle swarm optimization' (PSO) dan 'firefly algorithm' (FA) digunakan untuk memaksimumkan jumlah beban yang tinggal dan pada masa yang sama memaksimumkan 'stability index' (SI) voltan dalam rangkaian pembahagian. Untuk menggunakan algoritma metaheuristik dalam skema UFLS untuk memilih gabungan beban terbaik dalam masa nyata dengan mempertimbangkan pelaksanaan masa, model 'artificial neural network' (ANN) dibina berdasarkan lengkung beban harian. Untuk menangani aspek kedua, pemantauan berterusan isyarat pelepasan dari frekuensi kedua derivatif pusat inersia untuk mengesan defisit kuasa baru semasa proses penanggal beban. Selain itu,

sistem persamaan inersia yang setara dianggarkan untuk mengukur defisit kuasa baru. Dalam kaedah ini, jumlah gumpalan dihitung akan diturunkan dengan betul dengan menggunakan pengoptimuman PSO binari untuk memilih kombinasi beban terbaik. Untuk menilai keupayaan kaedah yang dicadangkan, sistem radial pembahagian bas IEEE 33 dengan pelbagai jenis DG dan sebahagian pembahagian rangkaian Malaysia dipilih untuk mengesahkan kaedah yang dicadangkan di MATLAB dan PSCAD / EMTDC X4 4.3.1.0 dan disimulasikan. Hasil simulasi mengesahkan bahawa algoritma hibrid yang dicadangkan dalam skema penanggal beban dapat menstabilkan voltan dan frekuensi rangkaian pembahagian pemulauan, dengan beban maksimum yang tersisa dan meningkatkan bas voltan. Skim UFLS yang dicadangkan-I dalam mod operasi juga mampu memulihkan frekuensi rangkaian dalam had yang dibenarkan (47.5-52.5 Hz). Di samping itu, dengan perubahan kuasa secara tiba-tiba semasa proses penanggalan beban, skema UFLS yang dicadangkan-II masih dapat memulihkan frekuensi dengan menanggalkan beban yang diperlukan dalam masa (0.2 saat) tanpa melepasi frekuensi.

Kata kunci: ‘Under frequency load shedding’ (UFLS), Peraturan frekuensi, ‘Particle swarm optimization’, algoritma ‘Firefly’, ‘Distribution generator’ (DG).

ACKNOWLEDGEMENTS

Along the way of completing this project, there are people helping me to work out this report. First of all, I am grateful to supervisor, Prof. Dr. Hazlie bin Mokhlis for all his great effort in guiding and advising me. His patience in guiding me with his tumultuous time to finish the project is much appreciated. Prof. Dr. Hazlie also organized the project guideline for me so that I am able to complete in time.

My special thanks reached out my supervisor, Prof. Dr. Saad Mekhilef of his professional advice and helpful comments related to the work. He has shared his ideas and suggestions in providing a better quality of work.

I wish to express my deepest gratitude to my parents for their support and sacrifice of living without me for long time. I would like to thank my wife, my son, my brothers, sisters, and my friends for their encouragement and support.

Lastly, I would like to thank and offer my regards to the people who support me in any respect during the completion of the work.

TABLE OF CONTENTS

LIST OF FIGURES

LIST OF TABLES

LIST OF SYMBOLS AND ABBREVIATIONS

ANN	:	Artificial Neural Networks
BFA	:	Binary Firefly Algorithm
COI	:	Centre of Inertia Frequency
DFIG	:	Doubly Fed Induction Generator
DG	:	Distributed Generation
DGs	:	Distribution Generations
EP	:	Evolutionary Programming
FA	:	Firefly Algorithm
FCWT	:	Full Converter Wind Turbine
GSA	:	Gravitational Search Algorithm
LAV	:	Least Average Value
MPPT	:	Maximum Power Point Tracking
PI	:	Proportional Integral
PMSG	:	Permanent Magnet Synchronous Generator
PSCAD	:	Power System Computer Aided Design
PSO	:	Particle Swarm Optimization
PV	:	Photovoltaic
RCB	:	Remote Circuit Breaker
RE	:	Renewable Energy
RESs	:	Renewable energy sources
ROCOF	:	Rate of change of frequency
SI	:	Stability Index
TLSA	:	Total Load Shed Amount
UFLS	:	Under Frequency Load Shedding

UVLS : Under Voltage Load Shedding

WECS : Wind Energy Conversion System

LIST OF APPENDICES

CHAPTER 1: INTRODUCTION

1.1 Overview

Energy consumption is currently an indicator of economic development and sustainability in many countries throughout the world. The global energy consumption resulted in the depletion of fossil fuel reserves and increased CO_2 emissions. According to the International Energy Agency (IEA), the total energy consumption in the world comes mainly from fossil fuels, which accounts for 78%, while 39.9% comes from crude oil, 15.1% natural gas, 12.2% biofuels, and 11.4% coal in 2014 (International Energy Agency). The detrimental effect of greenhouse gas emissions (GHG) on the environment prompted many countries to amend their respective energy policies to include more renewable energy (RE) sources. For instance, the European Union (EU) intend to replace 20% of the electricity generated from fossil fuels with RE sources by 2020 (T. E. U. C. Report, 2005). In North Africa, the total RE consumption has increased from 27 million tons in 2006 to 97.1 million tons in 2016 (Energy, 2017). Malaysia also seeks a new energy target to boost electricity generated from renewable energy sources to 11% by the end of 2020 (Hashim & Ho, 2011).

RE sources are incorporated into the power system in the form of Distributed Generation (DG). According to the IEEE standard, DG is defined as the "*sources of electric power that are not directly connected to a bulk power transmission system*" (Photovoltaics & Storage, 2007). A DG is installed in a distribution network as a small electrical power generator with a capacity of less than 10 MW (Barker & De Mello, 2000). There are various types of DGs, such as micro-turbine, conventional diesel, a solar photovoltaic (PV) system, fuel cells, and wind turbine. It plays an important role towards improving reliability, power quality, power efficiency, and economics. Also, the proximity of DGs to load sites resulted in reduced power losses in distribution networks. Interconnecting DG with distribution network is a common endeavor nowadays. Many

power utility companies around the world report significant DG penetration in their respective distribution networks. The United States (USA) has increased its DG capacity from 9579 MW in 2004 to 22636 MW in 2008 (IEA. Report, 2002), while the UK has increased its installed DG capacity from 1.2 GW in 1994 to over 12 GW in 2008 (Jenkins, 2010). The World Alliance for Decentralized Energy (WADE) reported that in 2004, many countries have a significant amount of DG penetration in their respective distribution networks, varying from 8.9% in Australia to 36% in Germany (WADE Report, 2006).

Despite the benefits of DG based on RE in solving environmental problems, the increasing trend of DG based on RE resources penetration in power system network reported several technical issues that needs to be resolved, such as the islanding operation of the distribution system.

1.2 Problem Statement

The increasing penetration level of DG in distribution networks is beneficial, but it also resulted in several problems. Problems include reduction of transmission power loss and the enhancement of energy efficiencies and improvement in voltage profile and power quality by assisting the central generating companies to reduce their load on their transmission system. Also, DG penetration improves the reliability of supply to customers in the intentional islanding operation of the distribution network. Hence, the operation of a distribution network in islanding mode could be an applicable choice, as long as its inherent issues are addressed.

The most important problem in islanding operations includes controlling the frequencies and voltages within allowed limits. Sudden imbalances in power generation and load demand due to the grid disconnecting could result in a rapid frequency drop. Furthermore, when power generation is lower than load demand, voltage drop could also

occur at the area farthest from the DG. Under frequency load shedding (UFLS) is an appropriate scheme for preventing a system from experiencing frequency collapse by disconnecting loads to restore the balance between the active power generation and demand. However, if the amount of load shedding is inappropriate, it might lead to power system blackouts (Chebbo, Irving, & Sterling, 1992). Recently, different approaches have been proposed to define the optimal amount of the load that should be removed in load shedding schemes. These new approaches were introduced, since conventional UFLS scheme does not account for the optimum amount of load shedding. Furthermore, the DGs ability to inject more power (from its reserve capacity) during islanded condition was also not accounted for.

Certain meta-heuristic optimization methods are used in planning load shedding schemes, such as genetic algorithm (GA) and particle swarm optimization (PSO) algorithm (Al-Hasawi & El Naggar, 2002; T Amraee, Mozafari, & Ranjbar, 2006; Kanimozhi, Selvi, & Balaji, 2014; Luan, Irving, & Daniel, 2002; Malekpour, Seifi, Hesamzadeh, & Hosseinzadeh, 2008; Rad & Abedi, 2008; Valujerdi & Mohammadian, 2012). The main aim of using meta-heuristic optimization is to minimize losses in distribution networks after islanding event quickly while improving the voltage profiles to reach allowable limits. In (Malekpour et al., 2008), GA was applied to the load shedding scheme to determine the optimal amount of load shedding with/without the presence of DGs in distribution networks. The optimization function was based on the minimization of load removal in the network system and power losses for both cases. The main drawback of using GA is the fact that it is time-consuming (Al-Hasawi & El Naggar, 2002; Kanimozhi et al., 2014; Luan et al., 2002; Rad & Abedi, 2008), rendering it unsuitable for a real-time applications. To achieve increased system reliability after load shedding, a hybrid meta-heuristic algorithm with voltage stability index can be explored for the determination of the maximum remaining loads after load shedding. The value

needs to be as close as possible to that of the active power generator in the system and improved voltage buses. A meta-heuristic algorithm cannot be used in load shedding with two objective functions in operation mode, as it takes longer to find an optimal solution due to the large number of selection in both population size and number of iteration. In order to avoid this, the function can integrate a meta-heuristic algorithm with an artificial neural network (ANN) to shorten its processing time, thus making it applicable for real-time applications.

Most DGs have small system inertias, which causes rapid system frequency drop when disturbances occur. Moreover, the limited spinning reserve of DGs may not able to compensate for huge power imbalances in a system, which could lead to sudden frequency drop. Shedding an amount of load that is close to the imbalance of power will help stabilize the frequency response. However, shedding too much or too little load could lead to a blackout. This has actually occurred in the past; the USA and Canada suffered from an intense blackout in 2003, affecting millions of people in 8 US states and 2 Canadian provinces (Chang & Wu, 2011; Pourbeik, Kundur, & Taylor, 2006; Zhao, Zhang, & He, 2009). Indonesia also suffered from an intense blackout in 2005 that affected 100 million people for 7 hours (C.-j. Zhang, Chai, Wang, & Zang, 2012). Although there are many under frequency load shedding techniques, only a few were proposed for islanded distribution systems with RESs (Anderson & Mirheydar, 1992; Karimi, Wall, Mokhlis, & Terzija, 2017; Laghari, Mokhlis, Bakar, Karimi, & Shahriari, 2012; Xu & Girgis, 2001). These techniques do not consider the occurrence of power deficit changes during the load shedding process, especially in the case where the RESs is connected to a distribution network and the system has a small inertia. It is therefore to estimate a new power deficit that could occur during the load shedding process in islanded mode, because in certain cases, this deficit could lead to system frequency collapse. A new UFLS scheme proposed in (Ketabi & Fini, 2015) estimated the power deficit for each

load shedding step. However, they only reported the nadir frequency response without showing the frequency when it reached its steady state. Also, their estimation of power deficit is inaccurate, due to them using only the response event (based on df_{COI}/dt) to calculate it. The real amount of total load curtailed from the system did not match the amount of load shed decided by the proposed UFLS scheme. This could result in overshooting the system frequency.

An appropriate amount of load shed should be taken into consideration when using the load shedding technique to maintain the system's frequency within an allowed limit. (Laghari, Mokhlis, Karimi, Bakar, & Mohamad, 2015) proposed a new fixed and random priority load shedding technique to determine a suitable combination of loads that needs to be shed. This technique is time consuming due to the many possible combinations of loads that needs to be determined prior to the load shedding process. An effective process should consider the determination of total load shed amount and the optimum load selection quickly. It should also be pointed out that the accuracy of the estimated power deficit and optimal amount of load curtailment can be observed based on either overshoot/undershoot frequency after load shedding.

Considering the limitation of the current UFLS scheme, this study proposed an improved UFLS in the context of (1) the ability to detect and estimate new power deficit during the load shedding process when sudden changes occur, such as DGs power variation, DGs disconnection, and load increment, and (2) the ability to obtain a close optimal combination of loads that need to be shed.

1.3 Research Objectives

This research intends to propose a new load shedding scheme to enable the operation of the distribution network in the islanded mode. The objectives are:

1) To formulate an optimization for load shedding planning by maximizing the loads' availability using Particle Swarm Optimization (PSO), Firefly (FA), and a hybrid of FA and PSO optimization.

2) To construct an ANN model for optimum load selection in the load shedding scheme during islanded distribution system.

3) To propose detection and estimation techniques for a new power deficit during the load shedding process based on the second derivative of frequency for detection and calculated inertia constant for estimation.

4) To integrate a power deficit detection and estimation technique with a flexible load selection approach via Particle Swarm Optimization (PSO).

1.4 Scopes and Limitations

1) This research took into account only two major technical issues; load shedding scheme for maximizing remaining loads in distribution network, and estimating a new power imbalance that occurs during the load shedding process in the islanding operation for a distribution system.

2) The islanding operation is tested on a modified IEEE 33 BUS networks and small Malaysian distribution network (29-bus), consisting of a mini hydro, wind turbine, and PV DG sources, which uses a rotating type DG made up of synchronous generators.

3) Models have been developed in PSCAD/EMTDC software, and many of the standard models available in the PSCAD software were used. However, new components were also developed for the proposed islanding detection techniques and the under frequency load shedding schemes. The necessary modules were developed using the PSCAD script via FORTRAN. A MATLAB code was also linked to PSCAD to increase programming flexibility and develop a simulation program for the proposed method.

1.5 Research Methodology

The research methodology is detailed in Figure 1.1:

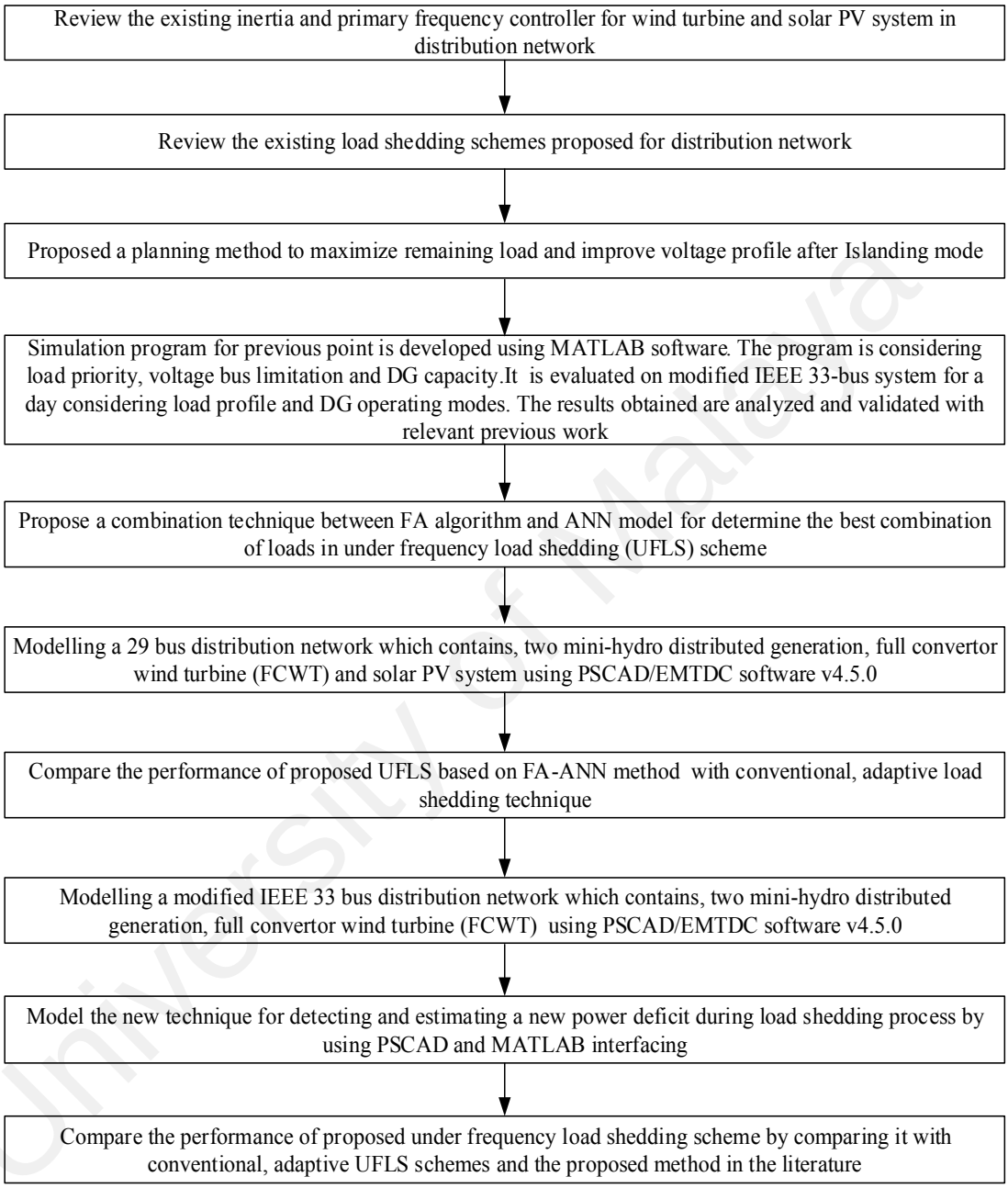

Figure 1.1: Flow chart of research methodology

1.6 Thesis Outline

This thesis is made up of seven chapters:

Chapter 1 details the intentional distribution network islanding issues post-DG penetration in a distribution network. The frequency issues following the distribution network islanding are presented in the problem statement. The objectives of the study are detailed, followed by the scopes and limitations of the research, and finally an outline of the research methodology and report outline.

Chapter 2 discusses the basics of power system stability. A definition of islanding mode, various frequency control schemes proposed for DGs-RESs, and the types of load shedding techniques are also presented. Technical papers related to load shedding will be reviewed as well.

Chapter 3 presents the fundamental concepts and methodologies of the proposed load shedding schemes for a successful islanding operation in the planning and operation modes. The proposed planning load shedding schemes are based on the meta-heuristic algorithm, which fulfils an optimum load curtailment and improves the voltage stability index (SI). The proposed operation of UFLS schemes is categorized into two schemes; UFLS scheme-I, which uses ANN with Firefly algorithm to select optimum load shedding, and UFLS scheme-II, which deals with any new power deficit during the load shedding process.

Chapter 4 presents the simulation results of the load shedding scheme in the planning mode. The results of the proposed hybrid firefly and Particle swarm optimization method of planning load shedding scheme are compared with the FA, PSO, EP and GSA based optimization algorithms in two cases. Both cases represent the load shedding with/without considering the priority limit.

Chapter 5 presents the simulation results of the UFLS-I in operation mode. This chapter details the comparative study between each of the proposed UFLS scheme-I, conventional UFLS scheme, adaptive UFLS scheme, and the method proposed by (Laghari et al., 2015) to highlight the significance of the flexible selection in load shedding scheme and to quicken the operational decision process of load shedding. This chapter also illustrates the effect of using the de-loading technique in RESs with the proposed UFLS scheme-I on the stability of system frequency.

Chapter 6 presents the simulation results of the proposed under frequency load shedding scheme-II. The modelling of conventional, adaptive, and Swing Equation-based UFLS schemes are also detailed in this chapter. The proposed UFLS-II is validated under different cases, such as islanding, DG tripping, change output power of full converter wind turbine (FCWT), and load increments. The results of the proposed UFLS scheme are then compared with conventional and other adaptive UFLS schemes reported in literature to highlight its advantages over the other schemes.

Chapter 7 concludes this report by summarizing the research contributions and presents possible future work in the context of this research.

CHAPTER 2: LITERATURE REVIEW

2.1 Introduction

The detrimental effect of GHG on the environment has prompted many countries to amend their respective energy policies to include more renewable sources. The interconnection of Distributed Generators (DGs) based on Renewable Energy Sources (RESs) in distribution systems benefit both power utility companies and customers, especially in the islanding mode. Islanding operation in a distribution network connected to DGs has the advantage of being able to continuously supply power to the loads even when disconnected from the grid. However, there are technical issues that need to be addressed in order to guarantee a successful islanding operation. The main challenge in a successful islanding operation is ensuring the stability of frequency and voltage of the distribution system.

This chapter begins with an overview of power system stability, distributed generation, and its operation modes and challenges pertaining to DGs in an islanding distribution network. It also discusses the operation of wind and solar PV system in the islanding mode for the support of the stability of frequency system. This chapter also reviews the many types of load shedding schemes, focusing on the application of the distribution system. Their respective advantages/disadvantages will also be elucidated.

2.2 Introduction to Power System Stability

The stability of a power system is an important issue in power system operations. Instability could result in major blackouts. In the context of a power system network, the improvement of power system stability, security, and reliability remain challenging issues. Therefore, it is important to detail the brief term definitions for stability, security, and reliability (Kundur, Balu, & Lauby, 1994), as follows:

1) Reliability is a network's ability to supply adequate electricity in order to keep up with continuous changes in consumer load.
2) Security refers to the ability of a power system to survive and withstand any disturbances without interrupting customer service.
3) Stability is the ability of a power system to be restored to its initial state following any disturbances in the electrical power system.

Generally, reliability is regarded as one of the most important issues in power system planning and operation. The electrical power system reliability can be realized by achieving security, which is achievable if the system is stable. Systems' security should be able to continue operating through impending disturbances, such as line tripping, generator tripping, or damaged equipment. Therefore, both reliability and security of a system can be enhanced by emphasizing system stability, which would allow the power system to realize new conditions and operating point post-disturbances.

In an electrical power system, stability can be classified into three main groups: rotor angle, frequency, and voltage (Kundur, Paserba, & Vitet, 2003). This study researched voltage stability and frequency stability. The former can be defined as "The ability of power system to maintain the acceptable voltage at all buses in the system under normal condition and after being subjected to disturbances". For that, the system is considered to be unstable when the system's voltage magnitude gradually declines post-system disturbances. During system disturbances, insufficient reactive power output from power generators can affect the system's voltage response, and could result in major failures (Xifan, Yonghua, & Malcolm, 2003). On the other hand, frequency stability in a power system can be defined as "The ability of a power system to maintain steady frequency following a severe system upset resulting in a significant imbalance between generation and load". In order to maintain the stability of system frequency, the load demand and

unintentional loss of load must match the power generation during imbalance condition. The unstable frequency condition leads to a loss of power generation in the islanded system. The problems of frequency stability result from insufficient generation reserve, weakness in a coordination between protection controller, and protection devices/failure in equipment response.

2.3 Distributed Generation:

The first Distributed Generation (DG) was reported alongside the first power plant, in 1882, by Thomas Edison, who called it the Pearl Steam Power Plant. It was capable of supplying electricity to 500 customers in New York City (Casazza, Casazza, & Delea, 2003). Later, due to progression in power transmission technology, it was able to produce power at one place and transmit it over long distances via high voltage cables to consumers at other locations. The advancement of a centralized generation of power and its transmission reduced the cost production of electricity (cost per kWh), which also led to enhanced reliability of supply. For instance, if one of a supply unit in a large interconnected system is unable to produce power, it will not affect the entire system. Centralized power generation dominated the power scene until the beginning of the 20th century.

In the last decade, interest in distributed generation has been increased, mainly due to technological advancement and increasing interest in environmental issues. According to the International Energy Agency (IEA), major factors that lead to increased developments concerning distributed generation include increased customer demand for higher reliable electricity, concerns about climate change, the electricity market liberalization, and constraints on the construction of new transmission lines (I. E. A. Report, 2002).

Nowadays, the majority of the power industry utilize renewable energy sources in distributed generations, due to increased interest in environmental problems. Renewable

energy sources, such as photovoltaic, wind, and hydro-power plants are able to decrease environmental pollutions by reducing the usage of fossil fuels. Hence, many countries and utilities around the world set targets towards increasing the application of renewable energy sources for the generation of electricity. This is evident by the growing usage of renewable energy in power generation (without including hydro) by 14.1% in 2016. 50 % of growth was contributed by wind energy, while 18% of it was due to solar energy. The Asia Pacific region contributed to 60% of this growth, making China the world's largest renewable power producer (Energy, 2017). The EU replaced 23.5% of their electricity generated from fossil fuels with renewable energy sources in 2012 (Eurostat, 2013). Malaysia has also started utilizing renewable energy sources for power generation. According to (Ahmad, Ab Kadir, & Shafie, 2011), Malaysia has produced 18,500 MW from small hydro power plants and aims to generate another 490 MW of power by 2020 (Ali, Daut, & Taib, 2012).

2.3.1 Distributed generation Operating Modes and Their Issues

Distributed generation can operate in two modes; grid-connected or islanded. In the former, the main grid governs the system operation, while in the latter, system control is recognized by the coordination of entire distributed generations. The descriptions of both are detailed below:

2.3.1.1 Distributed Generation Operation in Grid-Connected Mode

Despite the widespread use of distributed generations integrated into the grid/distribution network due to the reduction of transmission losses and dependence on fossil fuel, there are some unresolved technical issues. These issues need to be addressed before the distributed generations can be utilized efficiently. The following are the main problems of distributed generation operation with grid-connected mode (Ackermann & Knyazkin, 2002).

(a) ***Problem of Reverse Power Flows in Distribution Network***

The distribution system is traditionally designed as a radial system, where power flows in a unidirectional from the generation level to distribution level by decreasing voltage. However, the presence of distributed generations in the distribution system causes the power to flow bi-directional due to increased voltage on the DG's connection point. For that, the use of distributed generation in distribution network could affect protective devices, such as fuses, automatic re-closers, and over-current.

(b) ***Problem of Voltage Flickers***

Voltage flicker is defined (Langella, Testa, & Alii, 2011) as "Voltage fluctuations on electric power systems due to illumination changes from lighting equipment". Sometimes, the distributed generation suffers from fluctuations in the operating voltage caused by its intermittent nature.

(c) ***Problem of Harmonics***

Harmonics are caused by the switching operation in power electronics converters, which presents a link between distributed generation and the entire main grid. The technology of the converter affects the magnitude and order of the harmonics as well.

(d) ***Problem of Short Circuit***

The increasing number of DG units in the distribution network also increased short circuits. Moreover, increased fault current may lead to a significant influence on protection devices in a distribution network. However, this short circuit fault relies on many factors, such as the number of distributed generation units in the distribution network and the type of generator. For instance, the fault current caused by the synchronous generator depends on the total synchronous reactance.

2.3.1.2 Distributed Generation Operation in Islanded Mode

According to (IEEE_Std_929-2000), the islanding mode operation is defined as "A condition in which a portion of a utility system that contains both load and distributed resources remains energized while isolated from the remainder of the utility system".

When islanding is formed, the main circuit breaker isolates the distribution network from the main grid. To increase the exploitation of distributed generators after islanding, the sources should be operated at their maximum rated power and be fed some critical loads from the islanded micro-grid. However, the islanding area is formed based on the number of DG unit, voltage levels, and the amount of sufficient generation to match the islanded load. To prevent the system from collapsing, the network is split into several islands, and the load is shed in order to balance the output power generation and critical loads (Ahsan et al., 2012). Figure 2.1 illustrates the three split island regions. Each one includes loads and distributed generators after disconnecting the distribution network from the main grid.

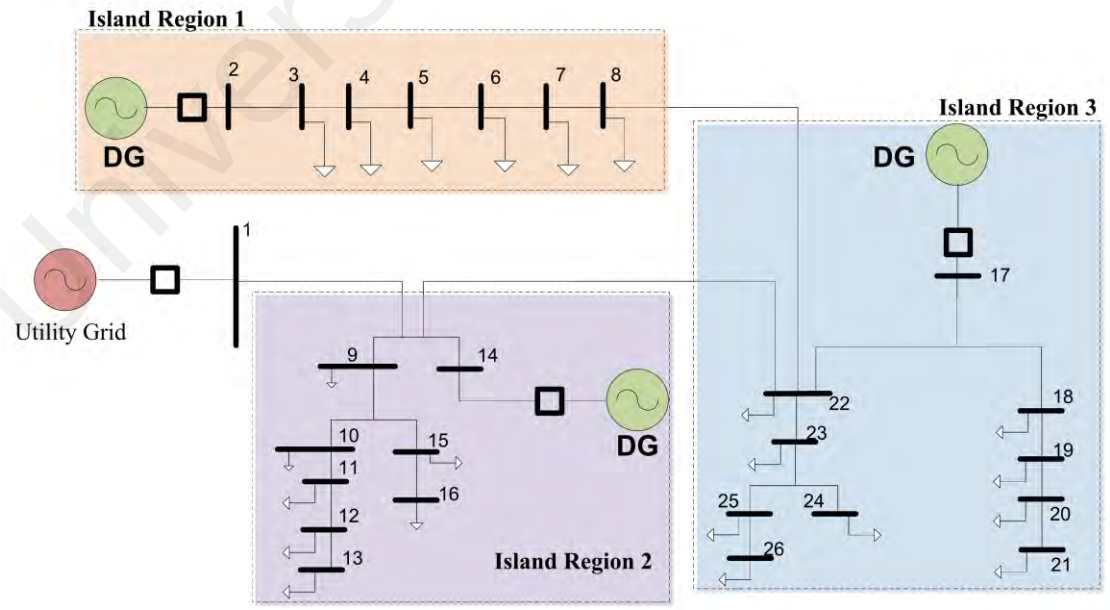

Figure 2.1: Operation of DG in islanding mode

This research handles an islanding operation where an islanded distribution network operates autonomously when disconnected from the main grid.

(a) *Problem of Small Inertial Response in Distributed Generation*

Usually, the system frequency is fluctuating continuously around its nominal values (50 Hz). This is mostly due to the decrement in the output power generation/increments in loads.

However, during islanding, unbalance occurs between output power generation and demand load. This causes a decline in system frequency with a rate of change of frequency (ROCOF). Based on the swing equation, ROCOF depends on two main factors, the amount of unbalance power and total system inertia. The following equation shows the relation between ROCOF and both power deficit and total system inertia (Kundur et al., 1994):

$$\frac{df}{dt} = \frac{f_0}{2H_{SYS}S_B}(P_m - P_e) \tag{2.1}$$

where df/dt is the rate of frequency change, H_{sys} is the total system inertia constant, S_B is the rating power of the generator, P_m, P_e are the mechanical power and electrical power, respectively, and f_0 is the system's frequency.

(b) *Frequency Control processes*

The frequency response is defined as the additional active power that can be delivered from a generating unit. It has two parts; primary and secondary responses. The former is available immediately after an event and can be sustained for a further 30 s, while the latter is available at 30 s after an event and can be sustained for a further 30 mins. Figure 2.2 illustrates the frequency response for the UK's power system.

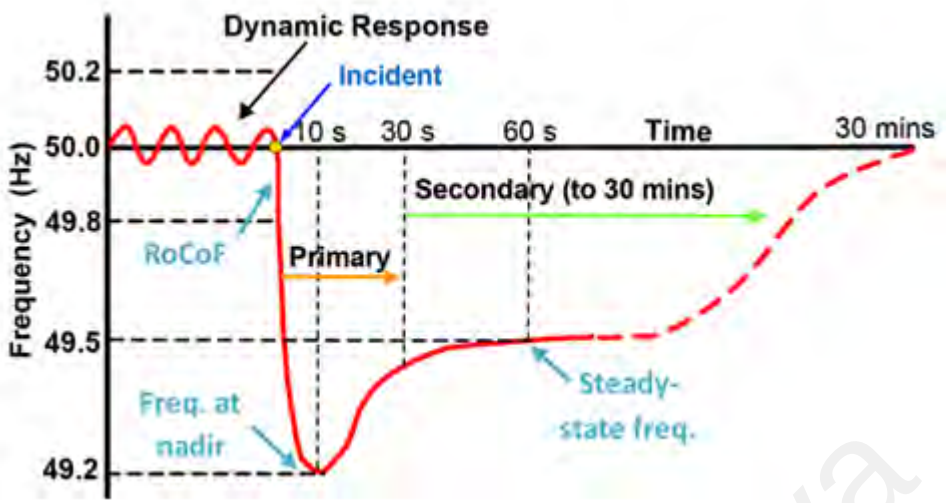

Figure 2.2: System frequency evolution after a contingency (National Grid) (Teng, Aunedi, Pudjianto, & Strbac, 2015)

i Primary frequency control

Primary frequency control is dictated by two mechanisms; inertial response and governor action. The former produces electrical energy from the release of kinetic energy stored in the rotating mass. This occurs due to the decrease in the speed of the synchronous generators, which is a fast response and proportional to ROCOF. It is available immediately after an event, and can be sustained for a further 10 s, as shown in Figure 2.2 (Díaz-González, Hau, Sumper, & Gomis-Bellmunt, 2014). Governor action uses a droop control loop to change the system's frequency by opening the governor valve to increase the turbine's output. This response is considered a slow response, and relies on the time lag of the prime mover and the dead band of the governor. Governor action is available at 20 s after an event, and can be sustained for a further 30 s, as shown in Figure 2.2 (Yu, Dyśko, Booth, Roscoe, & Zhu, 2014).

ii Secondary Control

Secondary control, followed by the primary control action in order to restore the system frequency within allowed limits.

iii Tertiary control

Tertiary control is used to compensate for the remaining unbalance of power after completing the primary and secondary responses. It relies on the power plants regulations based on an organizational structure of the power system.

In fact, due to the decrease in the installation synchronous power stations with increasing volume of grid-connected converters generation such as full converter wind turbine and solar PV system will not only lead to a decrease in the number of generators participating in frequency regulation, but also continued decrease of the total system's inertia constant. For instance, Figure 2.3 shows the forecasting of the total system inertia constant in the UK for the next 18 years.

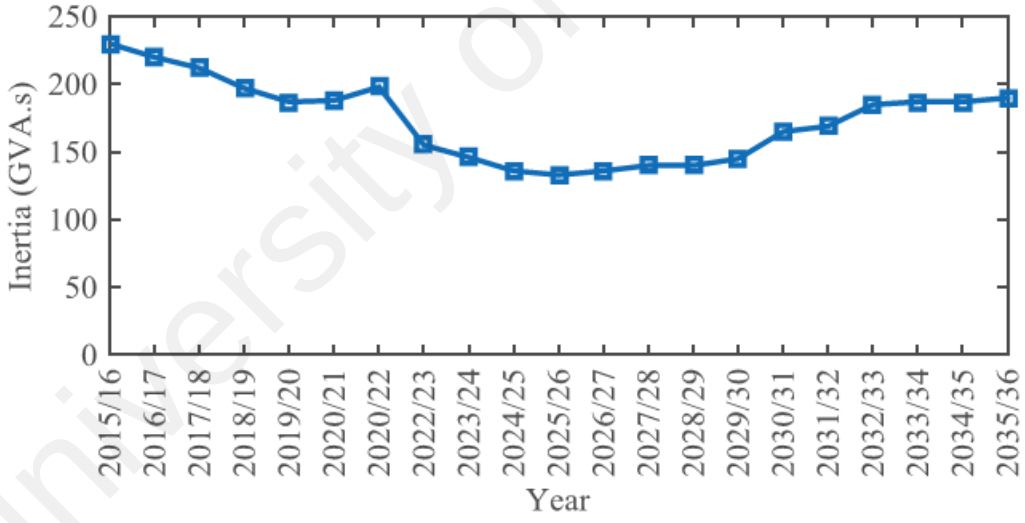

Figure 2.3: Decreasing system inertia constant that caused by the contribution output power from Renewable energy sources (F. M. Gonzalez-Longatt & Alhejaj, 2016)

The system's frequency decreases rapidly, which precludes the other controllers from recovering the unstable frequency.

The replacement of a large number of the DG based on the synchronous generator by the DG based on renewable energy resources reduces the total spinning reserve in the

whole system due to operating at their maximum power point. In the islanding mode, the total spinning reserve is used to regulate the system's frequency. Therefore, the reduction in the total spinning reserve results in increased deviated system frequency, which could result in a blackout (Ulbig, Borsche, & Andersson, 2014).

Three controllers are required to keep the system's frequency within an allowable limit in the islanding mode. The inertia controller is needed to increase the inertial response of the power system, frequency regulation is used to regulate the system's frequency, and under-frequency load shedding (UFLS) scheme is used to shed loads if both inertia and frequency controllers are unable to recover the system's frequency. The following sections detail literature on these controllers for wind turbine and solar PV systems.

2.4 Inertia and Frequency Regulation Controllers Proposed for RESs

Generally, frequency regulation is commonly used for two types of RESs; wind turbine and solar PV system. Figure 2.4 shows the techniques for wind turbine and solar PV systems.

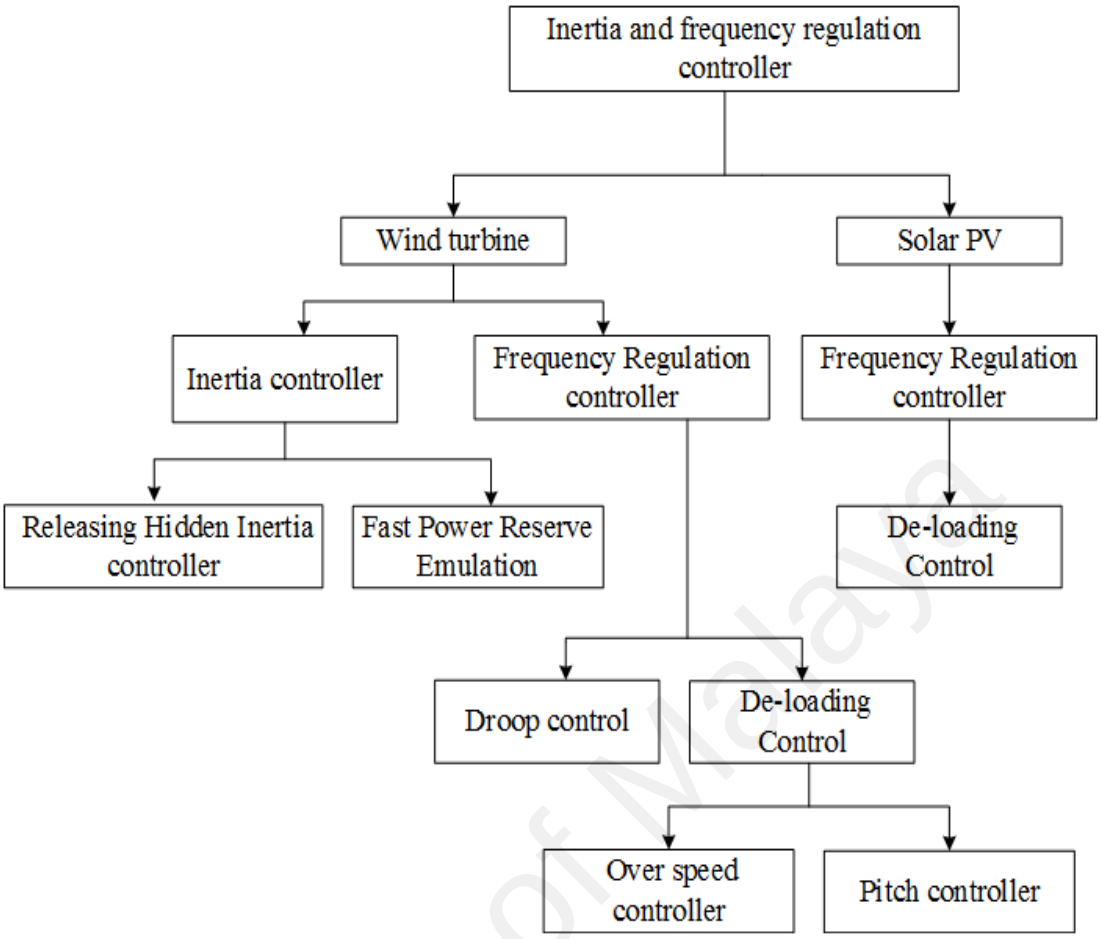

Figure 2.4: Inertia and frequency controllers designed for wind turbine and solar PV system

2.4.1 Wind Turbine and its inertia and frequency regulation controllers

Wind energy is the most used renewable source, which provided more than half of renewable growth in the world (British_Petroleum, 2017). The global wind industry is widespread in more than 80 countries, of which China, US, Germany, India, Spain, UK, Canada, and France had installed capacities of more than 10 GW (Global_wind_energy_outlook, 2016).

Fixed Speed Induction Generator wind turbines (WT-FSIGs) are widely used in offshore wind farms. They require system adjustments to adapt to changes in wind speed in order to maximize their energy efficiency. Their output power is the range of ~kWs. With the rapid development of aerodynamic and power electronic technology, the wind

turbine response at variable speed operations has reported significant improvements. The DFIG, with a back to back (B2B) power converter, is used in wind turbines, as it improves the energy efficiency while allowing for partial power control, both of which are crucial for dealing with speed changes and increased power ratings, from 1 - 5 MW (SIEMENS, 2014). With the reduction in the cost of power electronic converters, the full-scale B2B power converters wind turbine is an excellent option. The full converter wind turbine (FCWT) provides greater flexibility towards meeting the full range of variable speed operation and high energy efficiency, rendering power ratings of—for example-between 4.5 - 7 MW (Sugimoto, Goto, Wu, Yokomizu, & Matsumura, 2002).

Variable speed operation of a wind turbine results in favorable outcomes, such as reduced friction, mechanical stress, noise, maintenance, and improved efficiency and reliability. Currently, there are two most commonly used variable speed wind turbine generator system, which are the wind turbine generator and permanent magnet synchronous generator (PMSG). The former is the doubly fed induction generator (DFIG), and is commonly used in variable-speed wind energy applications with B2B power electronic converter. DFIG comprises two parts; the stator windings are directly connected to the AC grid via a transformer, while the rotor windings are connected to the AC grid via slip rings and three phase power electronic converters. The main and important feature of DFIG is that it is able to achieve a maximum energy conversion-efficiency over a wide range of wind speeds (F. Wu, Zhang, Godfrey, & Ju, 2006). This type of variable speed wind turbine power generation system uses a multi-stage gearbox and partial-scale power electronic converter to connect the wind turbine generator to the AC load/grid. The second type of wind turbine based on a variable speed wind energy conversion system (WECS) is a permanent magnet synchronous generator (PMSG). It is a synchronous machine, where the field flux is generated by permanent magnets instead of field excitation windings (Strachan & Jovcic, 2010).The direct drive of the multi-pole

synchronous generator is directly connected to the wind turbine, implying that it is capable of operating at the same low rotational speed as the wind turbine, enabling power extraction even at low wind speeds. This removes the need for a gear-box (Ahsanullah, Dutta, & Rahman, 2012), and the direct drive PMSG reports 35% lower losses relative to the DFIG (Liserre, Cardenas, Molinas, & Rodriguez, 2011).

The wind turbine extracts kinetic energy from the air flow via the blades. The conversion of air flow power to the main-shaft power can be optimized via the optimization of the pitch angle controller, which keeps the power generation at low and medium wind speeds (regions 2 and 3 in Figure 2.5), all of which are geared towards increasing the amount of captured energy. The power extracted from the air flow via the wind turbine blades can be calculated using the formula below:

$$P_m = \frac{1}{2}\rho\pi R^2 V_W^3 C_P(\lambda,\theta) \tag{2.2}$$

Where P_m is the mechanical power extracted from the wind, ρ is the air density, R is the rotor radius, V_W is the wind speed, and $C_P(\lambda,\theta)$ is the aerodynamic power coefficient, which depends on the pitch angle θ and the tip speed ratio λ, resulting in:

$$C_P(\lambda,\theta) = \frac{1}{2}\left(RC_f - 0.22\theta - 2\right)e^{-0.255\frac{RC_f}{\lambda}} \tag{2.3}$$

where $\lambda = R\omega t/V_W$, C_f is the blade design constant coefficient and ωt is the rotational speed of the wind turbine. From Equation 2.2, it can be seen that the wind turbine achieves its maximum power production if the C_P is maximum for a given pitch angle.

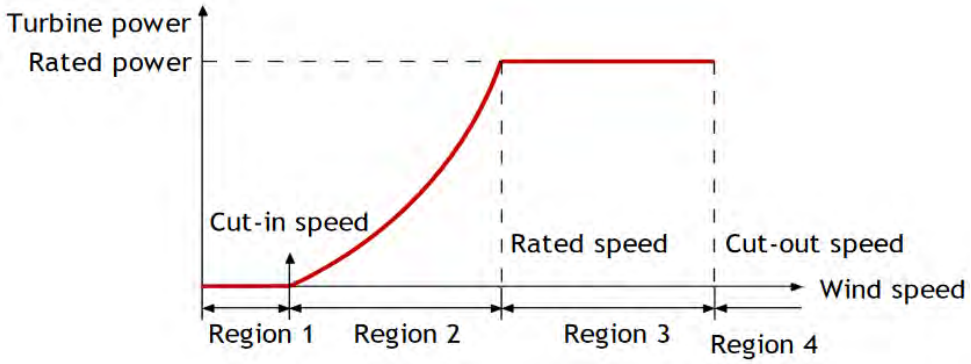

Figure 2.5: Wind Turbine Power Curve (Lydia, Kumar, Selvakumar, & Kumar, 2014)

It can be seen in Figure 2.5 that the power curve is split into four distinct regions. Region 1: Standby mode, Region 2: Control to maximize power, Region 3: Control to rated power, and Region 4: Turbine shut down. As Region 2 consists of low wind speeds and is below the rated turbine power, its blades run at maximum efficiency for extracting maximum power. Region 3 is a transition region that is mainly concerned with keeping rotor torque and noise low.

In region 2 (refer to Figure 2.5), the blade pitch angle is kept at it maximal conversion angle (near 0 deg) and the machine is kept at the peak of the C_P vs λ curve -as shown in Figure 2.6- via generator torque control using measurements of the generator's speed. In region 3, the pitch angle is moved away from its maximal power conversion angle based on the measurements of power.

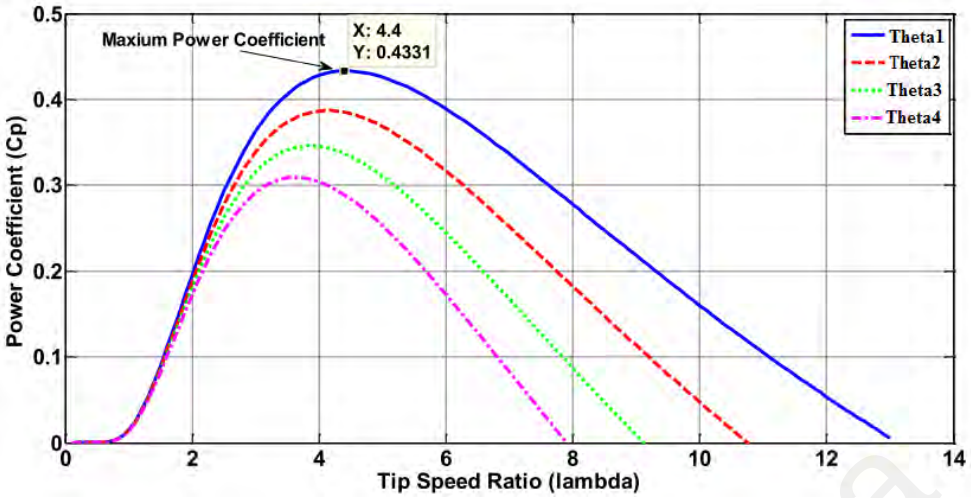

Figure 2.6: Power coefficient curves with different pre-setting pitch angle (Melício, Mendes, & Catalão, 2008)

The pitch angle controller is shown in Figure 2.7 (Hwas & Katebi, 2012). It usually consists of PI controller and a servomechanism system. The pitch angle range and its corresponding rates of change are limited. Beyond the rated wind speed, the speed deviation can be regulated by this pitch angle controller to increase θ_1 until it reaches its maximum limit of θ_4.

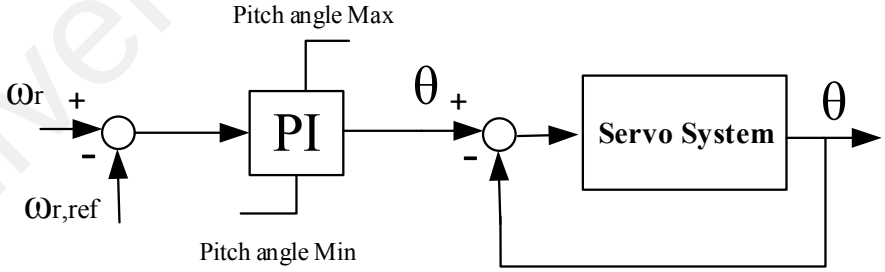

Figure 2.7: Pitch angle controller for variable speed wind turbine (Hwas & Katebi, 2012)

It should also be pointed out that there are other control techniques for wind turbines, such as torque gain control. The generator torque control is usually utilized in region 2 (Johnson, Pao, Balas, & Fingersh, 2006). In this state, the main objective is to maximize

the power captured from the wind, and this is only possible if the torque generator is used to optimally operate the turbine at a constant pitch angle of θ, as shown in Figure 2.8.

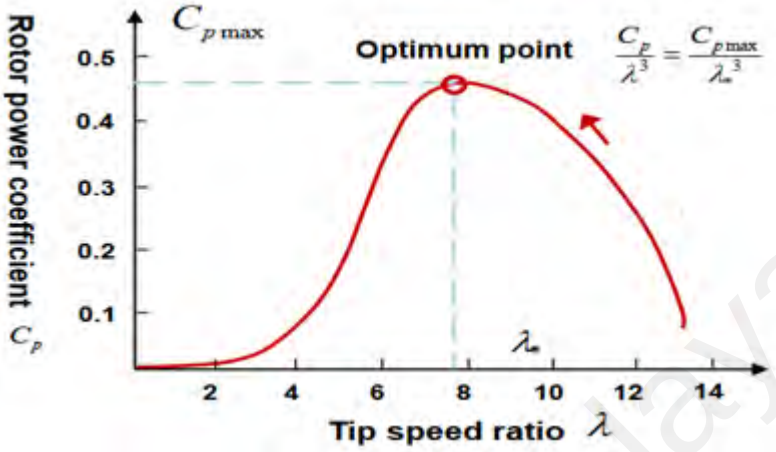

Figure 2.8: Relation between rotor power coefficient and tip speed ratio

The Torque control law is defined as:

$$\tau_g = K(\omega_g)^2 \tag{2.4}$$

Where the gain K is given by blade parameter:

$$K_{opt} = \frac{1}{2}\rho A R^3 \frac{C_{p,max}}{\lambda_*^3} \tag{2.5}$$

Where A is the rotor swept area, R is the rotor radius, and λ_* is the tip-speed ratio where the maximum power coefficient $C_{p,max}$ occurs.

The main features of the $k\omega^2$ law is that it brings the turbine to optimal point only using a rotor speed, as illustrated in Figure 2.8. It also does not need wind speed information. Figure 2.9 shows the block diagram of the optimal torque control method.

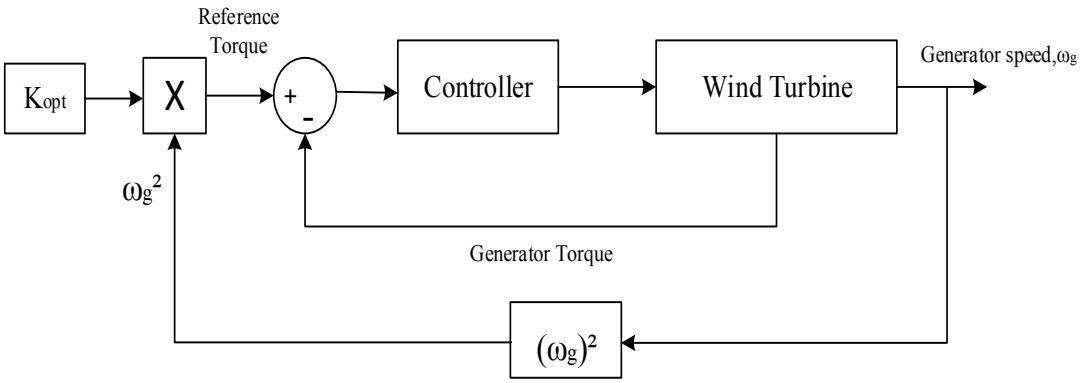

Figure 2.9: Block diagram of optimal torque control method (Abdullah, Yatim, & Tan, 2011)

In order to vary the speed of the wind turbine, the maximum aerodynamic efficiency is obtained by controlling the turbine's rotational speed to keep the tip speed ratio constant at a predefined value that corresponds to the maximum power coefficient over the range of operational wind speeds (Ackermann, 2005).

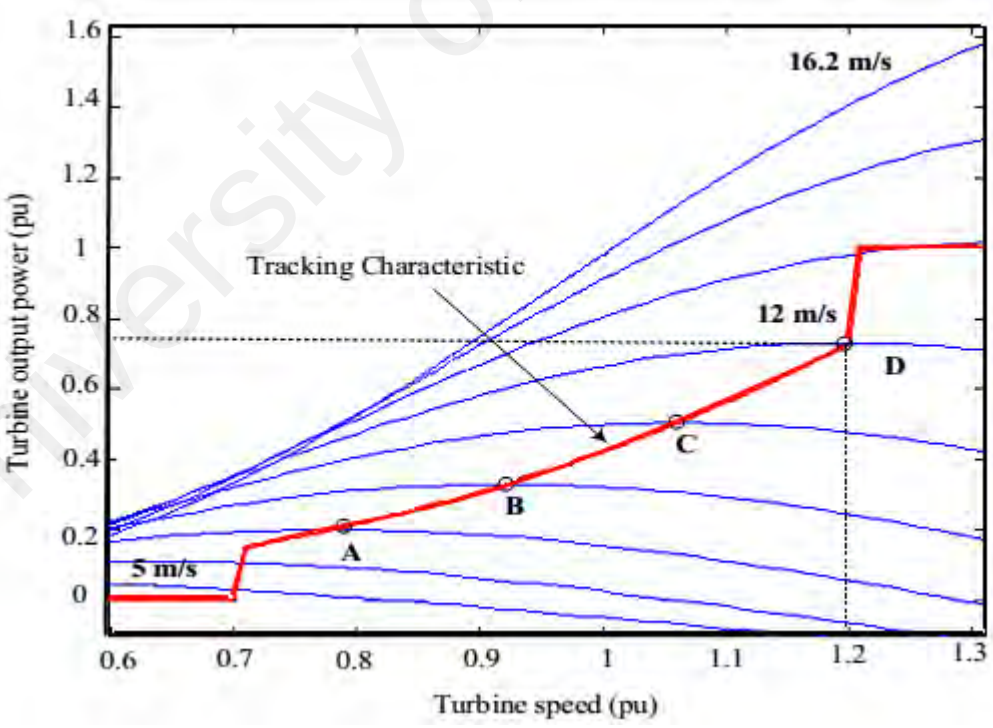

Figure 2.10: Power against rotating speed characteristics at (Pitch angle β=0) (Lamchich & Lachguer, 2012)

The maximum power point can be determined by keeping the speed of the wind turbine within the speed limits and pitch regulation after the rated speed, as seen in Figure 2.10.

As pointed out previously, primary and secondary controls are usually the formed frequency control of the power systems. For that, wind power requires participating in an active power to achieve primary and secondary frequencies. Controllers of wind turbine can be added to the Variable speed-wind turbine (VSWT) subsystems to allow for a transient support to the frequency. However, a wind turbine does not directly provide frequency response due to a decoupling between the wind turbine and grid via power converters. They can enable the primary frequency control by frequency regulation controller and an inertial controller.

2.4.1.1 The inertia controller

The inertia controller aims to temporarily increase power output during frequency disturbance. In order to be able to do this and increase power production, it require a form of energy storage. Thus, the wind turbine generator store a large amount of kinetic energy. The inertia controller can be formed using two basic approaches; releasing the hidden inertia and emulate a fast-power reserve. The hidden inertia controller is a simple control loop added to the power converter controller in order to create an active power control signal (inertial power P_{Hsyn}), following a version of the swing Equation (F. Gonzalez-Longatt, Chikuni, & Rashayi, 2013; Morren, De Haan, Kling, & Ferreira, 2006).

$$P_{Hsys} = 2H_{SYS}f_{sys}\frac{df_{sys}}{dt} \tag{2.6}$$

where H_{sys} express the emulated inertia and f_{sys} is the system frequency per unit. The implementation of releasing hidden inertia controllers is shown in Figure 2.11. The inertia controller leads to reduced maximum ROCOF and increased nadir frequency.

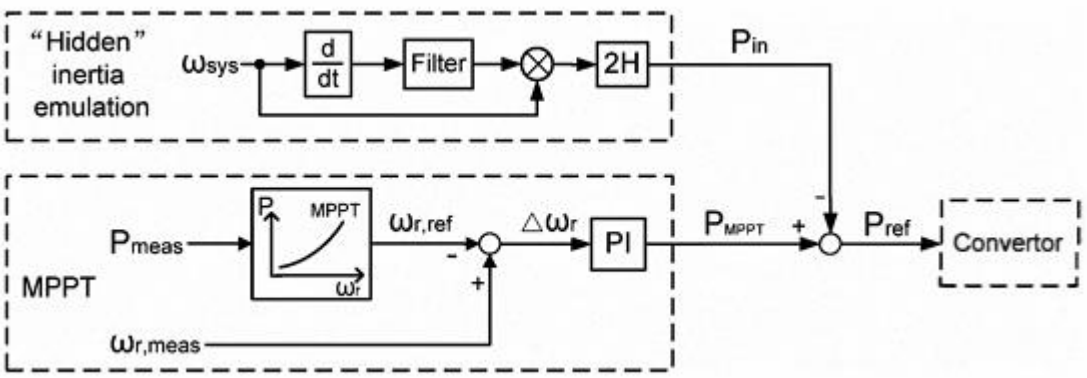

Figure 2.11: Hidden inertia controller (F. M. Gonzalez-Longatt, Bonfiglio, Procopio, & Verduci, 2016)

The fast power reserve emulation aims to release the kinetic energy stored in the rotating mass of the wind turbine (Hansen, Altin, Margaris, Iov, & Tarnowski, 2014; Ullah, Thiringer, & Karlsson, 2008). The fast power reserve controller is designed to provide constant power for a short period of time (Zhou et al., 2010). The simple integration of kinetic energy stored in the wind turbine rotor derives the fast power reserve (Wachtel & Beekmann, 2009):

$$P_{constant}t = \frac{1}{2}J\omega_{r0}^2 - \frac{1}{2}J\omega_{rt}^2 \tag{2.7}$$

Where $P_{constant}$, is the constant amount of active power, t is the time duration for the fast power reserve, ω_{r0} is the initial rotational speed, and ω_{rt} is the rotational speed at the end of the inertial response. Thus, this fast power reserve can be achieved by controlling the rotor speed setpoint to allow wind turbine rotor to release kinetic energy, as depicted in Figure 2.12.

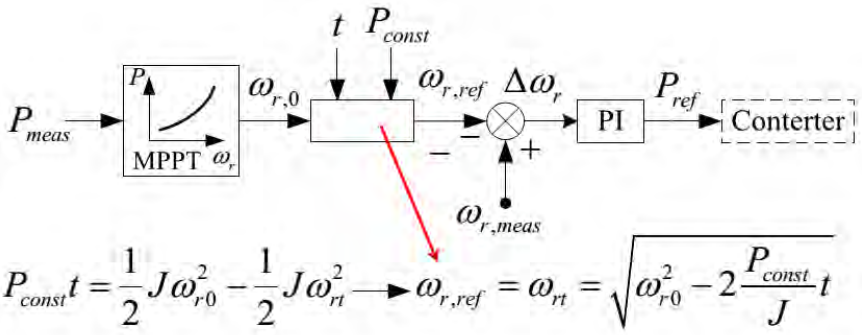

Figure 2.12: Fast-power reserve emulation controller (F. M. Gonzalez-Longatt et al., 2016)

2.4.1.2 Droop controller

The droop controller is described by a steady-state frequency characteristic, as shown in Figure 2.13.

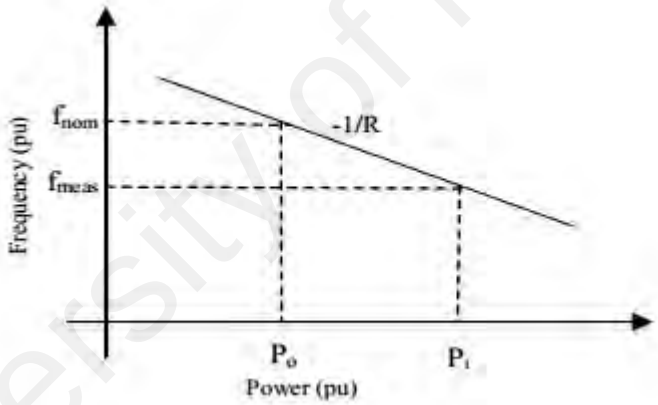

Figure 2.13: Frequency droop characteristic

It produces an active power change that is proportional to the frequency deviation. In a modern wind turbine, when the system frequency falls from f_{nom} to f_{meas}, the wind turbine increases its output power from P_0 to P_1 to compensate for the frequency deviation (Eid, Rahim, Selvaraj, & El Khateb, 2016)

The active power is adjusted according to linear characteristics, and is detailed in (Josephine & Suja, 2014; Mishra, Zarina, & Sekhar, 2013):

$$\Delta P = P_1 - P_0 = -\frac{f_{meas} - f_{nom}}{R} \tag{2.8}$$

where R is the droop constant and f_{meas} and P_0 are the new frequency and wind turbine output power, respectively. f_{nom} and P_1 are the initial operating points. The droop controller significantly impacts the frequency nadir, but it does not significantly affect the initial ROCOF after frequency disturbance. Figure 2.14 shows the droop speed controller for the supporting frequency.

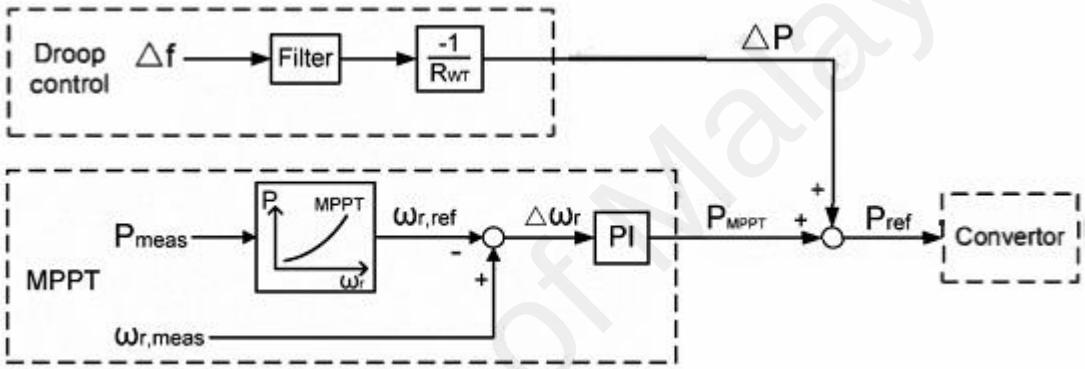

Figure 2.14: Frequency support scheme with droop speed control (Yao & Lee, 2011)

2.4.1.3 De-loading Control:

When the wind speed is below the rated value, the traditional VSWT always operate on the maximum power point tracking (MPPT) condition with the constant blade pitch angle ($\theta = 0$). This operation mode allows for the extraction of maximum power from wind energy. Meanwhile, when the wind speed increases and exceeds the rated value, the pitch angle begins to increase in order to keep the output of the active power on its rated value. However, at the MPPT condition, a short-term frequency droop control can be achieved using the kinetic energy obtained from the wind turbine rotor mass, since there is no wind turbine reserve power.

The maximum power-tracking curve is shown in Figure 2.15. The given MPPT curve can be used in order to illustrate the power reference of the active power control of VSWT at any rotor speed.

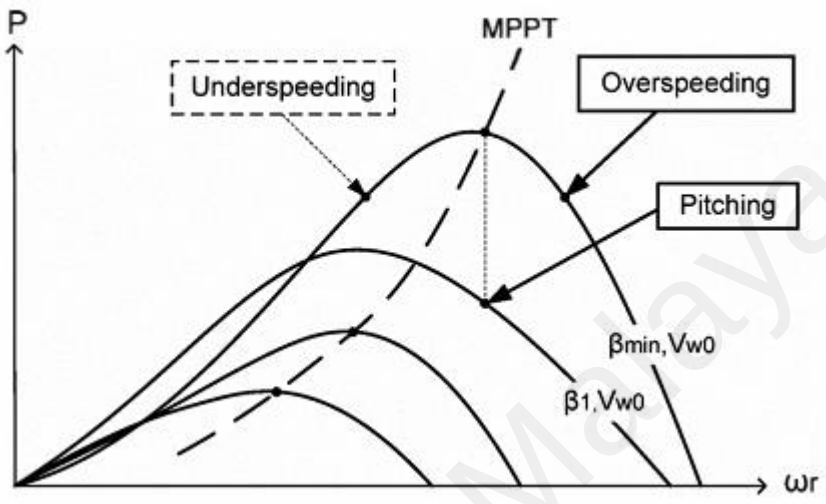

Figure 2.15: MPPT curves and de-loading possibilities: Over-speeding and Pitching (Alsharafi, Besheer, & Emara, 2018)

Depending on the de-loading control, wind turbines could save some active power for use as reserves. The de-loading operation can be dictated by over- speeding control and pitch angle control, or a combination of both, as per Figure 2.15.

(a) ***De-loading by pitch angle control***

As pointed out previously, a pitching control is one of the de-loaded methods. Its principle of operation is based on decreasing the pitch angle to limit the active power production to a value lower than its nominal value by keeping the rotational speed constant. When the system frequency decreases, the pitch angle is regulated as the difference between the frequency reference and actual frequency measurement. Figure 2.16 depicts the schematic pitch controller, which includes the primary frequency control droop.

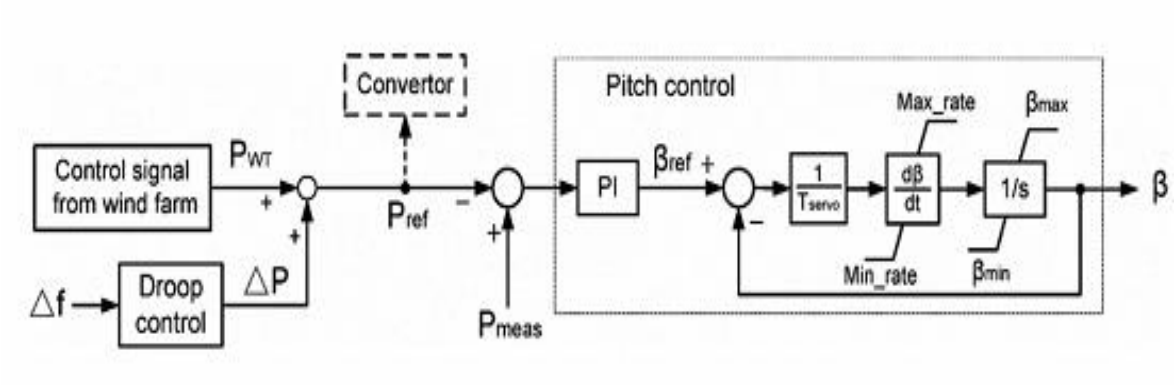

Figure 2.16: Pitch control schematic (Alsharafi et al., 2018)

Figure 2.17 shows the application of pitching control and increasing speed rotor and the de-load techniques at the (P-ω) curve. It can be seen that the point (X) is the maximum power operating point. When applying pitch control, the operating point moves from (X) to (Y) at similar rotor speeds.

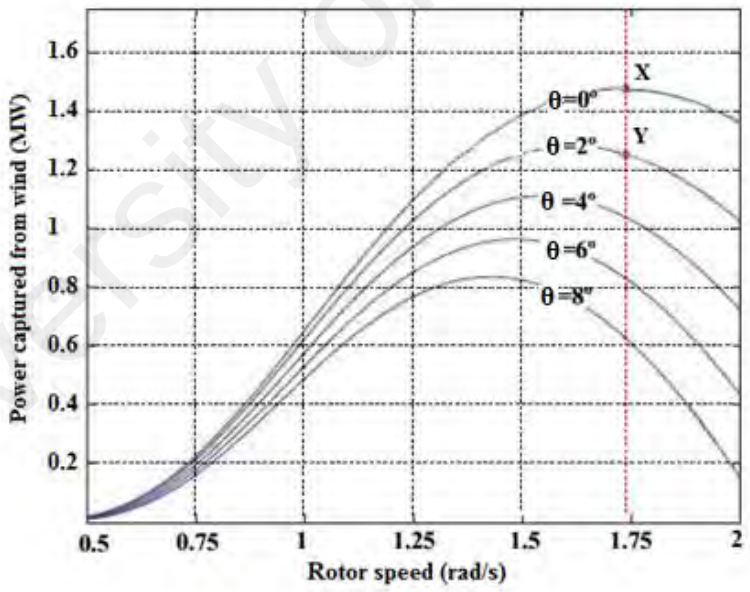

Figure 2.17: (P-ω) curve when applying pitching control for a wind turbine at speed 10m/s (Castro, Fuerte-Esquivel, & Tovar-Hernández, 2012)

(b) ***De-loading by Rotational Speed Control***

A speed control method operates the wind turbine at non-optimal working point in the power rotational speed (P-ω) curve by increasing/decreasing the rotor speed (over-

speeding or under-speeding) at a pre-set power by keeping the pitch angle constant. The wind turbine is forced to generate less active power than its optimum value by increasing the rotor speed to reserve some active power (Castro et al., 2012). When the frequency decreases as a result of a sudden load increase/loses a large supply of generators, reserve active power is injected into the AC grid. Contrarily, the decrease in the rotor speed reduces the output power but leads to an increase in active power production transiently, since the rotor releases kinetic energy in this situation. The main drawbacks of the under-speeding de-load method is that when the rotor speed increases, the active power will be consumed by the generator for acceleration, and it will take a long time for it to be restored to its original speed. This could also lead to a small signal stability. Consequently, the increasing rotor speed is preferred. Figure 2.18 illustrates a 95% de-loaded active power curves of the maximum available power curve.

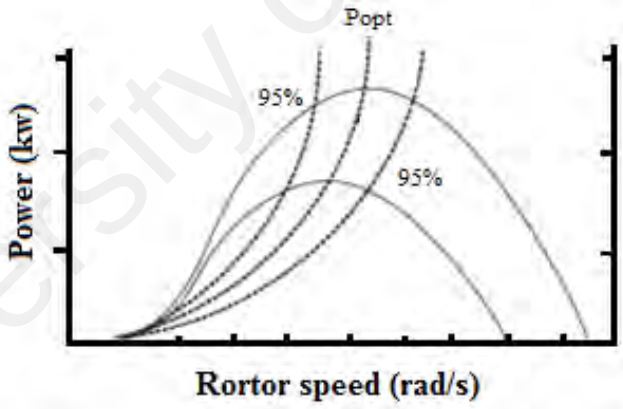

Figure 2.18: A de-loaded active power curves by changing the rotor speed

Figure 2.19 shows a general scheme for a VSWT rotational speed controller.

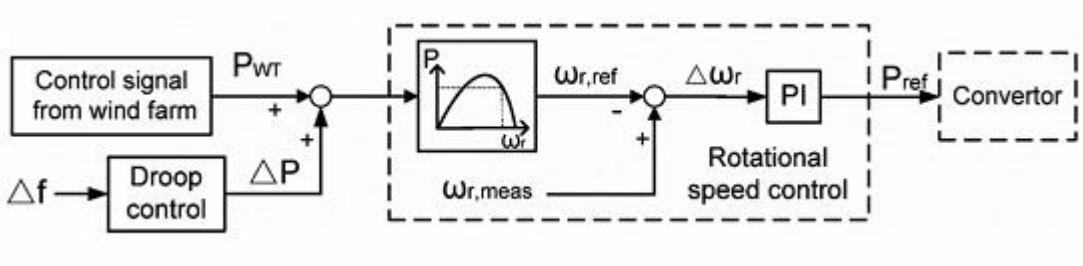

Figure 2.19: Rotational speed control for VSWT (Mahmud, 2016)

The cooperation between pitch angle and speed controller for a variable speed wind turbine was also detailed in (Díaz-González et al., 2014). They proposed three operating modes, depending on the range of wind speed, and a decision algorithm to manage the cooperation between pitch angle and the over-speed controller. This algorithm determines the power set value for the pitch angle controller and the power margin for the over-speed controller. (De Almeida & Lopes, 2007) used the cooperation between pitch angle and over-speed controller to allow the wind turbine to participate in frequency regulation. However, this time, the controllers decided on the reserve power value based on the network operator request. (Z. Wu, Gao, Wang, & Gu, 2012) reported that the same frequency regulation controllers used for the DFIG wind turbine were redesigned and implemented in the PMSG to enable this type of wind turbine to contribute to primary frequency control. (Tielens et al., 2012; Zhangjie, Xiaoru, & Jin, 2012) proposed the pitch angle and overspeed controllers, coordinated with the droop control. These controllers are activated by wind speed ranges to enable the DFIG-based wind turbine to participate in frequency regulation. Furthermore, the over-speed control strategy uses wind speed measurements to determine the sub-optimal power based on the de-loading tracking curve and saves this value in the lookup table. Table 2.1 shows suitable de-loading techniques based on the range of the level speed.

Table 2.1: De-loading techniques based on the range of the level speed

Parameter	Operating Regions for Wind Turbines		
	Low wind speed range (3-7) m/s	**Medium wind speed range (8-13) m/s**	**High wind speed range (13-25) m/s**
Operation Conditions of Wind Turbine	Always Wind turbines operate at partial load. The rotating speed of the turbine does not reach its rated value at any time.	Mostly Wind turbines operate at partial load. The rotating speed of the turbine reaches its rated value transiently.	Wind turbines operate at full load. The rotating speed of the turbine reaches its rated value. The power extracted from the wind should be not to exceed the ratings of the generator
De-loading Techniques Used	Over speeding techniques are used only.	Over speeding techniques are used and Pitch Control techniques may be used depends on its rated value of the rotating speed.	Pitch Control techniques are used only for applying de loading and regulate the rotational speed.

2.4.2 Frequency Regulation Controllers Proposed for PV

Nowadays, high levels penetration of photovoltaic (PV) into the distribution networks and using it in place of conventional source unit result in insufficient reserve capacity of frequency regulation. As a result of high cost of installation solar PV system, several MPPT techniques have been used to harvest maximum power from this source (De Brito, Galotto, Sampaio, e Melo, & Canesin, 2013; Faranda & Leva, 2008; Hua & Shen, 1998). Thus, the use of MPPT techniques in a solar PV system is unable to provide any reserve power to regulate system frequency under island condition.

To allow the photovoltaic system to participate in frequency regulation, many researchers proposed a de-loading technique for solar photovoltaic system, such as

(Rahmann & Castillo, 2014; Zarina, Mishra, & Sekhar, 2012a, 2012b). Figure 2.20 illustrates that the solar PV system operates at maximum power point (MPP) when dc voltage reaches to V_{MPP}. Thus, P_{MPP} represents the maximum power that can be produced from the solar PV system. In addition, the de-loading technique is shown in Figure 2.20, which is carried out by forcing the dc voltage of PV system (V_{MPP}) to operate beyond V_{MPP} by increasing the voltage by value (ΔV). This technique can provide some reserve power for use in frequency regulation.

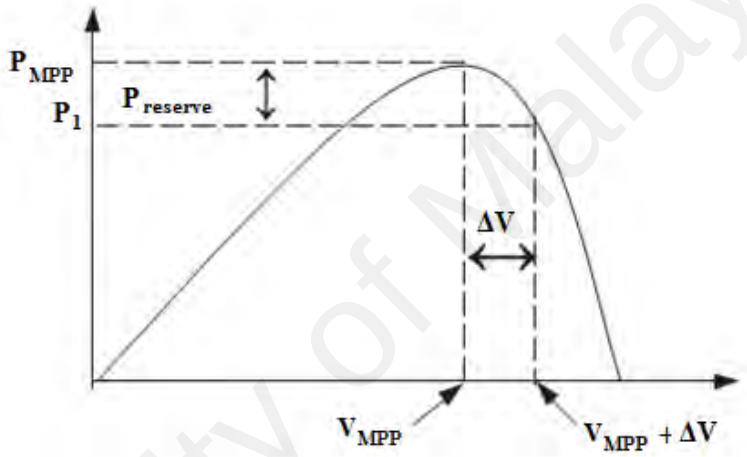

Figure 2.20: The principle of how may reserve power in the PV system

(Zarina et al., 2012a, 2012b) proposed a controller for de-loading technique, as seen in Figures 2.21 and 2.23.

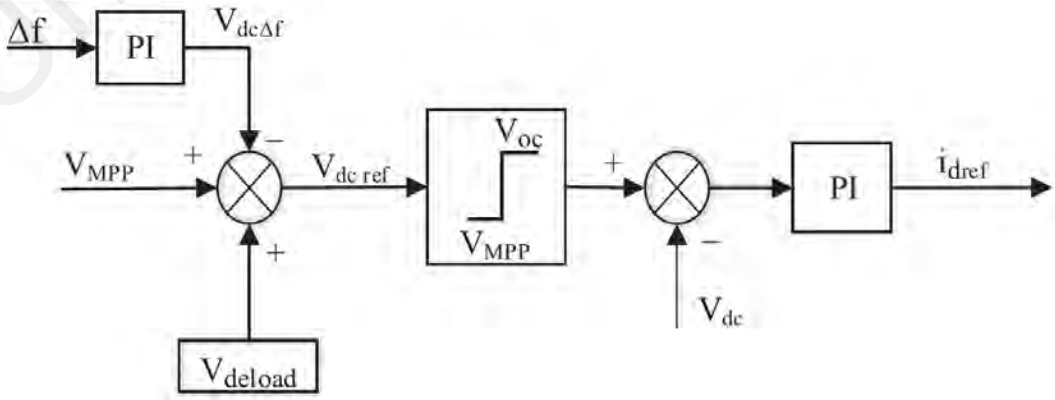

Figure 2.21: **Controller for deloaded solar PV (Zarina et al., 2012b)**

It can be noticed that the change in output power from the PV will not only depend on the V_{MPP} value, but also on the frequency deviation, as per Equation 2.9.

$$V_{dc,ref} = V_{MPP} + V_{deload} - V_{dc\,\Delta f} \tag{2.9}$$

The operation of the de-loaded controller, proposed by (Zarina et al., 2012a, 2012b), is illustrated in Figure 2.22. In normal conditions, solar PV is working at point 3 to reserve some power. When the system's frequency begins to decline, the solar PV voltage is reduced based on the control signal related to frequency deviation, making the PV operational at point 2.

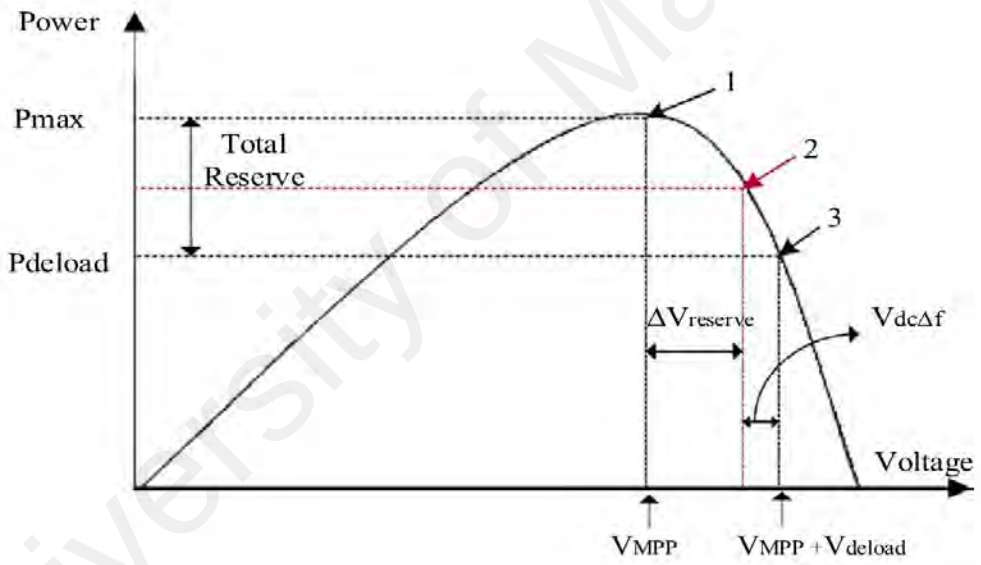

Figure 2.22: Solar PV with de-loading technique (Zarina et al., 2012a)

Indeed, the previous controller suffers from an unequal distribution of frequency regulation capability due to not accounting for the remaining amount of reserve power in each PV unit. In this situation, the solar PV unit, which has less reserve power, equally contributes to frequency regulation compared to the solar PV unit, which has more reserve power. Therefore, some of the PV units, which have less reserve power, will reach MPP faster, and will not be able to contribute any further to frequency regulation. To solve this problem, a new modification to the previous controller was also proposed by (Zarina et

al., 2012b). A new control signal can be added to represent the remaining reserve power $\Delta V_{reserve}$, as shown in Figure 2.23. The reference voltage of the new controller is given by Equation 2.10, which clearly shows that the output power released from the PV units are not only based on frequency deviation, but also on the reserve power available for each.

$$V_{dc,ref} = \left(V_{MPP} + V_{deload} - V_{dc\,\Delta f}\right) - \left(\Delta f \times \Delta V_{reserve} \times K_{P2}\right) \qquad (2.10)$$

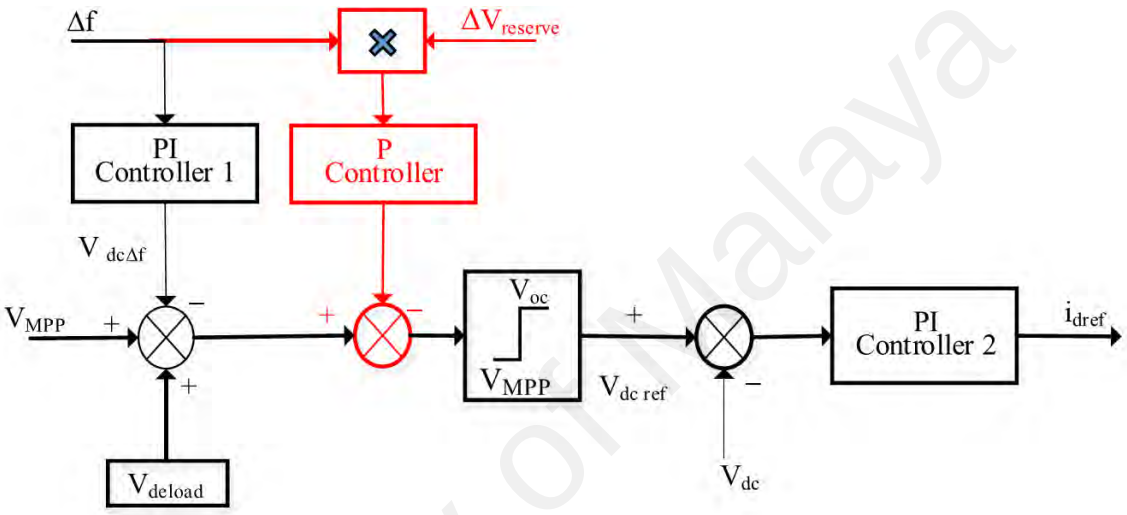

Figure 2.23: Improved controller for de-loaded PV (Zarina et al., 2012b)

In addition, (Pappu, Chowdhury, & Bhatt, 2010) introduced another method to get a reserve power for solar PV system using a de-loading technique in order to regulate the system frequency. The traditional fraction open circuit method of the maximum power point voltage (V_{MPP}) is defined by:

$$V_{MPP} = k \times V_{oc} \qquad (2.11)$$

Where k is the ratio of V_{MPP} and V_{oc} (open circuit voltage). The ratio k varies within (0.71 - 0.78). In order to realize the de-loading technique, the fractional open circuit method needs to be modified. In this situation, the PV system operates at a point below MPP by changing the fraction k of the open circuit voltage within (0.8 to 0.95).

(Okou, Akhrif, Beguenane, & Tarbouchi, 2012) proposed a frequency regulator that includes a frequency control module and a power control module. In normal conditions, the reference power of the power control module must be less than the MPP of the solar PV units. The difference between the maximum and reference powers can be used to support the grid when the frequency deviation becomes considerable. On the other hand, the adaptive frequency scheme was used in the frequency control module based on nonlinear control to calculate the active power signal P*, as shown in Figure 2.24. The output value of the frequency control module is related to the frequency deviation. In a power unbalance condition, the reference power of power control module is updated to determine the new output power of the solar PV by regulating the duty cycle of pulse width modulation (PWM) in the power converter.

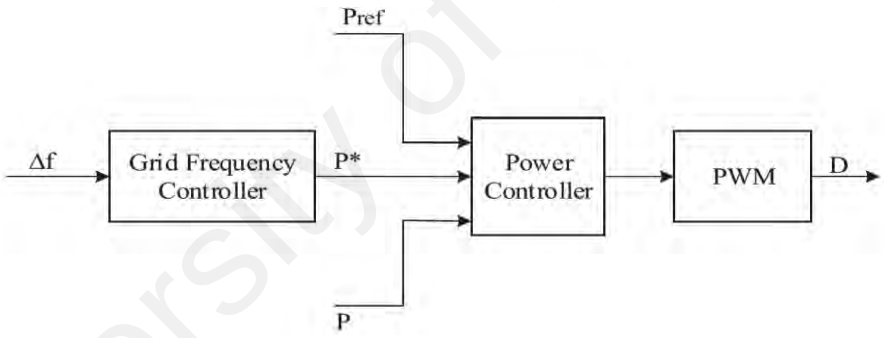

Figure 2.24: Solar PV frequency regulator (Okou et al., 2012)

Finally, the Table 2.2 shows the summary of the frequency regulation for wind turbine and solar PV proposed in literature.

Table 2.2: Summary of frequency regulation of wind turbine and solar PV that is proposed in the literature

Types of RESs	Proposed technique	Applied controller	References	Power loss	Time response	Features
Variable speed wind turbine	Inertia response	Hidden inertia emulation	(F. Gonzalez-Longatt et al., 2013; Morren et al., 2006)	No power loss	Fast response	Modification of DFIG/PMSG power reference by *df/dt* and Δf of network frequency.
		Fast power reserve	(Wachtel & Beekmann, 2009)			It is used to compensate the power loss for a short period and save time for other slower generators to participate in the frequency control.
	De-loading	Pitch control	(De Almeida & Lopes, 2007)	Some power is lost due to the de-loading technique	Slow response due to mechanical control	-High installation cost, exploiting wind farm below its maximum power extraction capability. -Prefer works when generator work close to rated power.
		Speed control (over-speed de-loading)	(Castro et al., 2012)		Fast response	It is more usable but should make sure the rotor speed does not exceed its upper limit.
Solar PV system	De-loading	Voltage controller based on PI	(Rahmann & Castillo, 2014; Zarina et al., 2012b)	Some power is lost due to the de-loading technique	Fast response due to the electronic converter	The controller does not adapt, instead, a classical PI is used without tuning.

2.5 Load shedding technique

As previously discussed, balancing power supply and demand is very important in an islanded distribution network. In some cases, the network faces a load increment over the generated power, with others generating power that exceed the loads' demand. Usually, the most common problem in island distribution network is being load rich, which results in frequency and voltage instability issues, and system blackout (Vahedi & Karrari, 2013).

In this situation, the applied load shedding technique is needed to restore the imbalance of power in an islanded system and prevent total system blackout during frequency and voltage instability issues. In literature, many researchers proposed load shedding techniques for this purpose.

Generally, load shedding techniques are commonly divided into two main categories; under-voltage load shedding technique (UVLS) and under frequency load shedding technique (UFLS).

2.5.1 Under Voltage Load Shedding (UVLS) Techniques

The UVLS schemes can prevent voltage drops in power systems. In many countries, voltage instability problem results in power blackouts due to tripping generator/overloading (El-Sadek, 1998; Verayiah, Mohamed, Shareef, & Abidin, 2014). Thus, imbalance in reactive power leads to decreased stability margin (Kaffashan, MORTEZAEE, & Amraee, 2016). To avoid further decline of voltage magnitude in the system, the UVLS scheme is conducted by power utilities to restore the power system voltage to its nominal value (T Amraee et al., 2006; Verayiah et al., 2014).

The UVLS techniques is commonly divided into two main categories; conventional load shedding and intelligent techniques.

2.5.1.1 Conventional Load Shedding Techniques

In 1998, UVLS have been applied on local buses based on a decentralized under voltage protective relays. A fixed value for the voltage threshold, time delays, and amount of loads to be shed are used in UVLS (Schlueter, 1998). However, this results in excessive load being shed from the system. Figure 2.25 shows the flow chart for conventional UVLS.

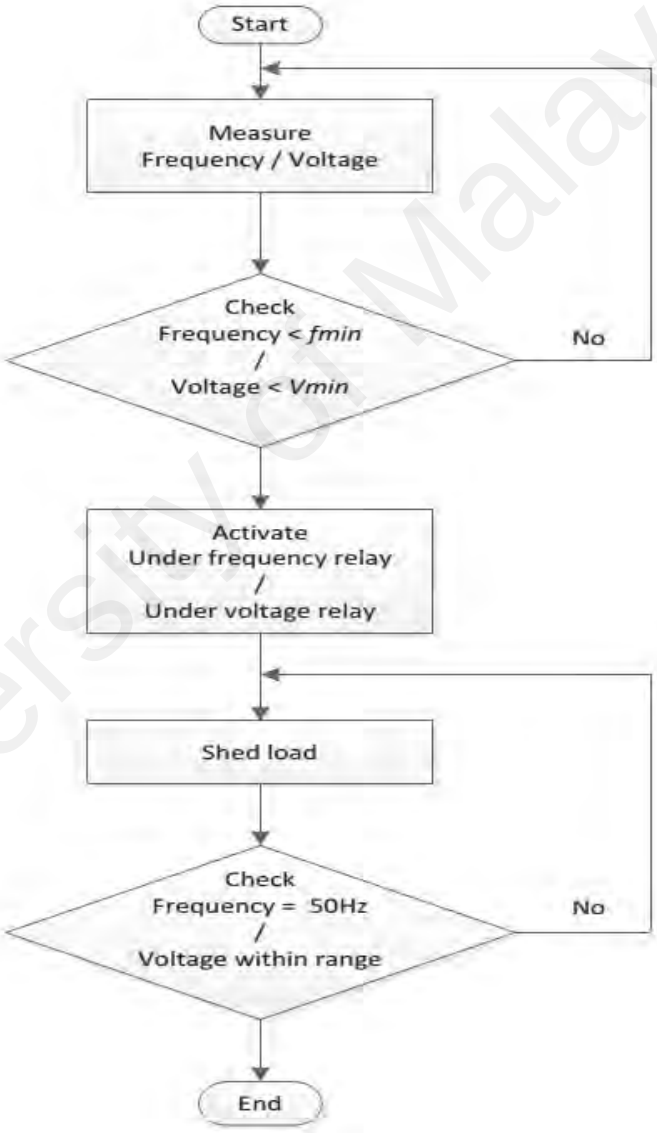

Figure 2.25: Flow chart of conventional load shedding

Conventional UVLS divides the total amount of load to be shed into a pre-set percentage of total load that will be shed when the voltage is reduced to its threshold

value. When the voltage is reduced to its first threshold value, the first pre-set percentage of the total load is curtailed. If there is a further lowering of the voltage and the voltage reaches its second threshold value, another pre-set percentage of the total load is curtailed, and so on. This process will stop when the voltage increases beyond its permissible limit. However, conventional UVLS suffers from achieving its optimum load shedding. Disturbance may occur in either local area system/wide area system (Turaj Amraee, Ranjbar, & Feuillet, 2011). This study focuses only on the local area, where the parameters at a particular node can be measured in order to calculate the voltage magnitude/voltage instability indicator. A number of authors have considered the local approach for detecting and evaluating voltage instability (Vu, Begovic, Novosel, & Saha, 1999; Wiszniewski, 2007). (Vu et al., 1999) focused on estimating the voltage collapse point based on the local measurement of bus voltage and load current. Also, (Wiszniewski, 2007) estimates the voltage stability margin by showing the effect of apparent power variation against the change of load admittance.

2.5.1.2 Intelligent technique

Currently, the structure of power systems is becoming very complex due to the significant increase in the integration of distributed generation. In this situation, the conventional load shedding scheme technique is inefficient. In order to prevent voltage collapse and system blackouts, a fast and accurate load shedding technique is required. The UVLS scheme, based on intelligent techniques, was implemented to determine the best possible load shedding scheme. Fuzzy logic control (FLC) was used in UVLS to determine the minimum load shedding in the desired loading margin in (Poshtan & Farinwata, 2006), and to avoid a risk of voltage collapse by minimizing peak loads in (Sallam & Khafaga, 2002). The Adaptive Neuro Fuzzy Inference System (ANFIS) was also used as a load shedding technique in (Haidar, Mohamed, & Hussain, 2010) to determine the amount of load curtailment in order to avoid cascading outage. In addition,

some meta-heuristic optimization methods are also used in load shedding schemes, such as genetic algorithm (GA) and the PSO algorithm. In (Malekpour et al., 2008), GA was applied in the load shedding scheme to determine the optimal amount of load shedding with/without the presence of DGs in distribution networks. The optimization function was based on the minimization of load removal in the network system and power loss in both cases. The main drawback of using GA is the fact that it is time consuming (Al-Hasawi & El Naggar, 2002; Kanimozhi et al., 2014; Luan et al., 2002; Rad & Abedi, 2008), making it unsuitable for real time applications. The PSO algorithm was implemented in UVLS to determine the optimal load shedding and prevent voltage collapse in (T Amraee et al., 2006).The UVLS scheme used the PSO algorithm to avoid voltage instability by determining the maximum loading point. It was noted by (T Amraee et al., 2006) that the PSO method can find the optimal solution more quickly relative to the GA method. The hybrid PSO and GA optimization were also proposed in the UVLS technique in (Valujerdi & Mohammadian, 2012), aiming to utilize an excellent optimization technique to determine the minimum amount of load shedding from GA characteristics and minimum computation time from the PSO features. Another hybrid optimization between PSO and Simulated Annealing technique was also implemented in the UVLS scheme in (Sadati, Amraee, & Ranjbar, 2009). The technique uses a static voltage stability margin to identify the global optimum amount of load shedding and prevent voltage instability with a minimum number of iterations. Commonly used optimization techniques, such as Evolutionary Programming algorithms (EP) and Genetic algorithm (GA), are limited in terms of computational time and premature convergence.

2.5.2 Under Frequency Load Shedding (UFLS) Techniques

UFLS is one of the most important protection systems, which results in the reduction of electrical load in the power system in order to avoid a system blackout after severe

disturbance (Zin, Hafiz, & Aziz, 2004). This section reviews the three types of UFLS techniques.

2.5.2.1 Conventional Load Shedding

Conventional UFLS is mostly utilized by power utility company due to it being simple and its lack of complicated relays. It curtails a specific amount of load when the system frequency declines under a specific edge (Karimi, Mohamad, Mokhlis, & Bakar, 2012; Laghari et al., 2015; Zin et al., 2004). In many systems, the total sum of load shedding is 30% of the rated capacity (Jiang, Yan, Ji, Liu, & Shan, 2010). Figure 2.25 shows the flow chart for a conventional UFLS.

The first curtailment might be inappropriate; therefore, if the frequency proceeds to decrease, further curtails are needed when the lower limits are surpassed. This continues until the system's frequency stop decreasing, or all the frequency sensitive relays work (Elmore, 2003). Figure 2.25 shows the overall concept of a conventional load shedding scheme. The threshold values of frequency limits and amount load to be shed at each frequency limits are decided from experience and simulations (Delfino, Massucco, Morini, Scalera, & Silvestro, 2001).The major drawbacks of the conventional UFLS is that it is unreliable in curtailing the correct amount of loads (V. Terzija & Koglin, 2002; Xu & Girgis, 2001), which can result in frequency overshoot (Shokooh et al., 2005). Generally, threshold values vary from one country to another, depending on the power system requirements. An example of a conventional UFLS is reported in (Zin et al., 2004), where three different conventional UFLS has been implemented in the Malaysian system network, consisting of 15-stage load shedding scheme in order to reflect 5610 MW, 5600 MW, and 5600 MW generation losses. The fixed amount of load is subsequently shed when the frequency of the system is unable to meet the settings' frequency.

2.5.2.2 Semi-adaptive load shedding

This type of UFLS focuses on the rate of change of frequency (ROCOF) when the system frequency decreases to a specific threshold due to the lack of generation (Kundur et al., 1994; Zin et al., 2004). When the ROCOF value is insignificant, the amount of load shed is small, and vice versa (Ahsan et al., 2012). This type of load shedding technique is preferred over conventional UFLS when the power deficit is low. However, if it is not, the operating curve of a semi-adaptive UFLS is similar to that of the conventional UFLS (Jiang et al., 2010).

2.5.2.3 Adaptive load shedding

This technique is proposed to estimate the power deficit that is unaddressed in conventional and semi-adaptive techniques. To realize the magnitude of disturbance in the system, an adaptive UFLS used the ROCOF (*df/dt*) (Karimi et al., 2012; Seyedi & Sanaye-Pasand, 2009; V. V. Terzija, 2006). The ROCOF of the system is measured after the disturbance due to the power imbalance in the system. Adaptive load shedding used a power swing equation to estimate the power imbalance, which can be obtained from following equation (V. V. Terzija, 2006).

$$\Delta P = \frac{2H}{f} \times \frac{\partial f}{\partial t} \tag{2.12}$$

Where ΔP is the power imbalance; H is the Inertia constant of generator; f is the nominal frequency (Hz); *df/dt* is the rate of change of frequency (Hz/s). After estimating the power imbalance, the adaptive load shedding technique curtailed the appropriate amount of load in order to stabilize the frequency.

Many adaptive UFLS techniques have been reported in literature. (Pasand & Seyedi, 2007; Seyedi & Sanaye-Pasand, 2009) proposed two centralized adaptive algorithms; response-based and a combination of response-based and event-based strategy. The

frequency response is regarded as the main measurement showing that the proposed scheme has the ability to shed optimum loads. When the frequency response overshoots, it means that the proposed load shedding scheme shed improper loads. The adaptive UFLS approach varied the frequency behavior due to un-optimum load shedding. (V. V. Terzija, 2006; Zin et al., 2004) reported that the adaptive UFLS technique suffers from overshooting frequency, which means that extra load has been shed. (Laghari et al., 2015) suggested an adaptive UFLS that sheds both random and fixed priority loads to address the aforementioned issue. The loads are selected by achieving the least error between the total combination of loads shed and total load amount that should be curtailed. Although this technique can shed the proper combination of loads, it is unsuitable for fast frequency changes and large power systems, as it is quite time consuming. (Delfino et al., 2001; Rudez & Mihalic, 2011) proposed the distribution of the total load amount that should be shed into five different stages, as per the threshold frequency value for each step. This offers an opportunity for primary frequency control of DGs to dispatch more active power. However, this requires extra adjustment of shedding steps for frequency control in order to minimize the curtailment loads. The load shedding scheme also faces a challenge when changes occur during load shedding. These changes could be from sudden decrease/increase of the DGs' output power, mainly if it is based on PV and Wind. Therefore, a new UFLS proposed in (Ketabi & Fini, 2015) estimated the power deficit for each load shedding step. However, they only reported the nadir frequency response without showing the frequency when it reaches the steady state. The accuracy of the estimated power deficit and optimal amount of load curtailment can be seen based on either overshoot/undershoot frequency post-load shedding. In that case, the accuracy of estimated power deficit in (Ketabi & Fini, 2015) is not immediately obvious.

2.5.2.4 Intelligent load shedding

Nowadays, the increasing integration of DGs with power systems makes it more complex. To overcome the traditional load shedding techniques problems, an intelligent load shedding scheme was used in order to shed the optimal load and keep the power system stable. Several intelligent load shedding schemes have been proposed. The optimal load shedding scheme based on Artificial Neural Network (ANN) for an isolated power system was proposed in (Cheng-Ting Hsu, Chuang, & Chen, 2011). In this technique, the inputs of ANN are the total generation, total load demand, and frequency drop rate, while its output is the minimum amount of load shedding. A comparative study was carried out to prove that the proposed load shedding is faster than the conventional technique. An ANN-based load shedding technique was applied on Taiwan's power system to increase its reliability (C-T Hsu, Kang, & Chen, 2005).The results confirmed that the ANN-based load shedding technique is suitable for real-time applications due to it shedding the exact amount of load. Moreover, (Hooshmand & Moazzami, 2012) suggested an optimal load shedding scheme based on the ANN technique, which they applied on a 39-bus New England power. The results confirmed that the proposed technique is capable of shedding an optimal load to stabilize the power system. (Sallam & Khafaga, 2002) suggested a new fuzzy UFLS method for an islanded microgrid. This technique is dynamic and robust in regulating frequencies in multiple cases. (H Mokhlis, Laghari, Bakar, & Karimi, 2012) presented a new fuzzy UFLS method for a distribution network in islanded form that is able to restore the frequency quickly. It uses frequency, the rate of change of frequency, and load priority to do this. (Ketabi & Fini, 2017) proposed a UFLS technique based on the forecast of the minimum frequency. In this technique, the system frequency samples are taken after disturbance, then, the PSO method is used to forecast the minimum frequency and shed the required loads. Table 2.3 shows the summary of UFLS techniques proposed in literature.

Table 2.3: Summary of UFLS techniques proposed in the literature

UFLS technique	Reference	Method used in UFLS technique	Detect and estimate power deficit	The ability to shed the appropriate loads	Priority of shedding loads	Remarks
Conventional UFLS	(Delfino et al., 2001)	Predetermined frequency step	Detect the power deficit but unable to estimate the value of power deficit	Shedding the fixed percentage of loads during disturbances, therefore, it Suffers from overshedding or undershedding loads.	Fixed priority load shedding	It is simple, but not suitable to implement in modern and complex power system There is no significant improvement when serious fault occurs
Intelligent UFLS	(Sallam & Khafaga, 2002)	Fuzzy logic	-Detect the power deficit and estimate the actual value of power deficit. -Unable to detect and estimate a new power deficit during shedding process.	Suffers from overshedding or undershedding loads.	Fixed priority load shedding	These techniques need to be trained to use operational network data, therefore it depends on network configuration.
	(Cheng-Ting Hsu et al., 2011)	ANN				

Table 2.3: Continued

UFLS technique	Reference	Method used in UFLS technique	Detect and estimate power deficit	The ability to shed the appropriate loads	Shedding loads priority	Remarks
Adaptive UFLS	Karimi et al., 2017)	Swing equation and Event based strategy	Detect the power deficit and estimate the value of power deficit. -Unable to detect and estimate a new power deficit during shedding process.	Suffers from overshedding or undershedding loads.	Fixed priority load shedding	-Accurate to determine the amount of load shedding -Cannot perform the optimum load shedding due to variation of frequency behaviour
	(Laghari et al., 2015)	Swing equation and Event based strategy	Detect the power deficit and estimate the value of power deficit. -Unable to detect and estimate a new power deficit during shedding process.	Appropriate shedding loads	Fixed and random priority load shedding	-Accurate to determine the amount of load shedding -Can perform the optimum load shedding due to variation of frequency behaviour
	Ketabi & Fini, 2015)	Swing equation	Detect the power deficit and estimate the value of power deficit. -Can estimate a new power deficit during shedding process.	Suffers from overshedding loads.	Fixed priority load shedding	-Inaccurate to determine the amount of load shedding -Cannot perform the optimum load shedding due to variation of frequency behaviour

2.6 Summary

This chapter provided an overview of power system stability, detailing various types of DG. The major topic addressed throughout this chapter is the frequency issue experienced in islanded distribution network due to the increasing penetration of RESs. To overcome these issues, several inertia and frequency regulation controllers were suggested. Based on literature, it was observed that the current inertia and frequency regulation controllers needs to be improved. Hence, this research proposes a modification in frequency controller for wind turbine and PV solar system for the distribution network. Various types of load shedding techniques have been reviewed in this chapter. The current techniques are unable to efficiently deal with a new power deficit during the load shedding process. Moreover, some existing load shedding technique still suffer from an over-shedding problem due to fixed priority shedding loads. Thus, this research will propose a new UFLS technique for detecting and estimating a new power deficit that occurs during the shedding process by shedding an optimal combination of loads.

CHAPTER 3: RESEARCH METHOLODGY

3.1 Introduction

This chapter details the modelling of the two-proposed load shedding scheme for planning and operation in islanded distribution networks, which is integrated with DG. These schemes consist of metaheuristic algorithms that is able to determine the most optimal amount of load shedding. The proposed scheme addressed the power changes that occurs during the load shedding process. This chapter also discusses the modifications of frequency regulation controller for the wind turbine and solar PV system, which is used in coordination with the load shedding scheme to restore the system's frequency to its reference value.

3.2 Overview of the Overall Proposed technique

This research proposes a frequency control scheme for islanded distribution networks with RESs. Figure 3.1 shows the diagram of the proposed frequency regulation, which consist of UFLS technique and frequency regulation of RESs (wind turbine and Solar PV system). The UFLS technique can be divided into the planning and operation modes. In both modes, the optimization technique was used to select random loads that should be removed from the system.

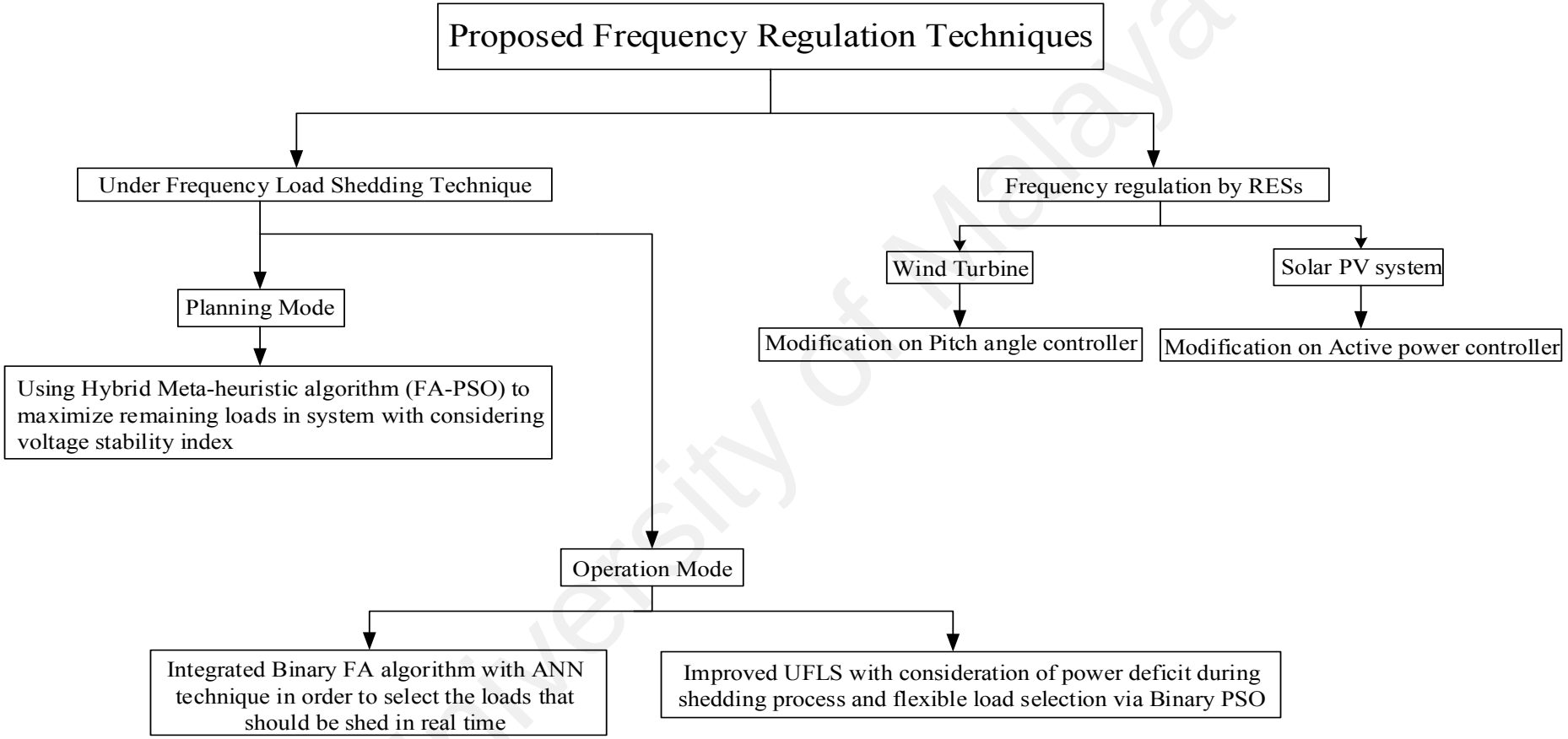

Figure 3.1: Diagram of proposed frequency regulation in distribution network

3.3 Optimal Load Shedding Planning by Using Hybrid Algorithm and Voltage Stability Index

This study integrates two algorithms to obtain an effective optimization algorithm known as Firefly Algorithm-Particle Swarm Optimization (FAPSO). The hybrid optimization aims to maximize the amount of load remaining and simultaneously maximize the voltage stability index in the distribution network. In this study, the Stability Index (SI) is used as an indicator to determine the load bus, which has the tendency to experience voltage collapse.

The Firefly algorithm (FA) is a newly designed algorithm that mimics the flashing technique of fireflies. A detailed explanation and formulation of the firefly algorithm will be given in section 3.3.2.3. A. FA has one demerit when finding a solution, it is sometimes trapped in a local optimum solution (Pal, Rai, & Singh, 2012). The firefly algorithm does not have a technique to remember the previous best solution of each firefly because the parameters in the firefly algorithm are fixed. Thus, it makes the fireflies move without taking into consideration its previous better solution. Moreover, FA also encounters some difficulties such as premature convergence and obtaining better solutions. On the other hand, the PSO algorithm is regarded as more common optimization algorithms and is applicable for many types of optimization problems. The PSO is a computational technique that depends on the movement of the swarm to determine the optimal solution in the search space. The swarm movement in the PSO algorithm in the search space takes its inspiration from a group of birds or bees. The major advantages of the PSO algorithm are simple context, easy implementation mechanism, and minimal storage requirements (Niknam, Narimani, & Jabbari, 2013). However, the PSO often faces some problems such as taking a long time to converge to optimal.

According to the previous explanation, despite the privileges of FA and PSO algorithms, they have some drawbacks, and in order to mitigate/minimize them, the two algorithms can be merged/ combined. The main goal of the proposed hybrid algorithm is realizing both local search using the flashing behaviour operation of Firefly in FA, and global search via PSO optimization. Therefore, it can be achieved that that through a balanced search between exploration and exploitation. This hybridization between FA and PSO serves the load shedding technique to find the optimum solution with less number of iteration in planning load shedding.

3.3.1 Voltage stability index

This section describes the voltage stability index formulation, referred to as the SI, which is used in the proposed load shedding scheme. The Stability Index (SI) was proposed in (Chakravorty & Das, 2001) to determine the weakest bus in a network that could lead to voltage instability when the load increases. In order to understand the SI, Figure 3.2 shows two buses in a power system model and its parameters. The line VSIs indicates the status of stability at the end of the line (received bus), while the bus VSIs indicates the status of bus stability. SI can be used in load shedding schemes and to evaluate critical loads in an islanded system. Thus, the load shedding problem can be formulated as an optimization problem using SI, and an effective optimization technique can provide a reliable solution to the problem. Therefore, this research considers the Stability Index (SI) for the load shedding scheme.

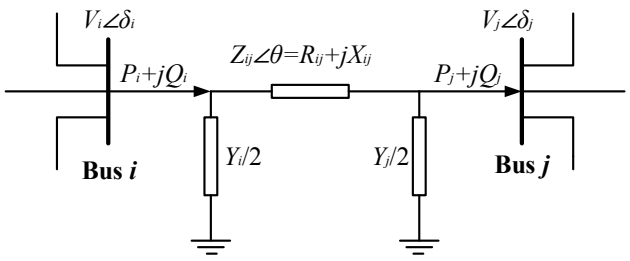

Figure 3.2: Two bus power system model

The symbols seen in Figure 3.2 are: V_i , V_j: voltage magnitude at the sending (i) and receiving (j) buses, respectively. P_i, Q_i: active and reactive power at the sending bus. P_j, Q_j: active and reactive power at the receiving bus. δ_i ,δ_j: voltage angle at the bus i and bus j, respectively. Y: line shunt admittance. R, X, θ: line resistance, line reactance, and line impedance angle. The line impedance amplitude is Z. The shunt admittances Y are neglected for simplicity.

The value of the index is given by:

$$SI = |V_i|^4 - \left[4\left(P_i X_{ij} - Q_i R_{ij}\right)^2 - 4\left(P_i R_{ij} - Q_i X_{ij}\right)^2\right]|V_i|^2 \geq 0 \qquad (3.1)$$

where SI is the voltage stability index; V_i is the sending bus voltage in pu; P_j and Q_j are the active and reactive load at the receiving end in pu, respectively; R_{ij} and X_{ij} are the resistance and reactance of the line i-j in pu.

In order to realize a more stable radial distribution network, the value of SI should be closer to one for all buses. When the SI value reaches zero, it indicates the voltage collapses in the buses carrying this value (Chakravorty & Das, 2001; Das, Kothari, & Kalam, 1995; Garg & Swami, 2014). Therefore, to avoid the possibility of voltage collapse; the SI of all nodes should be maximized. In the proposed algorithm, SI values will be calculated for each bus in the network and sorted in an ascending manner. The bus having the lowest value of SI will be considered in the fitness function.

3.3.2 Load shedding scheme - planning mode

3.3.2.1 Formulation of objective function

In this study, the optimization aims to maximize both the sum of load remaining after the load shedding process and the voltage profile of distribution network. In order to

achieve an excellent fitness value of the objective function, an approach that combines weighted objectives into a single objective method was selected. This means that the two objectives can be virtually separated by giving each its specific weight in the optimization process. In order to improve it, the objective function (*of*) needs to be formulated to minimize the objective function one (of_1) and objective function two (of_2) in the following manner:

$$Minimize \quad of = w_1 of_1 + w_2 of_2 \tag{3.2}$$

where:

$$w_2 = 1 - w_1 \tag{3.3}$$

$$of_1 = A \times \left[\frac{1}{\sum_{T=1}^{L} P_{remain,T}}\right] \tag{3.4}$$

$$of_2 = \frac{1}{SI_{system}} \tag{3.5}$$

where w_1 and w_2 are fixed positive weight values, w_1 is chosen to be in the range of [0–1], and it is used in the optimization algorithm to minimize the objective function *of* and determine the priority of two terms of_1 and of_2. *T* represents the load bus number and *L* represents the number of the load buses in the distribution network. *A* is a reference value to make of_1 unit-less and addable to the of_2 term, which is equal to 1 MW in this study. P_{remain} represents the remaining loads after the load shedding process for each bus. SI_{system} represents the lowest value of SI from all values of SI for load buses. The lowest value of SI refers to the weakest bus in the distribution network. This value is selected to improve all the voltage buses in the distribution network within allowable limits during the load shedding process.

In order to assign the proper weightage values in Equation 3.2, an analysis needs to be carried out by varying the value w_1 from 1 – 0, with a step size of 0.1. This is done to observe the significance of each weightage set (w_{set}) towards the objective function. To evaluate the performance of each weightage set, a performance index based on the Least Average Value (LAV) needs to be derived. The LAV is calculated using:

$$LAV = \frac{\Omega_1 + \Omega_2}{2} \tag{3.6}$$

where:

$$\Omega_1 = \frac{of_{1,wset,\alpha} - minimum\left(of_{1,overall}\right)}{minimum\left(of_{1,overall}\right)} \tag{3.7}$$

$$\Omega_2 = \frac{of_{2,wset,\alpha} - minimum\left(of_{2,overall}\right)}{minimum\left(of_{2,overall}\right)} \tag{3.8}$$

where $w_{set,\alpha}$ represent of_1 and of_2 values at weightage set α (where α = 1, 2, . . ., 11). $of_{1,\text{overall}}$ and $of_{2,\text{overall}}$ represent the overall of_1 and of_2 values. The performance index based on LAV (η_{LAV}) is expressed as:

$$\eta_{LAV} = \frac{1}{LAV} \tag{3.9}$$

It should be pointed out that the aim of the η_{LAV} is to estimate the least point representing the minimum value of both objective functions (of_1 and of_2) simultaneously. Therefore, by determining the largest value of η_{LAV}, proper weightage values can be determined, leading to the maximum remaining load in the distribution network with a high value of SI.

3.3.2.2 Constraints

Equality/inequality constraints that should be fulfilled for load shedding are:

(a) ***Equality in Power Flow***

The total power generated by DGs should be equal to the total load and total loss in the network after load shedding:

$$\sum_{\Omega=1}^{D} P_{DG,\Omega} = \sum_{\mathrm{T}=1}^{L} P_{Load,\mathrm{T}} + P_{Loss} \tag{3.10}$$

$$\sum_{\Omega=1}^{D} Q_{DG,\Omega} = \sum_{\mathrm{T}=1}^{L} Q_{Load,\mathrm{T}} + Q_{Loss} \tag{3.11}$$

Where P_{DG} and Q_{DG} are the active and reactive powers generated from the DG, respectively. Ω represents the DG number. D represents the total numbers of the DG units in the distribution network. P_{Load} and Q_{Load} are active and reactive loads in the distribution network after load shedding optimization for each bus, respectively. T represents the load bus number. L represents the total numbers of load buses in the distribution network. P_{Loss} and Q_{Loss} are the total active and total reactive losses in the distribution network after load shedding optimization, respectively.

(b) ***Limitation of Bus Voltage***

The voltage magnitudes at all buses after load shedding should be within permissible limits, as shown below:

$$V_{i,min} \leq V_i \leq V_{i,max} \tag{3.12}$$

where V_i is a voltage for i bus, and both of $V_{i,min}$ and $V_{i,max}$ range between ±10% of its nominal value, respectively.

(c) ***Limitation on the Amount of Load Shed at Each Bus***

The allowable amount of load shedding for any selected load bus should be in limited priority value. In other words, the minimum value of load remaining after load shedding at each bus is not less than the set value, as follows:

$$S_{i,priority} \leq S_{i,after\_shedding} \leq S_{i,before\_shedding} \tag{3.13}$$

where $S_{i,priority}$ is the minimum amount of load power that must be maintained for load bus number i. $Si_{,after\_shedding}$ and $S_{i,before\_shedding}$ represent the load power before and after the application of the load shedding process, respectively.

(d) ***Limitation on DG Capacity***

After islanding is formed, the DGs should work at the maximum output power ($P_{DG,max}$) to compensate for power shortages in the distribution network. The limit of generator power (P_{DG}) is given by:

$$P_{DG} = P_{DG,max} \tag{3.14}$$

3.3.2.3 Load shedding optimization algorithm

The proposed strategy aims to determine the optimal load shedding with minimum power losses while improving the voltage profile. This work solves the optimal load-shedding problem using the hybrid FA and PSO (FAPSO) technique and compares its' results with each FA, PSO, EP, and GSA algorithms. A detailed description of the FA, PSO and proposed algorithms are presented in the following section, while the EP algorithm was detailed in (Chakravorty & Das, 2001), and the GSA algorithm was detailed in (Rashedi, Nezamabadi-Pour, & Saryazdi, 2009).

(a) ***Firefly algorithm (FA)***

FA is a recent nature-inspired meta-heuristic optimization method. This algorithm was designed by Yang (Yang, 2010). Fireflies are small insects that are capable of producing light to attract other fireflies. They release light flashes as a signal. There is an inverse relationship between light intensity attraction '*I*' of fireflies and the distance '*r*'. Hence, most fireflies are visible only up to several hundred meters. To execute this algorithm, the fitness function is articulated based on the fluorescence light behavior of fireflies. For simplicity, it is imagined that the light intensity attractiveness of firefly is determined by its brightness '*I*', which is in turn connected to the fitness function. The main feature of the FA is based on the flashing characteristics of the firefly (Gandomi, Yang, & Alavi, 2011). The brightness '*I*' of a firefly can be selected as I_r proportional to the fitness for a maximization problem. Therefore, the I_r varies according to the well-known inverse square law, as shown in Equation 3.15.

$$I_r = \frac{I_s}{r^2} \tag{3.15}$$

where I_s is the intensity at the source *r*.

When the brightness '*I*' of a firefly increased, the Fireflies attractiveness, β, will increase, and vice versa. Thus, the attractiveness of the Fireflies is strongly proportional to their brightness. The fireflies' attractiveness, β, can be defined as:

$$\beta(r) = \beta_0 e^{-(\gamma r^2)} \tag{3.16}$$

where β_0 is the attractiveness at $r = 0$; γ is the coefficient of the light absorption; *r* is the distance between any two fireflies *y* and *z* at firefly (f_y) and Firefly (f_z), respectively.

The Cartesian distance can be determined using:

$$r_{yz} = \sqrt{\sum_{k=1}^{d}(f_{y,k} - f_{z,k})^2} \tag{3.17}$$

Where $f_{y,k}$. $f_{z,k}$ are the k^{th} component of the spatial coordinate f_y and f_z of k^{th} Firefly, respectively. d is the dimensionality of the problem. The movement of fireflies, where the new Firefly y,k ($f_{y,k}^{t+1}$) is attracted to previous Firefly z,k ($f_{z,k}^{t}$), can be determined by:

$$f_{y,k}^{t+1} = f_{y,k}^{t} + \beta_0 e^{-\gamma r_{yz}^2}\left(f_{z,k}^{t} - f_{y,k}^{t}\right) + \alpha(rand - 0.5) \tag{3.18}$$

where the second term is caused by the attraction, while the third term, governed by the randomization parameter α, is responsible for the insertion of certain randomness in the path followed by the firefly, and *rand* is a random number between 0 and 1.

(b) *Particle Swarm Optimization (PSO)*

PSO is another meta-heuristic method used by most researchers for the optimization problem. It was originally proposed by Dr. Eberhart and Dr. Kennedy in 1995 (Eberhart & Kennedy, 1995). The major principle of PSO is created according to the behavior of birds or fish searching for food. The advantage of using PSO over other optimization techniques is its simplicity and the fact that it requires very little adjustment to a few set parameters. Due to this fact, PSO has been widely used in a variety of applications.

Let a number of k particles in a swarm be initialized with positions $x^t_k = (x^t_1, x^t_2, x^t_3, \ldots, x^t_k)$ and velocities $v^t_k = (x^t_1, x^t_2, x^t_3, \ldots, x^t_k)$, and the fitness is calculated based on particle positional coordinates as the input values. Then, the particles are moved into new positions using the equations below (Baran & Wu, 1989):

$$x_k^{t+1} = k_k^t + v_k^{t+1} \tag{3.19}$$

$$v_k^{t+1} = wv_k^t + c_1 r_1(P_{best} - x_k^t) + c_2 r_2(G_{best} - x_k^t) \tag{3.20}$$

$$w = w_{max} - \frac{w_{max} - w_{min}}{iter_{max}} \times iter \tag{3.21}$$

where, x_k^t and x_k^{t+1} are the current position of the particle k at iteration t and $t+1$, respectively; v_k^t and v_k^{t+1} are the current velocity of the particle k at iteration t and $t+1$, respectively; c_1 and c_2 are the weighting factors; r_1 and r_2 are a random number between 0 and 1; w_{max} and w_{min} are the maximum and the minimum weight of the initial, respectively; iter and $iter_{max}$ are the current iteration number and the maximum iteration number, respectively. Each particle updates its position and velocity based on its own searching experience called P_{best}, and on the experience from the other particle called G_{best}.

(c) *Proposed Method: Hybrid of FA and PSO (FAPSO) Optimization*

In this method, the capability of the FA is integrated with the PSO to increase its chance for not being trapped in a local solution and quicken speed convergence. The FAPSO share similar procedures to that of the FA. However, the movement of fireflies in FAPSO is modified, where new firefly ($f_{y,k}^{t+1}$) can be randomly mutated by:

$$f_{y,k}^{t+1} = f_{y,k}^{t} + \beta_0 e^{-\gamma r_{yz}^2} + c_1 r_1 \left(f_{Gbest,k}^{t} - f_{y,k}^{t}\right) + \alpha(rand - 0.5) \tag{3.22}$$

The steps for implementation of FAPSO method is as follow:

1. Generate array of random fireflies.
2. Initialize P_{best} and G_{best}.
3. the fitness of initial population based on light intensity of fireflies is determined.
4. While (stopping criteria is satisfied)
5. For y= 1:k (k fireflies)

6. For z = 1:k
7. Calculate light intensity I by using Equation (3.15).
8. Determine the distance between $P_{best\text{-}fy}$ and $G_{best\text{-}fy}$ by using Equation (3.17).
9. If (I(y) < I(z))
10. Moving of Firefly y towards firefly z using Equation (3.22)
11. End If
12. The new solution is calculated and the light intensity value is updated.
13. Updating both of P_{best} and G_{best}.
14. End for z
15. End for y
16. End while
17. Rank the fireflies in descending according to their light intensity.

In the proposed method, the light intensity attraction step of each particle is mutated by a modified mutation function in the FAPSO operator. For that, each particle is randomly attracted towards the G_{best} position in the same population. Local search in different regions is implemented by the attractiveness step of the FA algorithm. The FAPSO algorithm outperforms the FA and PSO algorithms in solving the optimization problems using the flashing behavior of fireflies.

3.3.2.4 Procedure of applying FAPSO algorithm in load shedding

The flowchart in Figure 3.3 shows the procedure of the proposed UFLS.

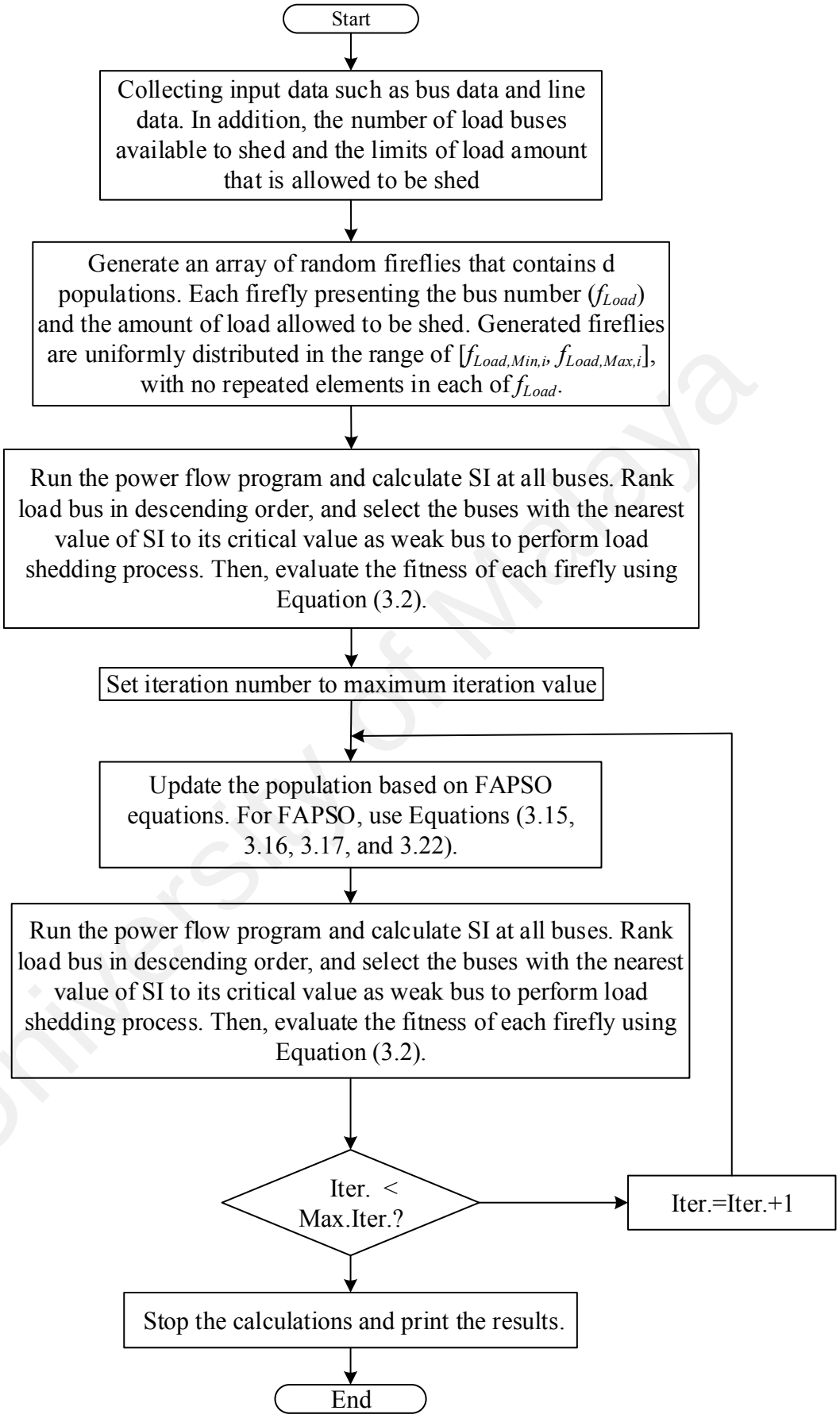

Figure 3.3: Proposed FAPSO algorithm flow chart

3.4 Methodology of proposed UFLS-I scheme in operation mode

The proposed UFLS scheme consists of two main modules: (1) Total Load Shed Amount Estimation Module (TLSAE), and (2) Load Shedding Controller Module based on ANN-Binary Firefly algorithm (LSCM-ANN_BFA).

3.4.1 Total Load Shed Amount Estimation Module (TLSAE)

The proposed UFLS scheme-I will only activate its process when it receives a tripping signal from an incoming grid substation breaker or DG breaker, indicating the formation of islanding or one of DG is disconnected. The amount of power deficit due to the formation of islanding or disconnected DG is equal to power incoming to the distribution network. On the other hand, the amount of power deficit during islanding is calculated based on the rate of change of frequency (ROCOF) for the sudden addition of the extra load to the distribution network. It is worth mentioning that the frequency of the center of inertia (COI) is considered in the UFLS whenever there is more than one generator in the islanded distribution network. The center of inertia frequency, in Hertz, can be determined using Equation 3.23:

$$f_{COI} = \sum_{i=1}^{N} H_i f_i \Big/ \sum_{i=1}^{N} H_i \tag{3.23}$$

Where N is the number of connected generators; H_i is the inertia constant of each generator in seconds; f_i is the frequency of each generator in Hertz. In this study, the value of 47.5 Hz and 52.5 Hz are assumed to be the allowable limits of system frequency. It should also be pointed out that when the system frequency is beyond these limits, the protection devices is activated so that it can disconnect all DGs, resulting in a blackout.

The amount of load to be shed can be minimized by utilizing the spinning reserve of the system, which depends on the generators' capacity. The total spinning reserve (TSR) of the system can be calculated using Equation 3.24.

$$TSR = \sum_{i=1}^{N} MGC_i - \sum_{i=1}^{N} AGP_i \tag{3.24}$$

Where N is the number of connected generators; MGC_i is the maximum generation capacity of i^{th} generator; AGP_i is the actual generated power of i^{th} generator.

When the TLSAE module senses any imbalance between the generated and demanded active power in the system during islanding mode, it calculates the power deficit in the system using:

1) Event based strategy – when one or more of generator supply like RESs are disconnected from the distribution network and/or the decreasing in output power generated by RESs (such as wind turbine and Photovoltaic).
2) Response based strategy – when the load suddenly increased in the islanded distribution network.

In the first strategy, the power deficit is estimated by detecting the status of generator breaker and recording the last generated power output prior to outage.

$$P_{deficit} = \sum_{j=1}^{M} P_{disconnected\ Source} \tag{3.25}$$

where $P_{deficit}$ is the imbalance power during islanding mode in per-unit, $\sum_{j=1}^{M} P_{disconnected\ \mathrm{Source}}$ is the sum of output power for tripped generators in per unit, and M is the number of trip generators. It can be noted from the last equation, when there is a

generator-tripping event, that the estimated power deficit is equal to the total generation loss in the system. To calculate the power deficit for RESs, Equation 3.26 can be used:

$$P_{deficit} = P_{RES,0} - P_{RES} \tag{3.26}$$

where $P_{RES,0}$ is the total output power generated by RESs at the source of RESs change event (like wind speed or sun radiation); P_{RES} is the total output power generated by RESs at 20 ms after the source of RESs change event.

The second strategy is based on the df_{COI}/dt. When there is a change in the rate of frequency caused by the load increment event, the power deficit can be calculated based on a power swing equation:

$$P_{deficit} = \frac{2 \times \frac{df_{COI}}{dt} \times \sum_{i=1}^{N} H_i}{f_n} \tag{3.27}$$

where $P_{deficit}$ is the imbalance power during islanding mode per-unit; df_{COI}/dt is the rate of change of center of inertia frequency at first disturbance in the system, Hz/s; H_i the inertia constant of ith connected generator; N is the number of connected generators; f_n is the rated value of frequency, Hz.

The primary frequency control of DGs is activated when the center of inertia frequency reaches 49.8 Hz to enhance the reduction in the declination in the frequency of the system (Liu & Chen, 2015). This value can be adjusted according to the needs of the protection. The magnitude of $P_{deficit}$ is utilized to determine the load shedding decision. If $P_{deficit}$ is less than a certain value (which reflects the small disturbance in the system), the load shedding process cannot be activated, while if $P_{deficit}$ exceeds this value, the load-shedding scheme is activated. These values can also be adjusted based on network conditions. To

improve the system frequency response and restore the frequency to its nominal value, the correct amount of load to be shed in the system can be calculated using:

$$TLSA = P_{deficit} - TSR \tag{3.28}$$

where *TLSA* is the total load shed amount.

After the TLSAE Module determines the loads to be shed, the Load Shedding Controller Module will initiate the corresponding load feeder to be removed in the distribution system with the right loads to be shed based on the power deficit estimation. In the next section will present the load shedding based on ANN-Firefly algorithm (LSCM-ANN_BFA).

3.4.2 Load Shedding Controller Module based on ANN- Binary Firefly algorithm

The proposed load-shedding scheme includes two main parts of offline and online studies. In order to create the ANN database, the network arrangement needs to be first specified, and the required data for this study will be prepared in two forms: load bus data and load that can be shed from the system. The necessary data for ANN training are collected from offline power system simulations using various contingency scenarios, such as unit and line outages in different loading conditions any TLSA in the system. In this step, the load shedding optimization problem can be solved using the Binary Firefly (BFA) algorithm to find the best combination of load curtailment for each TLSA from minimum to maximum values for every ΔTLSA.

This section is divided into two stages; (1) creating the data set for ANN by using the BFA to find the best combination for each TLSA, and (2) training these data by ANN. In real time application, the output of ANN determines the best combination of load buses to be closed to TLSA within the least possible time by using the data received from the offline BFA optimization method.

3.4.2.1 Binary Firefly optimization

In the load shedding technique, the Binary Firefly optimization is used to choose the best loads combination to be shed, which is to be close to *TLSA.* In this section, the BFA determines the best combination loads for TLSA for every ΔTLSA in MW from the minimum expected value of TLSA in MW to the maximum expected value of TLSA in MW. Both values depend on the nature of the distribution network. The values of each load buses are obtained from the daily load curve for the distribution network. The proposed load shedding based on BFA has two choices for each bus; either removing all loads on the bus or leaving the loads without shedding.

To illustrate the BFA method, let the TLSA be 1.2 MW, and 11 loads in (MW) are defined by the daily load curves at specific times. The length of each firefly depends on the number of loads that can be removed from the distribution network, so the length of the firefly is selected based on the nature of the distribution networks. The value of each element in firefly has two probabilities; '0', which represents the load demand bus leaves without shedding, and '1', which represents the complete load demand of load bus removes from networks. The best load combination that fulfils the minimum value of (TLSA - ∑Pi_Combination), namely when ∑Pi-Combination closest to TLSA is the best loads combination. As noted in Table 3.1, the best firefly is f_{50} because the value of (TLSA - ∑Pi_Combination) is the smallest value.

Table 3.1: Find the best combination of load removing when power deficit is 1.2 MW

Firefly No.	Binary Firefly Value	∑Pi-Combination (MW)	TLSA - ∑Pi-Combination (MW)
f_1	10101101010	$P_{L2}+P_{L4}+P_{L6}+P_{L7}+P_{L9}+P_{L11}$ =0.95	0.25
f_2	01000101011	$P_{L1}+P_{L2}+P_{L4}+P_{L6}+P_{L10}$ =1	0.2
f_3	11110000001	$P_{L1}+P_{L8}+P_{L9}+P_{L10}+P_{L11}$ =1.1	0.1
.	.	.	.
.	.	.	.
.	.	.	.
f_{50}	**00111000111**	**$P_{L1}+P_{L2}+P_{L3}+P_{L7}+P_{L8}+P_{L9}$ =1.195**	**0.005**

The objective function F can be presented in the following form:

$$F = \left| TLSA - \sum P_{i-combination} \right| \tag{3.29}$$

The inequality constraints that should be fulfilled for the load shedding are:

(1) Active and reactive power generation inequality constraint:

$$c_1 \times P_{Gi} \leq P_{Gi} \leq c_2 \times P_{Gi} \tag{3.30}$$

$$c_1 \times Q_{Gi} \leq Q_{Gi} \leq c_2 \times Q_{Gi} \tag{3.31}$$

Where P_{Gi} and Q_{Gi} are the active and reactive powers generated from the DGs, respectively, while c_1 and c_2 are 0.8 and 1.2, respectively.

(2) Limitations of bus voltage: The voltage magnitudes at all buses after load shedding should be within permission limits, as shown below:

$$V_{i,min} \leq V_i \leq V_{i,max} \tag{3.32}$$

Where, V_i is a voltage for i bus, and $V_{i,min}$, and $V_{i,max}$ range between ±10% of its nominal value, respectively.

(3) Limitations on the amount of load shed at each bus

The allowable amount of load shedding for any selected load bus should be in limited priority value. In other words, the minimum value of load remaining after load shedding at each bus is not less than the set value, as follows:

$$0 \leq \Delta S_i \leq S_i \tag{3.33}$$

Where S_i, ΔS_i are the maximum demand load at each bus and change of power load demand, respectively.

The problem of finding the best combination of load is solved using BFA in the following manner:

Step 1: Input data are determined, such as the active power of load buses and voltage, the power output of DGs, and the value of TLSA.

Step 2: The basic firefly parameters are set as β_0 =1, γ =1 and α =0.8.

Step 3: Generate random initial populations of firefly (*f*), where in this case there is two states for load bus either zero, which represents the load demand bus leaves without shedding or one which represents the complete load demand of load bus removes from networks, taking into consideration all the limitations and constraints as follows:

$$f = \begin{bmatrix} L_{11} & \cdots & L_{1n} \\ \vdots & \ddots & \vdots \\ L_{m1} & \cdots & L_{mn} \end{bmatrix} \tag{3.34}$$

where *m* indicates the population size; *n* is the number of load buses that can be applied load shedding process on it.

Step 4: Start the iteration by finding the best combination of load to be shed in order to obtain a close value of totally of active power of the combination of loads to be shed to the TLSA value.

Step 5: Evaluate the fitness for each of the population (1 to m) using Equation 3.29. This means evaluating the summation of active power of load buses to be shed.

Step 6: Rank the population according to the light intensity (low to high fitness) and save the best value in the following manner:

$$[F_{Index}] = sort(f)$$
$$F_{best} = F(1) \tag{3.35}$$

Step 7: Update all fireflies on matrix *x* (state of load bus) and rank the movement by taking into consideration all the limitations and constraints using the following equations:

The firefly attractiveness β is presented as Equation 3.16. The Cartesian distance between any two fireflies *l* and *j* (represented by row of the *x* matrix) can be expressed in the form of Equation 3.17. The movement of fireflies, where firefly *y* is attracted to brighter firefly *z*, is determined by Equation 3.18.

Step 8: Repeat the steps from step 4 until completing the maximum iteration number.

Step 9: Stop the process and print the best solution, which represents the best combination of load removing and plot the total fitness during the iterations.

The optimal combination of load shedding selections by the BFA optimization is generated to be a training data set for Neural Network (NN), which will be detailed in the next section.

3.4.2.2 Artificial Neural Network (ANN) based intelligent load shedding model

ANN is one of the artificial intelligence techniques that has been used to determine the best combination of load to be shed for a given TLSA. In load shedding, the training data set of ANN is generated by the actual system stability behavior (C-T Hsu et al., 2005). However, in this work, the training data set is generated from the best solution of BFA i.e. TLSA and the best combination of load. From the best value, the input of the network is TLSA and the output is the best combination of load to be shed. The feed forward network model is used, which consists of three layers called the input, hidden, and output layers, respectively. The training date set of the network is given as per Equations 3.36 and 3.37.

$$Input: training\ data, TLSA\ (MW) = \begin{bmatrix} {}^{min}TLSA \\ {}^{min}TLSA + \Delta TLSA \times 1 \\ {}^{min}TLSA + \Delta TLSA \times 2 \\ \vdots \\ {}^{max}TLSA = {}^{min}TLSA + \Delta TLSA \times z \end{bmatrix} \quad (3.36)$$

$$Output: training\ data, The\ best\ combination\ of\ load\ to\ be\ shed$$

$$= \begin{bmatrix} {}^{best}combination_{load\ shed\ 1} \\ {}^{best}combination_{load\ shed\ 2} \\ {}^{best}combination_{load\ shed\ 3} \\ \vdots \\ {}^{best}combination_{load\ shed\ z} \end{bmatrix} \quad (3.37)$$

Where z is the total number of *TLSA*, which needs to be calculated for the best combination of loads to be shed.

Using this data set, the network is trained and output of the network is denoted as ${}^{NN}combination_{\,Load\ shed}$. The general structure of the ANN network is given in Figure 3.4.

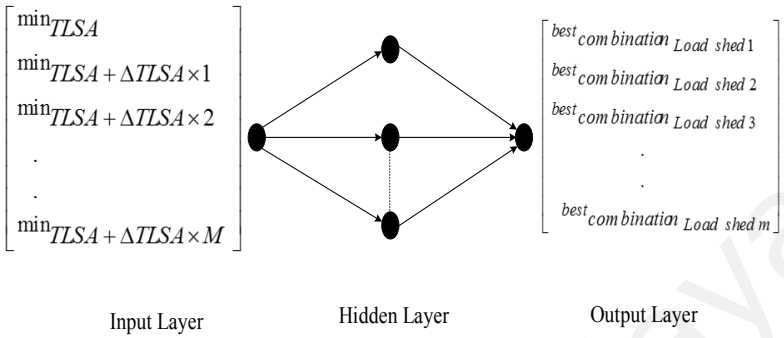

Figure 3.4: Mechanism of an artificial neuron

The Back Propagation (*BP*) training steps involved in the neural network are explained below:

Step 1: Initialize the input, output and weight for each neuron. Here, *TLSA* is the input of the network and the best combination of load to be shed is the output of the network.

Step 2: These data sets are given to the classifier and determine the BP_{error} , as follows:

$$BP_{error} = {}^{best}combination_{\,Load\ shed} - {}^{NN}combination_{\,Load\ shed} \tag{3.38}$$

In Equation 3.38, ${}^{best}combination_{\,Load\ shed}$ is the target output and ${}^{NN}combination_{\,Load\ shed}$ is the output of the network.

Step 3: The output of the network is calculated to be:

$${}^{NN}combination_{\,Load\ shed} = \sum_{m=1}^{M}\left(w_{1m}({}^{NN}combination_{\,Load\ shed}(m)) + Threshold\ value\right) \tag{3.39}$$

$${}^{NN}combination_{\,Load\ shed}(m) = \frac{1}{1+\exp\left(-w_{1m}\times\left({}^{best}combination_{\,Load\ shed}\right)\right)} \tag{3.40}$$

where ${}^{NN}combination_{Load\ shed}$ is the input at neuron i, W_{1m} is the weight of going from node 1 to node m, m is the number of neurons in the previous layer, *Threshold value* is the bias of neuron. Equations 3.39 and 3.40 denote the activation function of output and hidden layers, respectively.

Step 4: Vary the weights of neurons by $w_{new} = w_{old} + \Delta w$, where, Δw is the change in weight, which can be determined using:

$$\Delta w = \lambda \times ({}^{NN}combination_{Load\ shed}) \times BP_{error} \tag{3.41}$$

where λ is the learning rate which varies from 0.2 - 0.5.

Step 5: Repeat the process from step 2, until BP_{error} gets minimized to a least value i.e., $BP_{error} < 0.1$.

Once the process gets completed, the network will be suitable for providing the ${}^{best}combination_{Load\ shed}$ for any *TLSA*. Figure 3.5 shows the ANN-BFA module with distribution network.

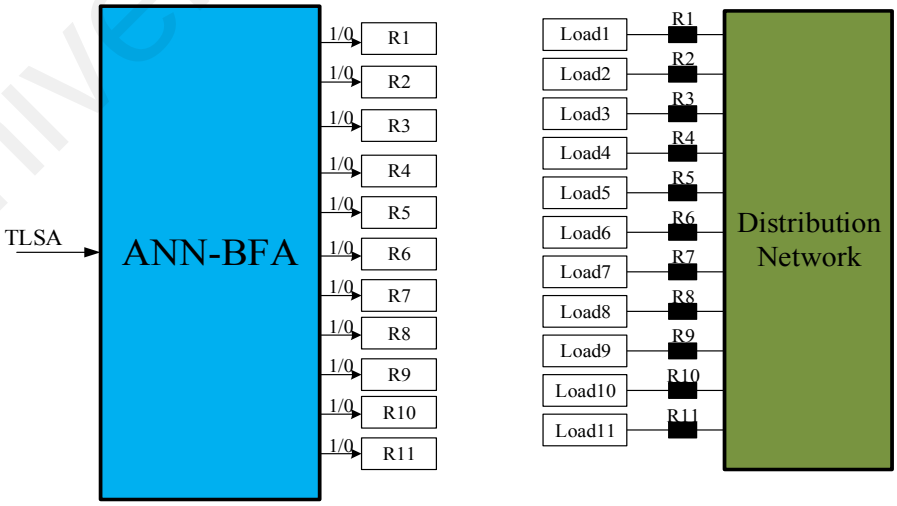

Figure 3.5: ANN-FA load shedding unit

3.5 Proposed UFLS-II technique with Consideration of Power Changes during shedding Process

This section details the proposed UFLS scheme that possess the ability to detect power deficit during the shedding process and accordingly adjust the amount of load shedding. This is achieved by continuous monitoring of the overshooting signal of the second frequency derivative of the center of inertia. Once detected, an equivalent system inertia constant is estimated in order to determine the new power deficit. The scheme is also equipped with an optimization algorithm to determine the best combination of loads close to the amount of power deficit, which helps minimize frequency overshoot/undershoot. The optimization technique selected for this section is the Binary Particle Swarm Optimization (BPSO).

The total load shed amount (*TLSA*) is determined by the Total Load Shed Amount Estimation Module (TLSAE), as mentioned in section 3.3.1. The total load shed amount (*TLSA*) was distributed in four shedding steps according to the following threshold frequencies: 49.5 Hz, 49.2 Hz, 48.9 Hz, and 48.6 Hz. The load shed amount for these frequency thresholds were set to 35%, 30%, 20%, and 15% of the total load shed amount (Ketabi & Fini, 2015). These values were selected to give a chance for the primary frequency response of the generator to inject more active power into the system at each step, and consequently reduce the lowering rate of change of the center of inertia frequency (df_{COI}/dt).

The distribution load shedding, based on four steps, increases the opportunity for the primary frequency response to contribute towards containing the deviation, which is preferable towards optimal shedding and minimizing the disconnected load while preventing the frequency from reaching its minimum value. The first step is to shed the largest percentage of load and quickly limit the rate of change of frequency to prevent a

severe frequency drop from occurring in the distribution network. This large initial shedding is preferred in distribution networks, as their low inertia and limited primary response resources can result in a large frequency drop.

Furthermore, the proposed UFLS scheme-I will use governors to respond to increase in its mechanical power, which leads to power injection with the objective to minimize load shedding. If the governors can prevent the frequency from decreasing, the *TLSA* is zero, and load shedding becomes unnecessary. In this UFLS scheme-I, and the value of $f_{min} = 47.5$ HZ and $f_{max} = 52.5$ Hz (Laghari et al., 2015). It should also be pointed out that when the system frequency is beyond these ranges, the protection relays of DGs will be activated to disconnect all of the DGs, which results in blackouts.

3.5.1 Selection of Loads for load shed by using Binary PSO

After the controller confirms the amount of load that can be shed from the system, the next step involves finding the best combination of load buses that can be disconnected from the network in four load shedding steps. The problem of determining the optimal combination of load shedding selections can be solved using the Binary Particle Swam Optimization (BPSO) technique. The steps pertaining to this module are outlined in Table 3.2.

Table 3.2: PSO steps to select the best combination of loads in distribution network

Step number	Procedure
Step1	Determine the Input data, such as the amount of load to be shed, PSO parameters such as weighting factors, and the number of particles.
Step 2	Generate an array of random particles with a random position (combination of load to be removed) and velocity. Each particle presents the combinations of random load buses to be shed that fulfil the pre-set limitation.
Step 3	Step 3: Evaluate the fitness value for each particle using the fitness function in 3.29
Step 4	Update the position and velocity of each particle based on its own searching experience, called P_{best} and on the experience from the other particle, called G_{best}. Update the particle position and velocity based on the Equations 3.19 ,3.20 and 3.21
Step 5	The same process is repeated until the optimal, or near optimal solution that has the minimum error as per the following equation is found. $f_{max} - f_{min} \leq 0.005$ or number of iteration >120
Step 6	Select the optimal combination load with the minimum absolute error. then, the signal send to the breakers by controller to shed the optimal load combination; the PSO algorithm repeats this process for the four shedding steps.

The assumed delay time of 200 ms includes control, communication, and Circuit Breaker (CB) operation times (Aponte & Nelson, 2006). It should also be highlighted that the communication links for transmitting signals control and data for load shedding control is assumed to be at high speed via mediums such as fiber optics (Ketabi & Fini, 2017).

3.5.2 Power Deficit Estimation Module

When a power deficit occurs during the load shedding process, the proposed load-shedding controller can detect and estimate new power deficits during the load shedding process. The detection is based on the negative overshoot of the second derivative of the center inertia of frequency. In order to describe this idea, a test system, shown in Figure

3.6, is modelled and simulated in PSCAD/EMTDC for the islanded condition, where the grid is disconnected from the system, and the load added while it is being shed. The system consists of three mini hydro generator units (G1, G2, and G3) connected to a group of system loads (Load1,…Load32). A utility grid is also connected to supply 3 MW to the system. The model does not include transmission lines. All circuit breakers (BRKA, BRKB, BRK3, BRK1,…,BRK32, and BRK-Grid) were modelled as ideal switching devices, while the system load was modelled as per (Karimi et al., 2012). Table 3.3 tabulate details pertaining to the test system.

Simulation first began with grid disconnection to form islanded condition. The power imbalance can be determined using Equation 3.25. Then, an extra load (0.25 MW) is connected after the first load shedding step.

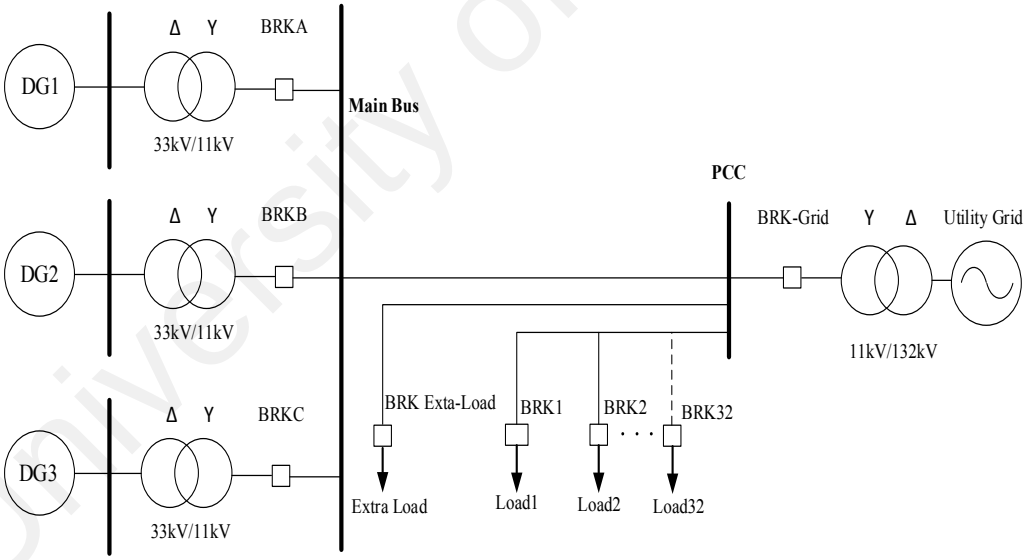

Figure 3.6: A model of a simple test system used for analysis of the frequency second derivative

Table 3.3: Test frame indices

Indices	Value	Indices	Value
Mini hydro rating (1 unit)	2MVA	Active power load for each load (Load1,…,Load 32)	0.25 MW
Active power supplied by grid utility	3MW		
Voltage (L-L)	11kV	Frequency	50 Hz
Total active power load	8 MW	Active power of extra load	0.25 MW

The results of the simulated events are shown in Figure 3.7 at the first derivative (rate of change of frequency) and second derivative of frequency over time for multiple events. It is clear that the high value of the active power deficit due to islanding leads to the first derivative frequency to move further away from zero. This means that the system's frequency starts decreasing compared to its reference value. On the other hand, the second frequency derivative value starts to decrease drastically, as shown in Figure 3.8. The power deficit caused by islanding is reflected on the higher negative value of the amplitude of the second derivative of the frequency curve. The load shedding process then takes place, and distributes itself in four steps of 1.044, 0.783, 0.651, and 0.522 MW at frequency thresholds of 49.5, 49.2, 48.9, and 48.6 Hz, respectively. The first load shedding step also effects the frequency first-derivative curve by causing a sudden step change towards a zero-frequency gradient. The second frequency derivative is also influenced by the load shedding steps, resulting in a positive impulse signal, as shown in Figure 3.8. However, when an extra load is suddenly added to the test system, the second derivative in Figure 3.8 immediately moves toward a negative value, exceeding the threshold value. Based on this significant change, the proposed scheme uses the second derivative to sense any changes (imbalance) in power during load shedding.

Patterns similar to the ones obtained in the simulation of the test system shown in Figure 3.6 were also reported in (Karimi et al., 2017; Hazlie Mokhlis, Karimi, Shahriari,

Bakar, & Laghari, 2013). Generally, Figures 3.7 and 3.8 show the behavior of first and second frequency derivatives during various events in any distribution network with four load shedding steps, respectively. Figure 3.7 illustrates the second derivative of the center of inertia frequency with time after islanding was formed and during the load shedding process, while Figure 3.8 shows the first derivative of the center of inertia frequency with the center of inertia frequency behavior after islanding was formed and during the load shedding process.

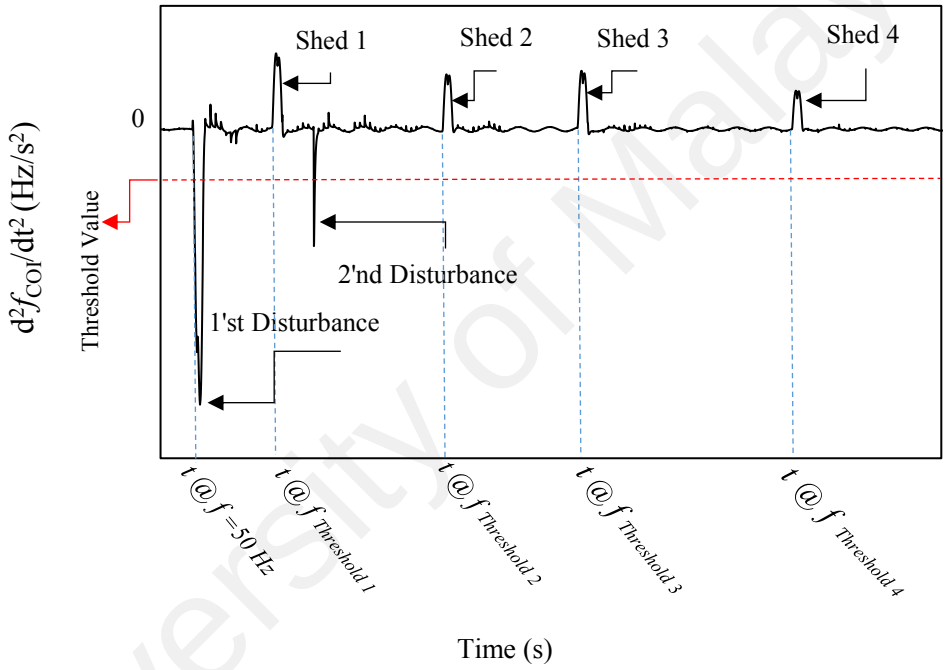

Figure 3.7 Monitoring the d^2f_{COI}/dt^2 is the indicator of changing in distribution network in general case for applying load shedding scheme and a sudden power deficit during load shedding process

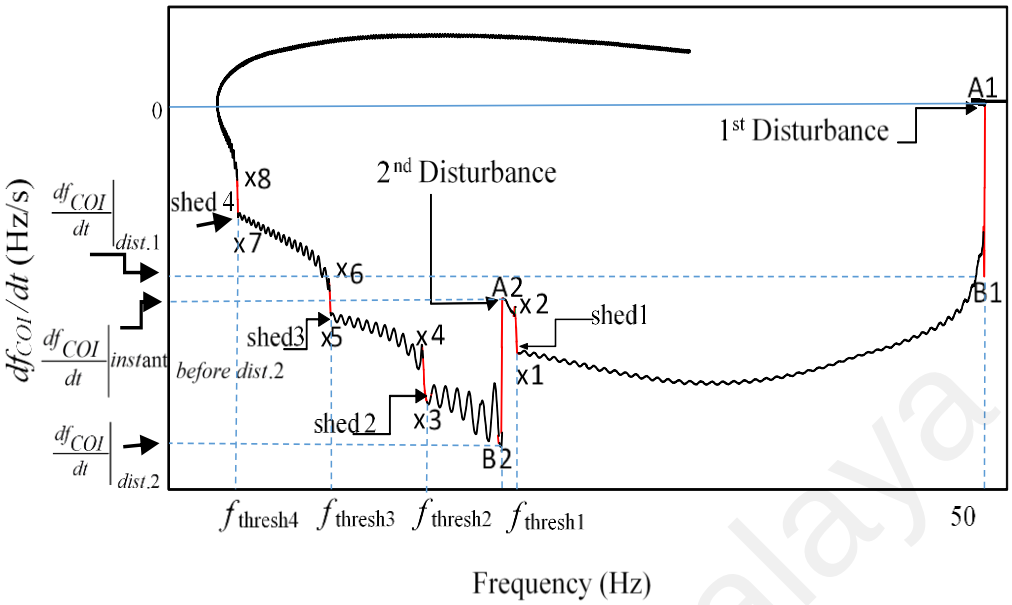

Figure 3.8: The relation between df_{COI}/dt with f_{COI} during load shedding in general case for applying load shedding scheme and a sudden power deficit during load shedding process

It can be seen from Figure 3.8 that when an islanding mode occurs-representing the 1st disturbance point - the (df_{COI}/dt) directly moves towards the negative side. The red line from A1-B1 represents$(df_{COI}/dt) \mid_{dist.1}$, which is used in the swing equation to estimate the first imbalance of power. The load shedding occurs at the four threshold frequency values, depending on the system network and control strategies technique. At each load shedding process, it increased (df_{COI}/dt) from x1-x2 at the first frequency threshold, x3-x4 at second frequency threshold, x5-x6 at the third frequency threshold, and x7-x8 at the fourth frequency threshold.

After detecting a second power deficit, the controller captured the first derivative of the center of inertia frequency $(df_{COI}/dt) \mid_{dist.2}$ that represents point (B2) in Figure 3.8, and brings the last (df_{COI}/dt) that represent point (A2) in Figure 3.8 before a new disturbance occur at $(df_{COI}/dt) \mid_{before\ instant\ dist.2}$.

To estimate the value of a new power deficit, we should estimate the equivalent inertia constant of the system. The following equation can be used to obtain the equivalent inertia constant of the system:

$$H_{eq,update} = \frac{(P_{deficit} - \sum_{k=1}^{l} P_{shed}|_{step\ k}) \times f_n}{2 \times \left| \left(\frac{df_{COI}}{dt} \mid_{before\ instant\ dist.2} \right) \right|} \tag{3.42}$$

where $H_{eq,update}$ is the new equivalent inertia constant of the system; k is the step shedding; l is the last step shedding before the second disturbance; $\sum_{k=1}^{l} P_{shed}|_{step\ k}$ is the total power load shed at step k before the second disturbance; $\frac{df_{COI}}{dt} \mid_{before\ instant\ dist.2}$ is the rate of change of center of inertia frequency before the second disturbance, Hz/s.

Based on the new equivalent inertia constant of the system (H_{eq}), we can now estimate the new imbalance power using equation (3.43).

Estimating the new total load to be shed resulting from the new power deficit ($P_{deficit,new}$) is added to the next load shedding steps. After that, the load shedding process repeats the steps described in section 3.4.1 prior to any new power deficit.

$$P_{deficit,new} = \frac{2 \times H_{eq,update} \left| \left(\frac{df_{COI}}{dt} \mid_{dist.2} - \frac{df_{COI}}{dt} \mid_{before\ instant\ dist.2} \right) \right|}{f_n} \tag{3.43}$$

As per previous explanations, the changes in the frequency second derivative is regarded as an indicator of all of the activities of the distribution network that affect its trajectory. In order to further explore the proposed method in the context of its application, an analysis of the frequency second derivative using the model of a simple test system needs to be performed. Finally, by applying the proposed method on the test

model in Figure 3.6 (adding an extra load (0.25 MW)), the new power deficit in the test system is estimated to be 0.258 MW.

3.6 Frequency control strategy for wind turbine and solar PV system in distribution network

Most RESs, such as variable speed wind turbine and solar PV system, are incapable of providing an active power reserve to enhance frequency stability when power deficit occurs. A de-loading operation is applied on wind turbine and PV system to generate less active power than its maximum value capability. Thus, the difference between the actual generation and available generation can be considered as the primary frequency reserve. The de-loading operation in wind turbine can be accomplished by pitch angle control/wind turbine generator speed control (Z.-S. Zhang, Sun, Lin, & Li, 2012).

Pitch angle can be used to de-load the wind turbine by increasing the blade's angle. Figure 3.9 shows the power-rotor speed curve for a variable speed wind turbine under different pitch angles. This figure illustrates the de-loading technique for a wind turbine. In this case, in order to create a primary frequency reserve, the pitch angle controller begins to increase the angle of the wind turbine blades and shifts the operating point from point A to point B without changing the rotor's speed.

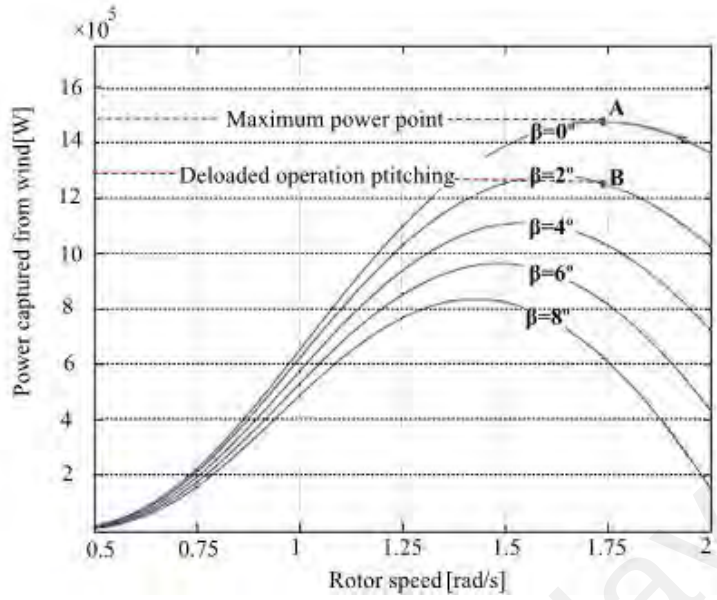

Figure 3.9: Power rotor-speed curves for different values of pitch angle for a 1.5 MW wind turbine (wind speed: 10 m/s) (Díaz-González et al., 2014)

In this study, in order to enable wind turbine to provide active power reserve margin for frequency support, an angle increment $\Delta\beta$ needs to be added to force the wind turbine to operate in the de-loading mode. The value of $\Delta\beta$ determines the de-loading level, namely, the capacity of active power reserve. A 10% de-loading level is set for frequency regulation study, and the modified pitch angle controller is shown in Figure 3.10.

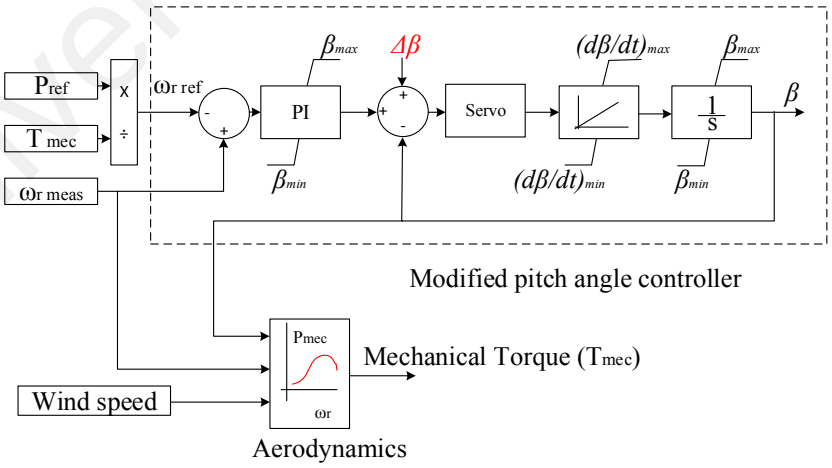

Figure 3.10: Modified pitch angle controller

For a de-loading technique in solar PV system, the PV generator needs to be properly derated to dispatch a reduced power output than its maximum possible value, making its

output controllable. This amount of reduced power is kept for use as a reserve to supply the transients whenever required.

From Figure 3.11, when the PV unit operates at (V_{MPP} +V_{deload}), which is a higher voltage than V_{MPP}, the power output will be P_{MPP} - P_{deload}. In this situation, the PV does not extract the whole available power. According to Figure 3.11, the operating point transfers from point 2 to point 3. Consequently, the reserve power ($\Delta P_{reserve}$) from the difference between P_{ref} and P_{MPP} can be used for frequency regulation when disturbances occur.

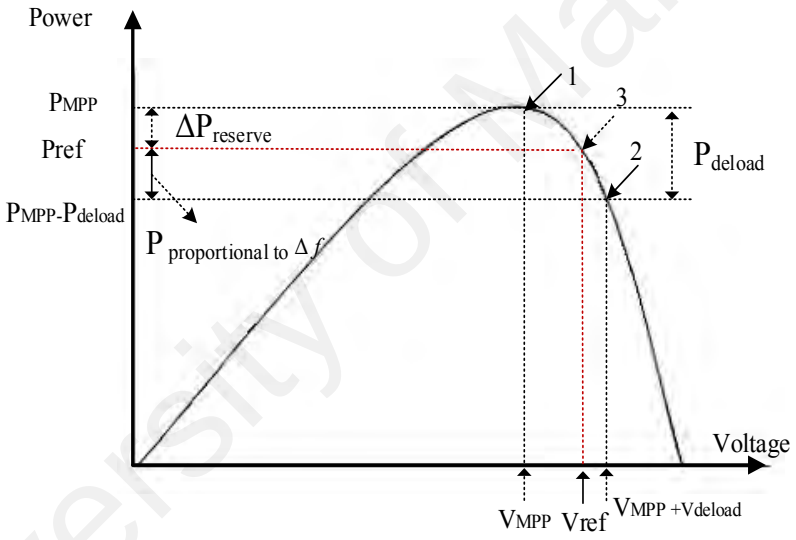

Figure 3.11: De-loading control for solar PV unit

For achieving a de-loading technique in a solar PV system, a modified Active Power Controller (APC) is proposed to enable the solar PV unit to regulate its frequency and operate in the distribution network after islanding mode, as shown in Figure 3.12.

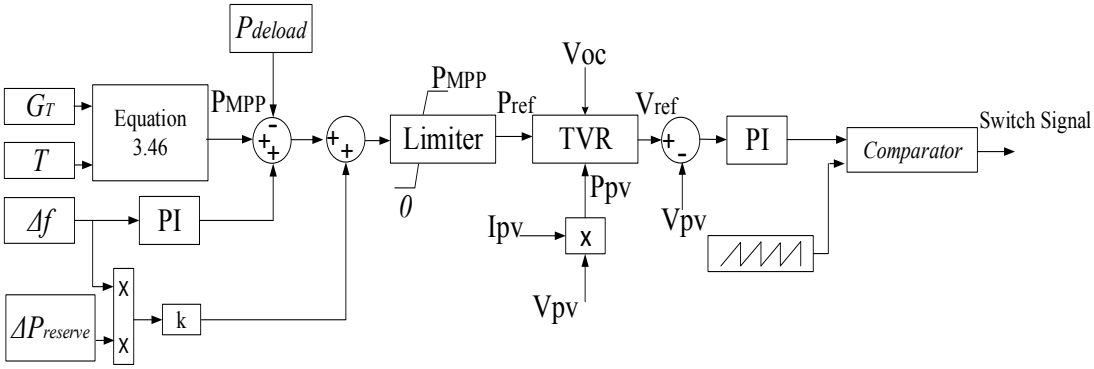

Figure 3.12: Active power controller for de-loaded PV, which considers the amount of available reserve

The active power control scheme for the de-loaded PV contains three main parts. The first, P_{deload} value, is used to decrease the solar PV output. The value of P_{deload} depends on the direction of grid power (P_{grid}). There are two cases that can be used to determine the value of P_{deload}. The first case is when there is a high penetration power from RESs in the distribution network, namely when the distribution network is connected to the grid and powers it via its DGs. In this case, the P_{deload} value equals the P_{grid} value to prevent the over-frequency directly after islanding from forming while offering a reserve power, which can be used in under frequency events during the islanding mode. The second case is when the distribution network is fed from the grid, the P_{deload} value equals 10% from P_{MPP} of PV system unit to offer a reserve power for use after islanding to avoid the under-frequency events, as used in FCWT (Liu & Chen, 2015). The output power reduction of the solar PV can be achieved by subtracting the value of P_{deload} from the maximum power point P_{MPP}. However, when the distribution network has excess power, the RESs has a high-power penetration related to loads in distribution networks, which can lead to over-frequency after islanding. The P_{deload} can also be updated during islanding by adding the imbalance power during islanding mode ($P_{deficit}$) when df_{COI}/dt is positive, due to the sudden decrease in the load amount in distribution system. Figure 3.13 shows the tracking voltage regulation (TVR) algorithm.

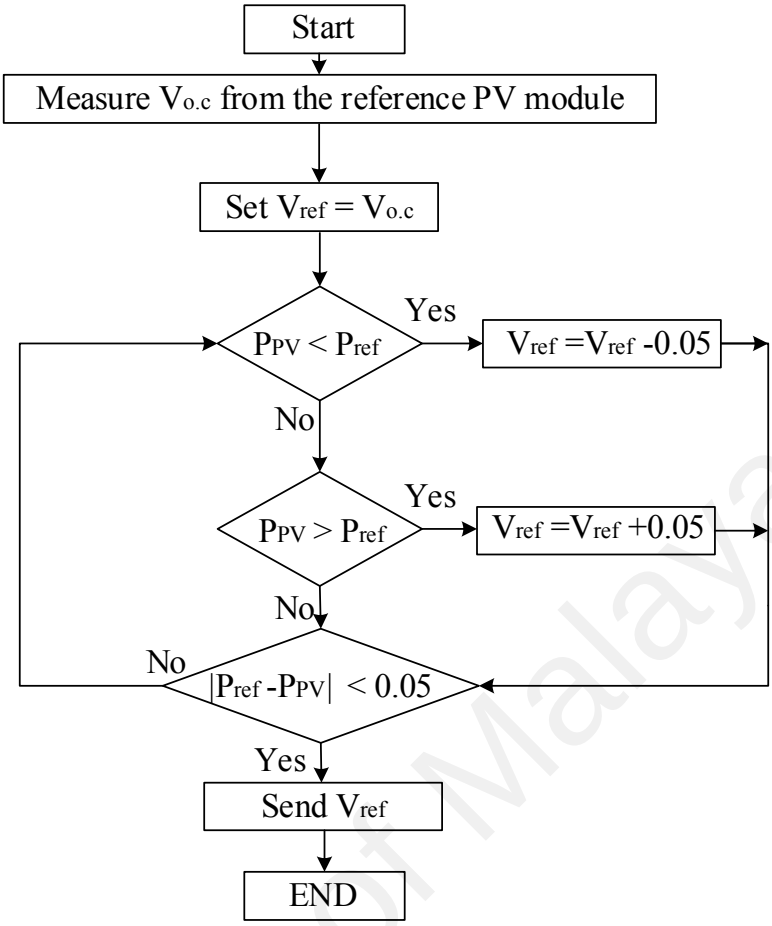

Figure 3.13: Block diagram of tracking voltage regulation algorithm

The P_{deload} for each PV unit can be calculated using Equation 3.44. It should also be pointed out that the solar radiation is assumed to be constant and equal for all solar PV systems units.

$$P_{deload} = P_{grid}/N \tag{3.44}$$

where N is the number of solar PV unit and P_{grid} is the power produced from RESs that flows from the distribution network towards the grid. Figure 3.11 illustrates the operation of de-loading control for PV unit when P_{grid} is the power of RESs flowing from the distribution network towards the grid. After islanding is formed in the distribution networks, the APC shifts the operating point from point 1 to point 2 in order to allow the solar PV to maintain some reserve power and stop the overshooting frequency.

The P_{ref} of the PV unit can be calculated using Equation 3.45. It should be pointed out that the second term of Equation 3.45, which corresponds to the reserve power available in the solar PV unit, influences the output only when the $\Delta P_{reserve}$ is non-zero. Also, when the available reserve power is large, it leads to increased power extraction due to the movement of P_{ref} to a position closer to P_{MPP}. Moreover, when the frequency instability occurs in the islanding distribution network, immediately, the power of the PV system increases from the deloaded point to new point based on Δf and $\Delta P_{reserve}$, as illustrated by Equation 3.45.

$$P_{ref} = \left(P_{MPP} - P_{deload} + P_{proportional\ to\ \Delta f}\right) + (\Delta f \times \Delta P_{reserve} \times K) \qquad (3.45)$$

As shown in Figure 3.11, the maximum power point controller is not used in this study, and the value of the maximum power point P_{MPP} can be calculated using Equation 3.46 (Liao, Xu, Sun, Bao, & Tang, 2017).

$$P_{MPP} = NI_m V_m \frac{G}{G_{ref}}\Big(1 + a\big(T - T_{ref}\big)\Big) \ln\Big(e + b\big(G - G_{ref}\big)\Big)\Big(1 - c\big(T - T_{ref}\big)\Big) \qquad (3.46)$$

where N represents the quantity of the PV panels in the PV power station.

I_m and V_m are parameters given by the PV panel manufacturer at standard test conditions of illumination intensity G = 1000 W/m^2 and temperature T = 25 °C. G_{ref} and T_{ref} are the reference values of illumination intensity and temperature, i.e. 1000 W/m^2 and 25°C, respectively. The compensation coefficients a, b, and c are the constants that can be tested by experimental data (Huang, Mao, Lu, & Wang, 2012).

3.7 Summary

This chapter presented the methodology of planning and operation load shedding schemes. In the former, a new proposed hybrid optimization algorithm consisting of FA and PSO algorithms intends to maximize both the total remaining loads present in the distribution networks and minimum value of Stability Index (SI) in the system. This chapter has also presented two proposed UFLS technique for the operation mode. The UFLS scheme-I used a BFA algorithm with the ANN technique in order to determine the optimal load shed from combinations of random loads. In the hybrid method, the BFA was used in two stages for framing the optimization model and generating the data set to train the network. The appropriate buses for load shedding were selected based on the minimum difference value between the total load combination and total load that should curtailed from the system. This chapter also proposed a method for detecting and estimating the new power changes that could occur during load shedding process.

Furthermore, the de-loading technique has been used in frequency regulation by modifying an active power controller for PV system and pitch angle controller in the wind turbine, which are applicable to the UFLS technique in a distribution network.

CHAPTER 4: PERFORMANCE OF THE PROPOSED UFLS TECHNIQUE IN PLANNING MODE

4.1 Introduction

This chapter discusses the performance of the proposed planning load shedding technique, which aims to simultaneously maximize the remaining load after the shedding process and improve the voltage profile. The effectiveness of the proposed methods is demonstrated using a modified IEEE 33bus test system. The line and bus data of the system are listed in Appendices A-1. In this chapter, the proposed method, referred to as the Firefly Algorithm-Particle Swarm Optimization (FAPSO), is compared with the Particle Swarm Optimization (PSO), Firefly (FA), Evolutionary Programming (EP), and Gravitational Search Algorithm (GSA) in order to measure the accuracy of the final solution and convergence speed for maximizing the remaining load after applying load shedding by improving the lowest Stability Index (SI) in an islanded distribution network. The impact of the proposed methods to the overall voltage profile is also detailed in this chapter.

4.2 Test system for planning load shedding scheme

The test system is a modified IEEE 33 bus radial distribution network with the addition of three DG units. The basic system data is adapted from (Baran & Wu, 1989). The system consists of a three-phase balanced system with 33 buses and 32 branches connected to the main grid. The rating voltage is 12.66 KV at 50 Hz, and its total load capacity is 3.715 MW and 2.29 MVAR of real and reactive power, respectively. The three DGs consist of two constant power generator (mini-hydro power generator) and one variable power generator (Photovoltaic (PV) system(. Table 4.1 provides the location of DGs and the active power rating for each DG at maximum power rating. The location of the DG is selected based on improve of voltage profile of load buses by trial and error. Figure 4.1 depicts the test system.

Table 4.1: Maximum active power Produced by DGs

DG number	Bus number	Type of DG	Maximum output power (MW)	Power factor
1	7	Mini-Hydro	0.85	0.8
2	25	Mini- Hydro	0.5	0.8
3	30	PV	0.837	1

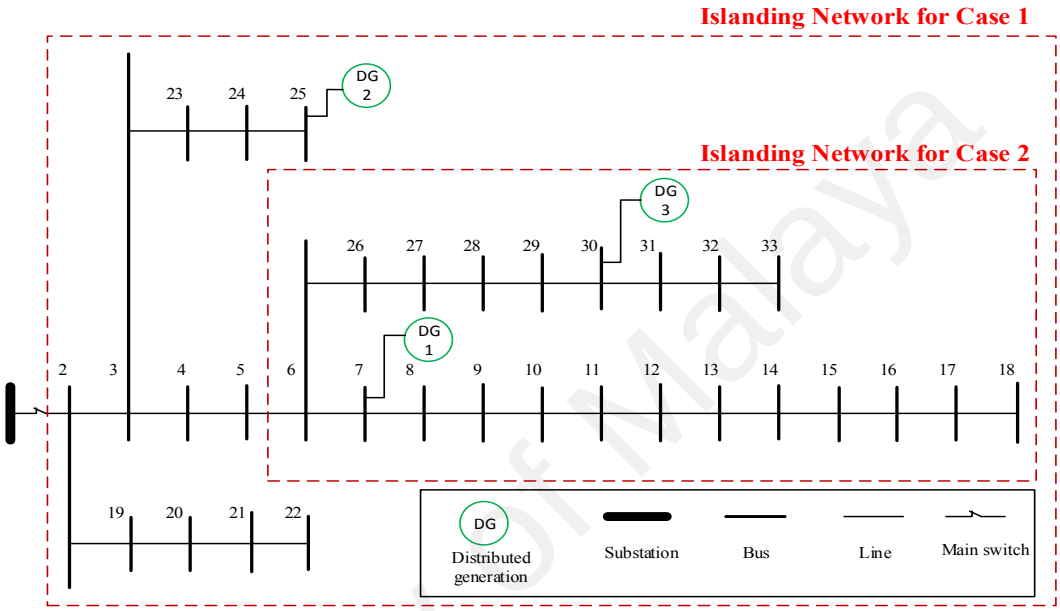

Figure 4.1: Test system for planning UFLS scheme

Figure 4.2 and Figure 4.3 show the hourly PV power generated in kW and hourly load profile levels in pu.

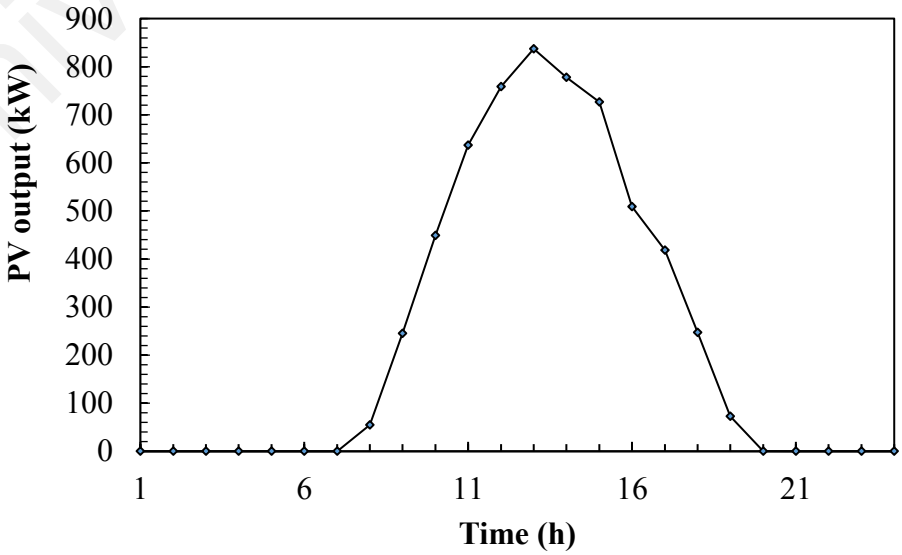

Figure 4.2: Hourly PV power production by DG3

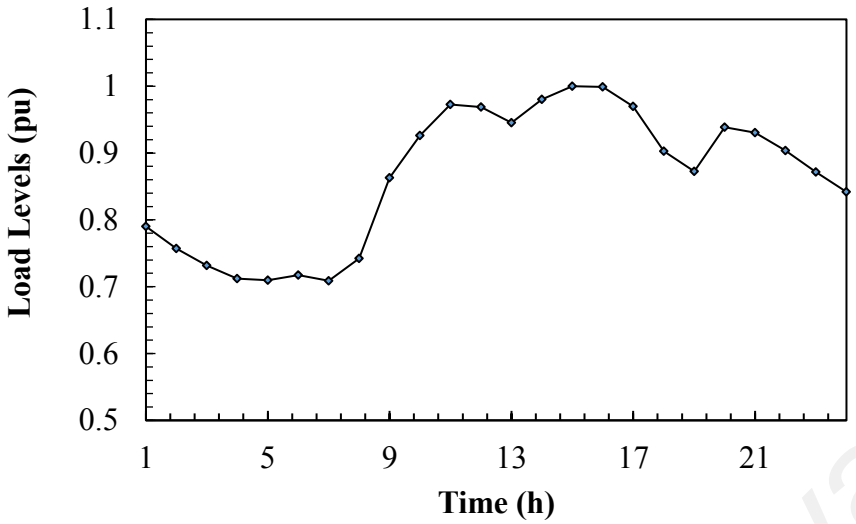

Figure 4.3: Hourly load profile for individual loads

The load priority percentage is shown in Table 4.2 by listing the percentages of the minimum power that should be connected to the distribution network at each bus.

Table 4.2: The minimum percentage of load priority limit for each bus (Khamis, Shareef, & Mohamed, 2015)

Bus No.	Percentage (%)	Bus No.	Percentage (%)
2	33	19	61
3	24	20	54
4	62	21	21
5	17	22	49
6	44	23	5
7	36	24	17
8	22	25	11
9	7	26	60
10	20	27	21
11	0	28	25
12	53	29	16
13	10	30	54
14	48	31	23
15	59	32	32
16	62	33	4
17	38	-	-
18	33	-	-

4.3 Results and Discussions

In order to analyze the performance of the proposed method (FAPSO) against the PSO, FA, EP, and GSA, the algorithms were implemented for load shedding. Table 4.3 shows the basic parameters for each algorithm.

Table 4.3: PSO, FA, FAPSO, EP and GSA Parameters Setting

Parameter	PSO	FA	FAPSO	EP	GSA
Population size (N)	50	50	50	50	50
Maximum iteration (n)	300	300	300	300	300
Parameters values that used for algorithm	w_{max}=0.9 w_{min}=0.4 c_1=2 c_2 =2	β_0 = 0.2 γ=1 α=0.8	β_0 = 0.2 γ=1 α= 0.8 c_1=2	-	G_0=100 α= 10

There is no absolute way to determine the values of population size and maximum iteration. The current values were determined via the trial-and-error approach. Meanwhile, the parametric values used for the algorithms in the load shedding process was selected based on (Badran, Mokhlis, Mekhilef, & Dahalan, 2017; Lu et al., 2018; Shi & Eberhart, 1999).

Two scenarios were considered to demonstrate the performance of the FAPSO optimization. In the first case, the proposed load-shedding scheme was tested by considering the location and load priority limit. The limit, in this case, refers to the minimum percentage of load amount that should remain at a particular bus after the load shedding process. The values are shown in Table 4.2.

In the second case, the proposed load-shedding scheme was tested by only considering its location, where the whole load connected to a particular bus was completely removed.

4.3.1 Optimal Load Shedding by FAPSO with Consideration of Priority Limit

The proposed load-shedding scheme based on FAPSO was applied on the test system with the intention of maximizing the remaining load and improving the voltages' stability index. The fitness value was evaluated using the Equations 3.2. The weightage set was varied from 0 to 1, with a step size of 0.1. Based on the highest η_{LAV} value tabulated in Table 4.4, the weightage set of $w_1 = 0.8$ and $w_2 = 0.2$ was selected as the best combination.

Table 4.4: Weightage set and corresponding performance index based on LAV by applying proposed load shedding with consideration priority limit at time 15:00 related to Figure 4.3

No.	w_1	w_2	Remaining load (MW)	Minimum value of SI	η_{LAV}
1	1	0	1.974802	0.951475	34.86
2	0.9	0.1	2.03936	0.950209	78.63
3	**0.8**	**0.2**	2.07637	0.956846	**4178.4**
4	0.7	0.3	2.034878	0.952472	79.10
5	0.6	0.4	1.890752	0.941886	17.49
6	0.5	0.5	2.068509	0.944912	119.49
7	0.4	0.6	2.031323	0.940203	49.77
8	0.3	0.7	2.03376	0.95338	80.36
9	0.2	0.8	1.987242	0.95048	38.57
10	0.1	0.9	1.784058	0.957304	12.22
11	0	1	1.114939	0.957304	2.32

In this case, the islanded system was formed when the main switch was opened. This scenario is represented as case number one in Figure 4.1. Figure 4.4 shows the hourly power of the total load demand, total power generation from DGs, and grid for 24 hours during the grid connection mode. The figure confirms that the power imbalance between the load demand and power supply from DGs is rather large, ~48–61% from the power generation curve to the maximum daily load curve. When islanding was formed, load shedding was required to balance the generation and load demand to cater for the huge imbalance of power.

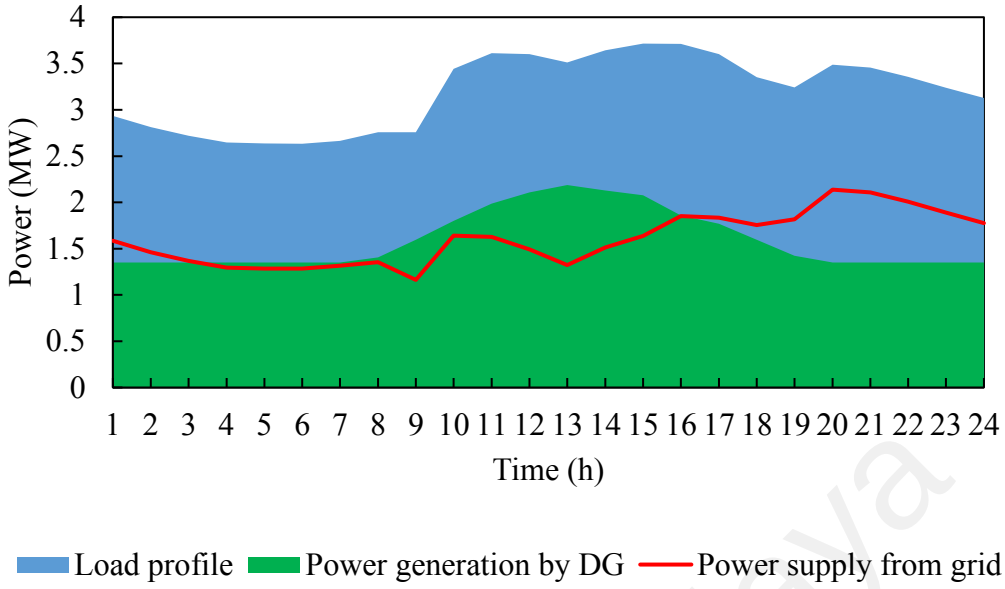

Figure 4.4: Daily load curve and power supply by grid and DGs

Since islanding could occur at any time, the proposed FAPSO for load shedding was tested every hour to determine its overall performance towards determining the optimal load shedding. Figure 4.5 illustrates the amount of load and power from DGs due to load shedding if it occurs at any hour (within 24 hours) for case 1.

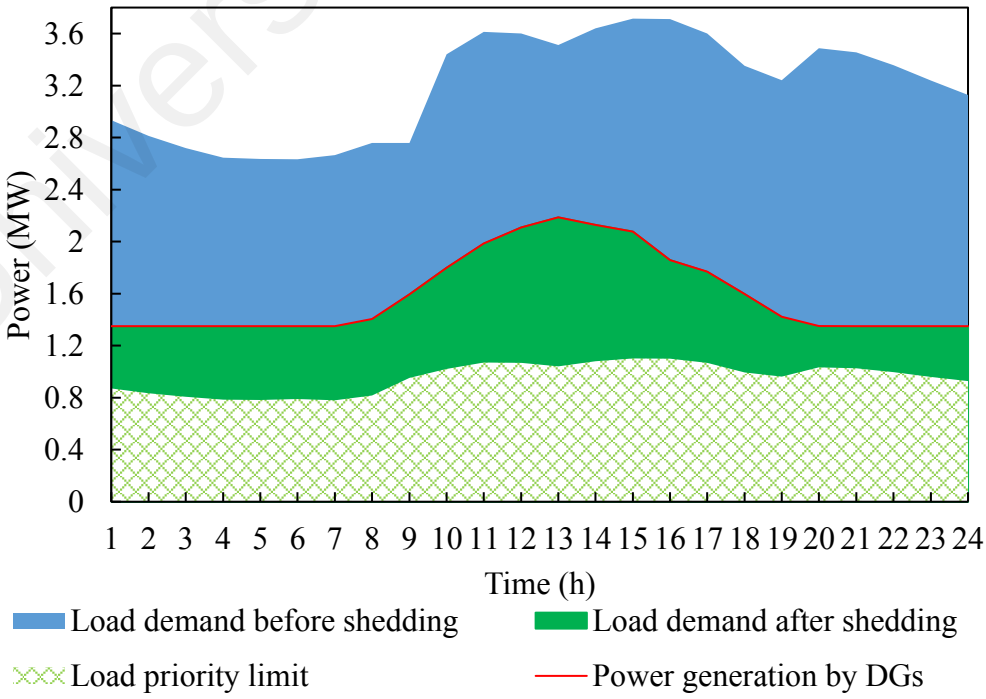

Figure 4.5: Load demand before/after applying the proposed load-shedding technique by hybrid FAPSO in case 1

It can be seen that the amount of the remaining load after the load shedding process is nearly identical to the amount of power being supplied. This shows that that the proposed load-shedding technique based on the FAPSO optimization can identify the minimum amount of load to be curtailed without removing extra loads from the network. It can also be seen that the proposed load-shedding technique based on FAPSO optimization was within the load priority limit requirement.

The load shedding result at 15:00 is taken as an example to discuss the performance of the proposed load shedding. At this time, the maximum load demand is 3.715 MW, as shown in Figure 4.4. However, the total power produce from DGs at this hour was only 2.0764 MW, and the power deficit was ~44%. Thus, 44% of the load must be shed from the distribution network to prevent the system from collapsing. After applying the proposed load shedding scheme, 1.6387 MW was removed, thus, the total remaining load was only 2.0763 MW, which closely matches the DGs' power output.

The convergence characteristic for the proposed load shedding technique using the FAPSO optimization is shown in Figure 4.6 at 15:00. It can be seen that the FAPSO converges and finds the solution after 157 iterations. Comparing the FAPSO results between the original load demands (black bar), remaining load after shedding (green bar), and load priority limit (red bar) for each bus are shown in Figure 4.7. From this comparison, it can be seen that load shedding fulfills the minimum load priority set in Table 4.2. There are also cases where the load at particular buses were not selected for shedding, examples being at buses 4, 24, 29 and 30.

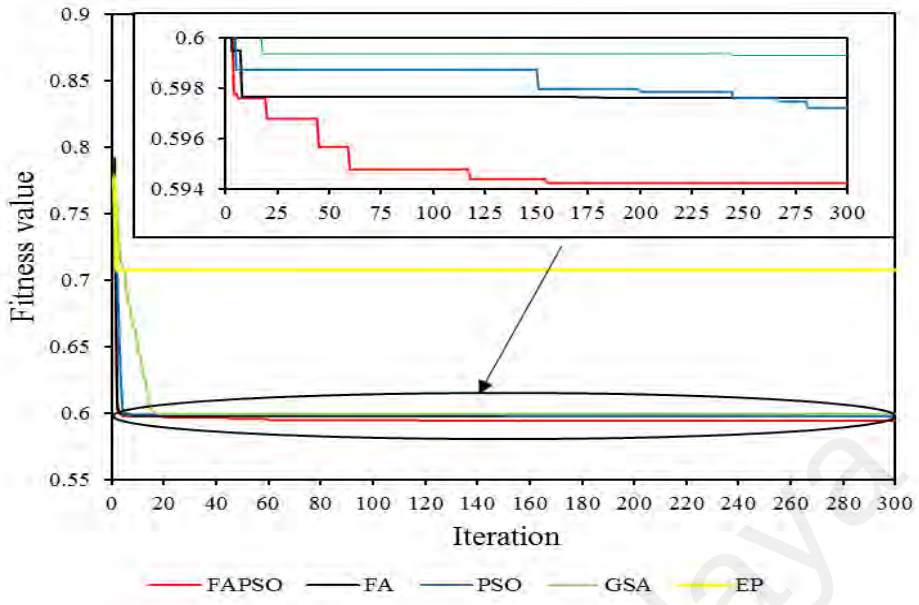

Figure 4.6: Convergence characteristic for FAPSO, FA PSO, GSA and EP optimizations for case 1 at time 15:00

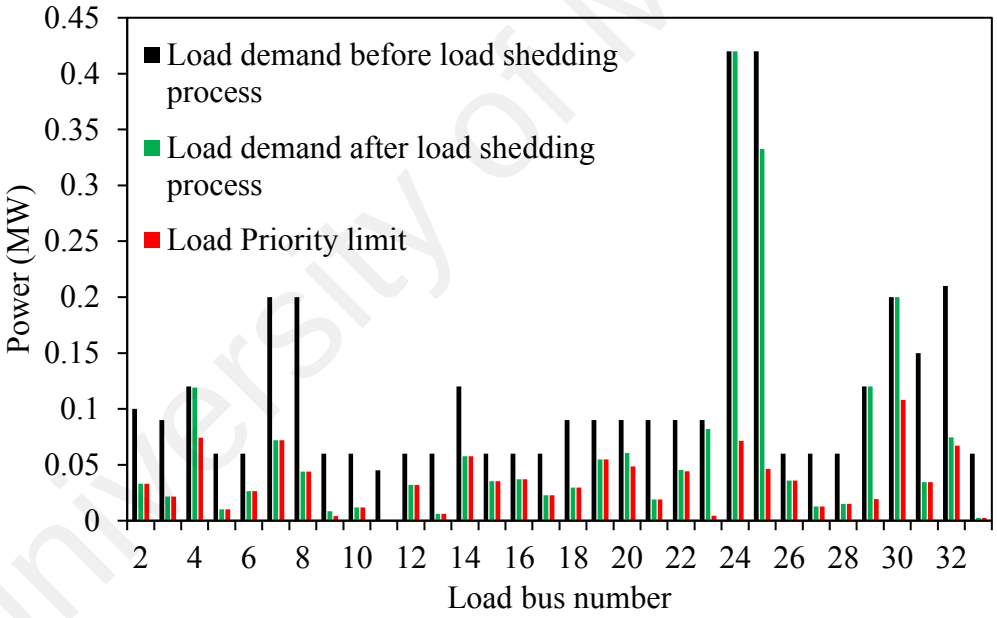

Figure 4.7: Loads demand at each bus after performing the proposed load-shedding technique at time 15:00 hour for island case 1 with their load priority limits

The load-shedding technique was also performed and tested using FA, PSO, EP, and GSA algorithms.

For this study, the same time i.e., 15:00 was selected. The voltage profile of the system before and when islanding occurs at 15:00 is shown in Figure 4.8. It can be clearly seen that islanding caused the overall voltage profile to decrease. However, when load

shedding was applied using FAPSO, FA, PSO, EP and GSA optimizations at 15:00, it can be seen that the voltage profiles after load shedding were all within the allowable limit, as per Figure 4.9. It can also be noted that minimum values of voltage profiles obtained using FA, PSO, EP and GSA optimizations are higher than the minimum value obtained using FAPSO. This took place due to the amount of loads that remaining in the distribution system using FAPSO optimization is larger than the others optimization techniques and the different amounts of load shed at particular buses. However, differences are regarded to be small. It should be noted, the minimum SI value before and after islanding form without applying load shedding are 0.89 and 0.5, respectively.

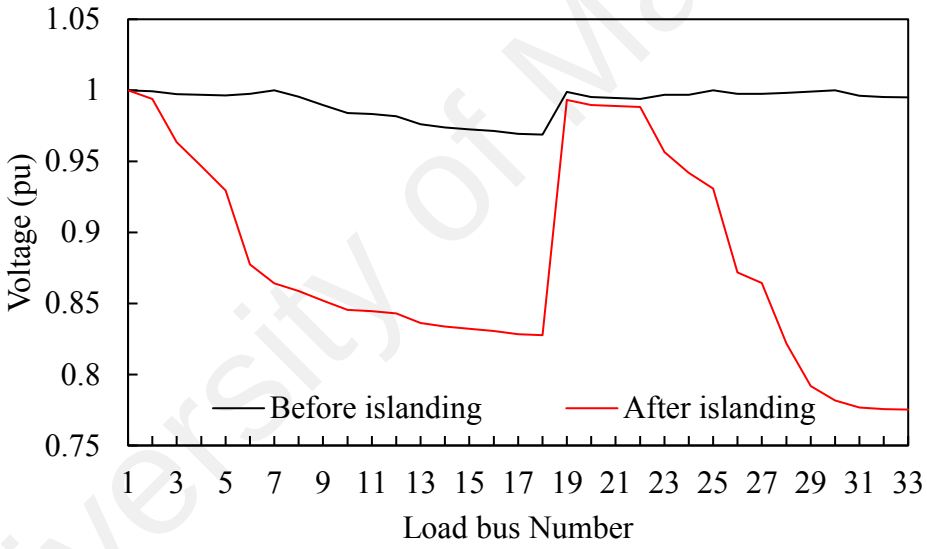

Figure 4.8: Voltage profile before and after islanding at time 15:00 without load shedding for case 1

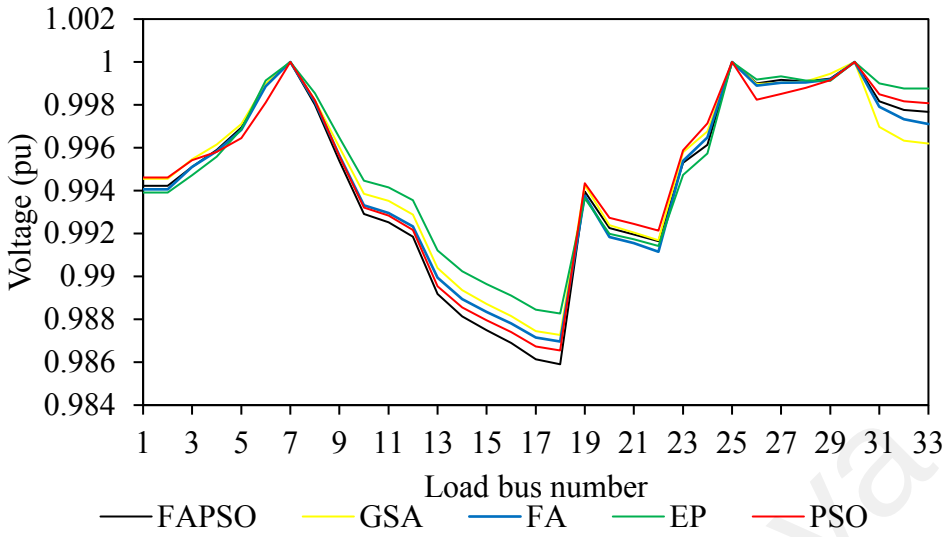

Figure 4.9: Voltage profile after applying techniques FAPSO, FA, PSO, EP and GSA optimizations at time 15:00 for case 1

After applying the load shedding technique based on both of FA, PSO, EP, and GSA optimizations, the total remaining load suggested by FA, PSO, EP, and GSA optimizations were 2.0643 MW 2.0649 MW, 1.61 MW, and 2.0594 MW, respectively. These values are less than the amount determined by the FAPSO technique (2.0763 MW), which proves that the FAPSO is better than FA, PSO, EP, and GSA algorithms in determining the optimal amount of remaining load, taking into account that the main objective of this study is to maximize the amount of load remaining without removing important loads from the system. The overall result of load shedding for all of the optimization methods is shown in Figure 4.10 for all of the buses. It can be seen that the FA, PSO, EP, and GSA shed more loads than FAPSO in the islanded system, where the percentage of total shed loads related to maximum acceptable shed value in the system were 63.16%, 63.14%, 80.55%, 63.35%, and 62.70%, respectively.

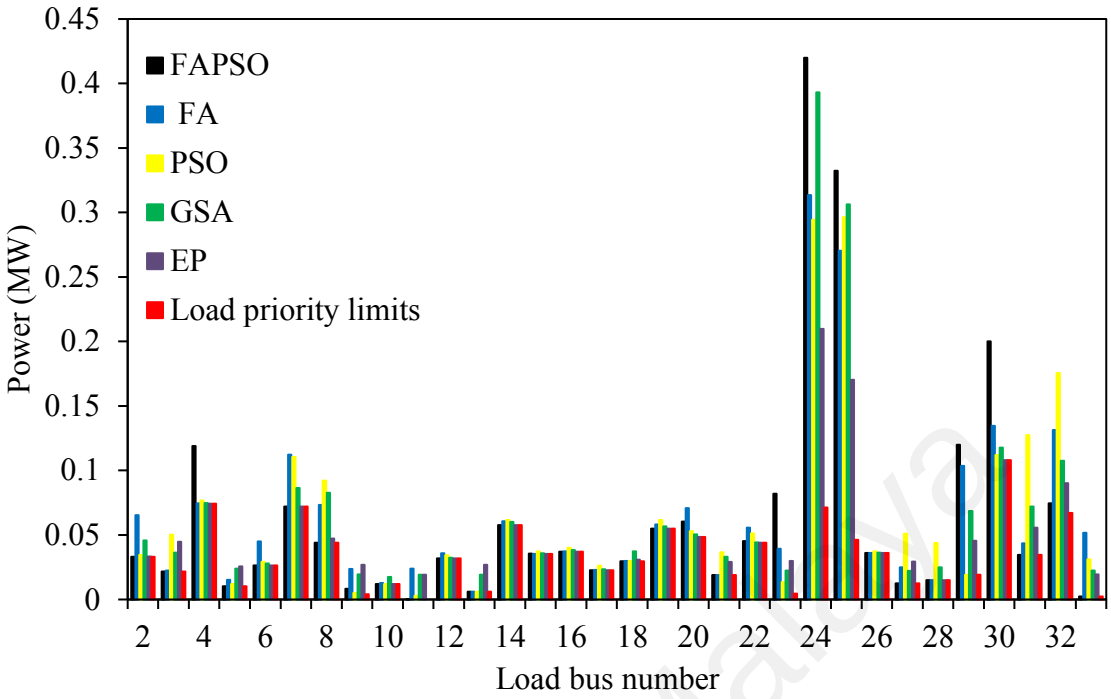

Figure 4.10: Load buses demand after implementing the load shedding process based on FAPSO, FA, PSO, EP and GSA optimizations at time 15:00 for island case1

4.3.2 Optimal Load Shedding by FAPSO without Consideration Priority Limit

In this case, the amount of load remaining is either zero or the complete load demand for each bus. To solve the IEEE 33 bus system using FAPSO, the length of the firefly was set to 33, consisting of all buses and encoding, as shown in Figure 4.11, based on the best remaining load combination that fulfils the minimum fitness value of the multi-objective function. This means that the proposed load shedding based on FAPSO have two choices for each bus; either remove all loads on the bus or leave the loads without shedding. This encode was used instead of a load priority limit.

Bus2	Bus3	Bus4	Bus5	Bus6	.....	Bus33
1	0	1	1	0		1

Figure 4.11: An example of one of the firefly content that is used in load shedding scheme with regardless priority limit

This case represents case number two in Figure 4.1. In this case, DG_2 was disconnected from the system concurrently when islanding was formed. A proposed load shedding

scheme was applied on a test system to evaluate the effectiveness of the hybrid FAPSO. The weightage set was varied within 0 - 0.1 with a step size of 0.1. Based on the highest η_{LAV} value observed in Table 4.5, the weightage set of $w_1 = 0.8$ and $w_2 = 0.2$ was selected as the best combination.

Table 4.5: Weightage set and corresponding performance index based on LAV by applying proposed load shedding without consideration priority limit at time 9:00

No.	w_1	w_2	Remaining load (MW)	Minimum value of SI	η_{LAV}
1	1	0	1.0876	0.95087	38.96
2	0.9	0.1	1.0876	0.99156	244.2
3	**0.8**	**0.2**	1.0876	0.99156	**244.22**
4	0.7	0.3	1.08	0.98675	99.3
5	0.6	0.4	1.083	0.98791	123.75
6	0.5	0.5	1.0789	0.98675	94.48
7	0.4	0.6	1.081	0.99134	137.75
8	0.3	0.7	1.08	0.99155	131.26
9	0.2	0.8	1.07	0.99067	78.29
10	0.1	0.9	1.0776	0.99156	114.48
11	0	1	0.44884	0.99968	1.427

Figure 4.12 shows the hourly power imbalance between the total load demand in the system and total power supply available by the DGs. Figure 4.12 demonstrates that the power imbalance between the load demand and power supply is huge, that is, 11.2% – 52% from power generation curve to maximum daily load curve.

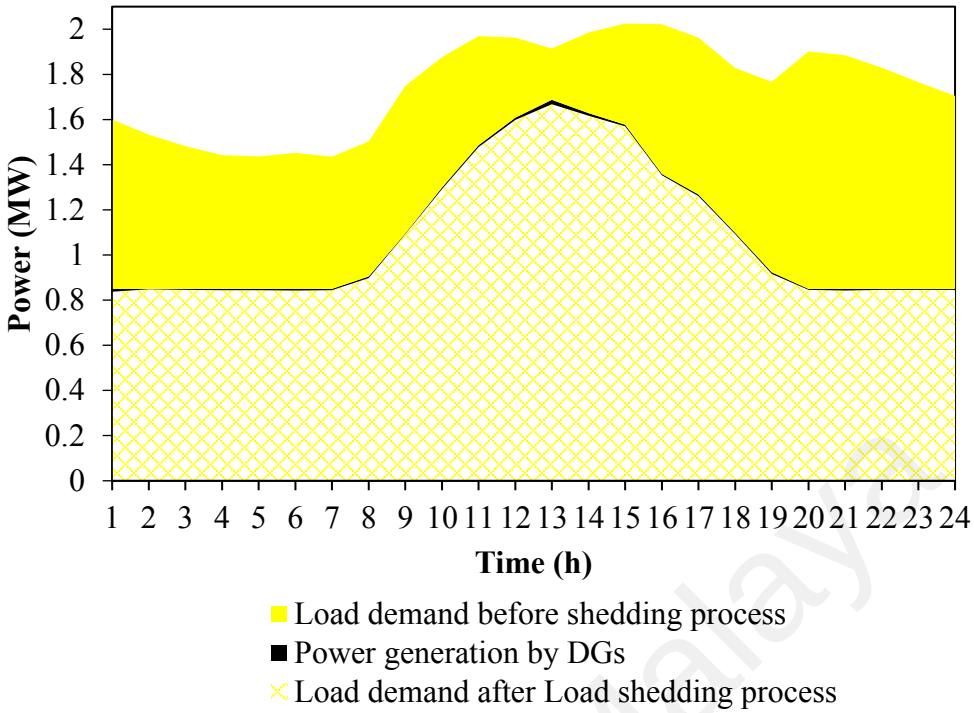

Figure 4.12: Load demand before/after applying the proposed load-shedding technique by Hybrid FA-PSO in case 2

Since islanding could occur at any time, the proposed FAPSO for load shedding is tested at each hour to analyze its overall performance towards determining the optimal load shedding. Figure 4.12 illustrates the amount of load and power from DGs as a result of load shedding if it occurs at any hour (within 24 hours). It can be seen that the amount of remaining load after the load shedding process nearly matches the amount of power supplied. This confirms that the proposed load-shedding technique based on the FAPSO optimization has the ability to identify the minimum amount of load that needs to be curtailed without removing any extra load from the network. To discuss the performance of the proposed load shedding, load shedding result at 09:00 can be used as an example. At this time, the load demand is 1.75 MW, as shown in Figure 4.12. However, the total power production at this hour was only 1.095 MW, and its power deficit is ~37.42%. Thus, 37.42% of the load must be shed from the distribution network to prevent the system from collapsing. After applying the proposed load shedding scheme, 0.659 MW

was removed. Thus, the total remaining load was only 1.091MW, which closely matches that of the DG's power output.

Similarly, the load-shedding technique was performed using FA, PSO, GSA, and EP algorithms. For this study, the same time, i.e., at 09:00, was used. The voltage profile of the system before load shedding at 09:00 is shown in Figure 4.13. It can be seen that when islanding occurs, the voltage magnitude at all buses dropped. However, with load shedding based on FAPSO, FA, PSO, GSA, and EP, it can be seen that the voltage profiles after load shedding are all within the allowable limit, as shown in Figure 4.14. It can also be noticed that some voltage profiles obtained using FA, GSA, and EP exceeded those obtained using FAPSO. This difference is due to the amount of load shed at particular buses. However, the differences are considered to be small. After applying the load-shedding technique based on each of FA, PSO, GSA, and EP, the total remaining load suggested by the FA, GSA, EP were 1.0703 MW, and 1.0832 MW, 1.04009 MW, respectively. These values were less than the amount determined by the FAPSO and PSO techniques (1.0876 MW), which proves that the FAPSO and PSO are better than FA, GSA and EP algorithms in finding the optimal amount of the remaining load, considering that the main objective of this study is to maximize the amount of load remaining in the system without the removal of important loads. However, it can be noted in Figure 4.14 that the voltage profile of FAPSO is better than PSO due to the SI of FAPSO being improved to levels better than the PSO.

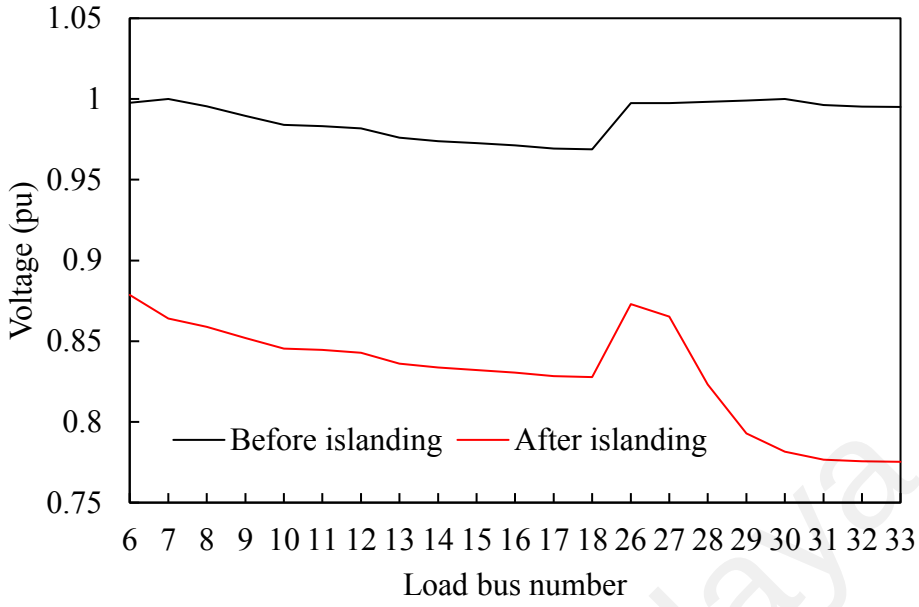

Figure 4.13: Voltage profile before and after islanding at time 9:00 for case 2

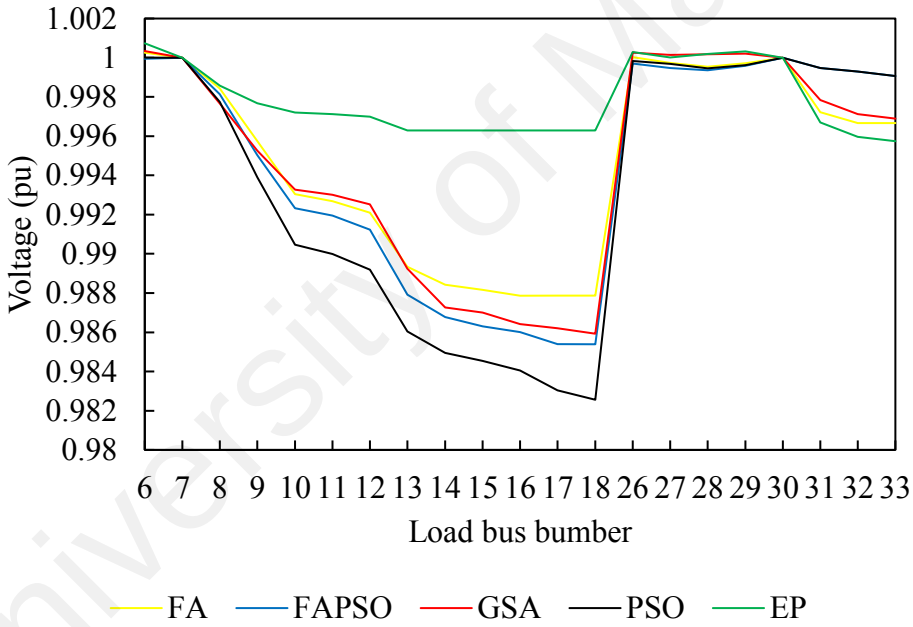

Figure 4.14: Voltage profile after applying load shedding techniques using FAPSO, FA, PSO, EP and GSA optimizations at time 9:00 for case 2

The convergence characteristic for the proposed optimal load shedding scheme using the FAPSO technique is shown in Figure 4.15 for this hour. It shows that the FAPSO converges and finds the solution after 20 iterations. Table 4.6 shows the buses that remain without shedding load buses.

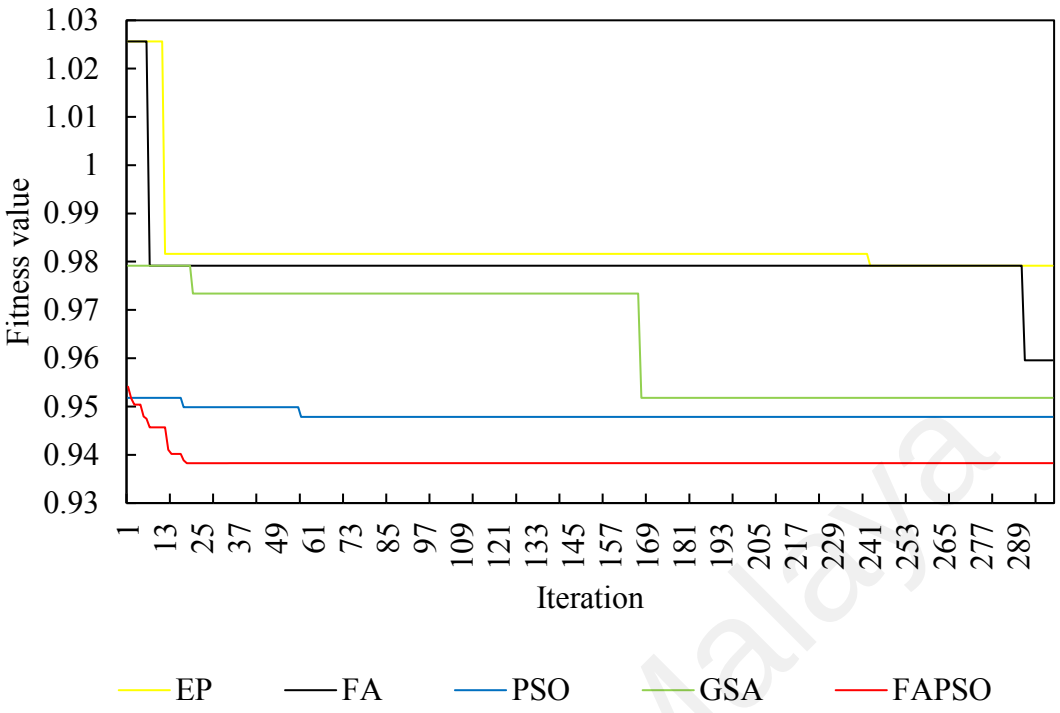

Figure 4.15: Convergence characteristic for FAPSO, FA, PSO, GSA and EP optimization for case 2 at time 9:00

Table 4.6: Buses number that is remaining without shedding for FAPSO, FA, PSO, GSA and EP optimization

Parameter	PSO	FA	FAPSO	GSA	EP
The No. of Buses that remaining without removing loads after load shedding process.	2,3,4 5,9,10 12,19,28 30,31,32,3 3	6,7,9,10,1 3,14,15,17 ,26,27,28, 29,30,33	6,7,8,26,27 ,29,30,31,3 2	6,7,9,10,11,1 2,13,14,18,2 6,28,29,30,3 3	6,7,10,11, 13,14,16,2 7,28,29,31 ,32

The proposed load shedding scheme based on FAPSO algorithm was compared with other load shedding scheme based on FA, PSO, GSA, and EP algorithms in the context of the maximized amount of the remaining load after the load shedding process and improving the minimum value of SI to prevent the system from collapsing using Matlab.

The work has been tested in two cases; the first takes into consideration the load priority limit with load shedding selection, as explored in Section 4.3.1, while Section 4.3.2 shows the second case, which regards the load priority limits as negligible in the

load shedding process. From the results, it was concluded that the proposed FAPSO algorithm outperformed FA, PSO, GSA, and EP algorithms in the context of the maximum remaining loads in the distribution network, voltage profile improvement, and speed convergence. Table 4.7 tabulates the summary of the comparison between the proposed load shedding based on the FAPSO optimization with each FA, PSO, GSA, and EP optimization for two cases. It can be seen from Table 4.7 that the load curtailment value done on the FAPSO optimization is the lowest, which keeps the voltage profile within the allowed limits.

Table 4.7: Summary for comparison in performance of FAPSO, FA, PSO, GSA and EP in load shedding technique

Case 1	**Applying optimal load shedding with consideration priority limit at time 15:00.**		
Algorithms	**Fitness**	**Minimum voltage of load bus**	**Load curtailment %**
PSO	0.59719	0.98654	44.43
FA	0.59759	0.98696	44.46
FAPSO	0.59424	0.98590	**44.11**
GSA	0.59929	0.987271	44.56
EP	0.70726	0.988271	56.66
Case 2	**Applying optimal load shedding without consideration priority limit at time 9:00.**		
Algorithms	**Fitness**	**Minimum voltage of load bus**	**Load curtailment %**
PSO	0.93858	0.98255	**38.594**
FA	0.95987	0.98786	39.659
FAPSO	0.94422	0.98539	**38.594**
GSA	0.9518	0.98592	38.929
EP	0.97917	0.99574	41.362

The simulation was conducted 100 times and the average fitness value, best solution, and standard deviation of each of FA, PSO, GSA, EP, and the proposed algorithm are listed in Table 4.8. It can be seen that the FAPSO outperforms the others in terms of average fitness, which makes it the best solution and standard deviation values in both cases, confirming that it is the best searching performance that is highly accurate.

Table 4.8 also reveals the average running time (in seconds) of each of FA, PSO, GSA, EP, and the proposed algorithm on load shedding scheme in 100 runs. It can be seen that the GSA is the faster algorithm to complete 300 iterations and find the final solution. However, it is interesting to note from Figures 4.6 and 4.15 that the proposed algorithm converges very fast relative to FA, PSO, GSA, and EP algorithms for load shedding scheme in both cases. This means that the proposed algorithm can reach the best solution quicker compared to the other algorithms. This confirms the efficiency of the FAPSO in reaching the sub-optimal value.

Table 4.8: Comparison of mean fitness value, best solution, standard deviation and average computational time for 100 runs on load shedding scheme

Case 1						
Population size / Max iteration	**Indices**	**Algorithms**				
		EP	**GSA**	**FA**	**PSO**	**FAPSO**
50/300	Average fitness	0.77924	0.59988	0.59939	0.59904	**0.59468**
	Best solution	0.70726	0.59929	0.59760	0.59719	**0.59419**
	Standard deviation	0.031476	0.00039588	0.00050378	0.0008866	**0.00032375**
	Average computational time (seconds)	661.21	330.01	760.58	655.7	708.11
Case 2						
Population size / Max iteration	**Indices**	**Algorithms**				
		EP	**GSA**	**FA**	**PSO**	**FAPSO**
50/300	Average fitness	0.98983	0.95319	0.96021	0.94712	**0.93988**
	Best solution	0.97917	0.9518	0.95987	0.94538	**0.93827**
	Standard deviation	0.05978	0.001801	0.0018817	0.003254	**0.00166**
	Average computational time (seconds)	650	335	758.89	621.8	654.78

4.4 Summary

This chapter used a metaheuristic algorithm in the planning load shedding scheme in order to maximize both the minimum Stability Index (SI) and the total remaining loads present in the system. The proposed hybrid optimization algorithm, consisting of FA and PSO algorithms, was applied on the modified IEEE 33 bus distribution networks. The effectiveness of the proposed method was tested with/without considering the load priority limit. The proposed method can retain the system stability and prevent the system from a complete blackout in two tested cases. The results of the proposed hybrid method were also compared with the FA, PSO, EP, and GSA optimization techniques. The comparison shows that the proposed method achieved the best maximum remaining load and simultaneously improved the voltage profile of the islanded system.

CHAPTER 5: PERFORMANCE OF THE PROPOSED UFLS SCHEME-I IN OPERATION MODE

5.1 Introduction

This chapter details the modelling of the distribution network used to validate the proposed UFLS scheme-I. The performance of the proposed UFLS scheme-I is validated on part of the Malaysian distribution network. It also deals with the validation of the proposed UFLS scheme-I using various case studies, such as islanding, DG tripping, and load increments. Furthermore, the proposed UFLS scheme-I is compared with the conventional and adaptive UFLS techniques in order to confirm its ability in shedding the optimal amount of power from the distribution network. This chapter presents a coordination of de-loading technique for RESs (wind turbine, PV system) and optimal under frequency load shedding (UFLS) scheme to solve the instability frequency in islanded distribution networks.

5.2 Test system modeling for proposed UFLS scheme-I

To validate the APC for RESs (wind turbine, PV system) and the operation of the proposed UFLS-scheme-I, one of the Malaysian distribution network was selected, as shown in Figure 5.1. This distribution network includes two mini-hydro units, three PV units, and one wind turbine unit. Each mini-hydro depends on synchronous generators; rated for each unit at a capacity of 2 MVA, with a maximum active power dispatch of 1.80 MW. In addition, each solar PV unit is rated 0.55 MWP, and the wind turbine is rated 1.453 MW. The load demand in the distribution network is fed by power generated from two mini-hydro units and three solar PV generation units, one wind turbine unit, and the rest of the power is generated by the main grid. Two feeders were used to connect the distribution network to the transmission grid, each one connected to a 30 MVA step down transformer (132 kV/11 kV). In order to increase the voltage from 3.3 KV to 11 KV, two transformer units of 2 MVA step up were connected to the mini-hydro units. To model

the mini-hydro DG components, the standard models for exciter, governor, and turbine in PSCAD/EMTDC library were used. In the mini-hydro model, the IEEE type AC1A excitation standard model was used for the excitation system and PID governor, while the pilot and servo dynamics were used for the hydraulic governor. The hydraulic turbine without a surge tank model and a non-elastic water column was selected for the turbine mini-hydro units. To determine the impact of integrating grid connected RES-based on power electronics on the frequency stability of distribution network after islanding, three solar PV units rated 0.55 MWP and a wind turbine rated 1.453 MW were used. The average RESs (solar PV system and wind turbine) capacity penetration level (RCPL) was ~64%, which can be expressed by Equation (5.1) (Liu, 2014):

$$RCPL = \frac{\text{total installed RES capacity (MW)}}{\text{total load capacity (MW)}} \times 100\% \tag{5.1}$$

The dynamic PV unit was modelled using PSCAD/EMTDC model for three solar PV units integrated in the distribution network. The wind turbine converts the kinetic energy in the wind into mechanical energy. The wind farm was modelled using standard models of exciter, wind governor, and wind turbine provided in the PSCAD/EMTDC library. The wind turbine can be operated at 1.453 MW, which represents its maximum generated power. The entire line was modelled according to a nominal π form, where the length of each line does not exceed 6 km. The following sections presents the details pertaining to each part of the test system's model.

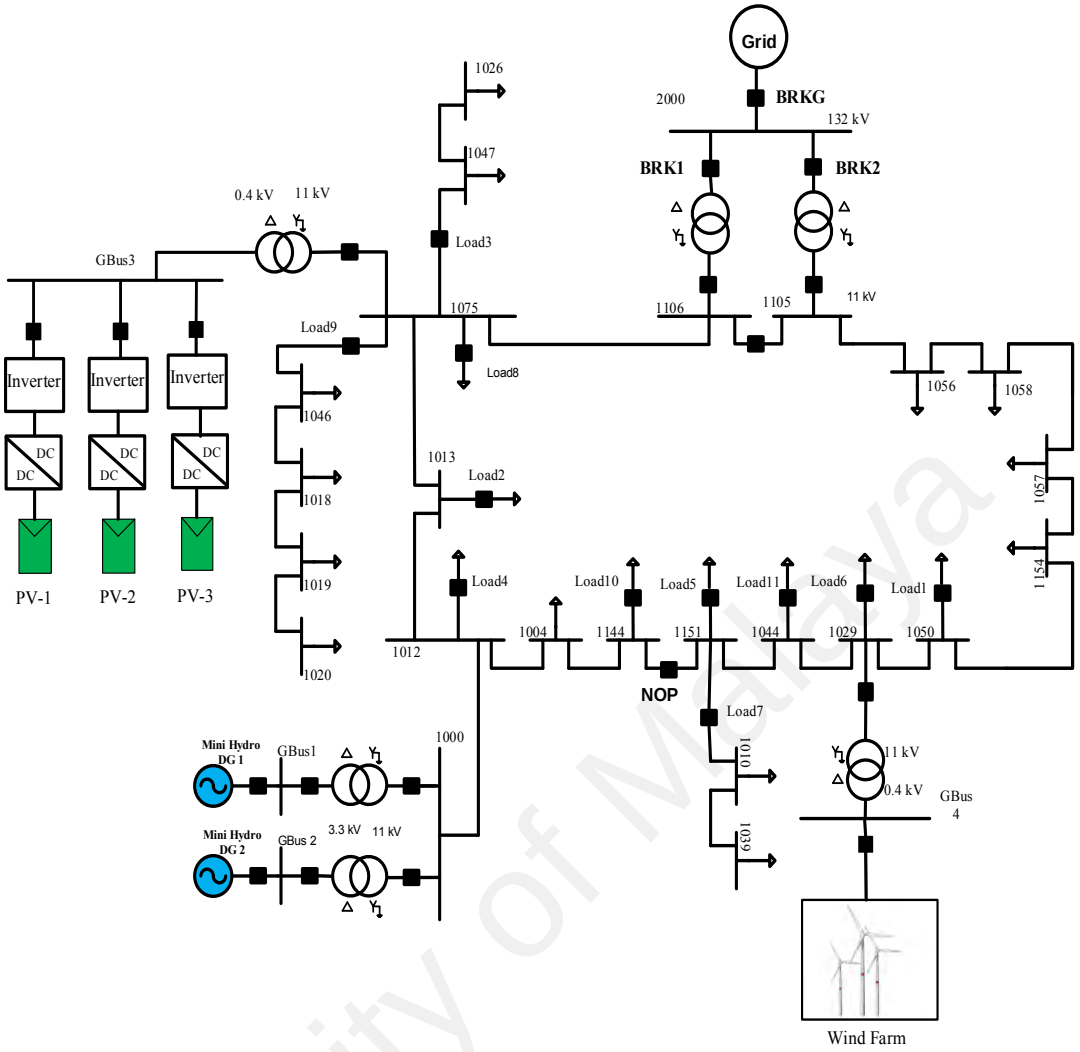

Figure 5.1: Test system for UFLS scheme-I

5.2.1 Modelling of Mini-Hydro DG

A simplified block diagram of a hydropower plant with essential features is shown in Figure 5.2.

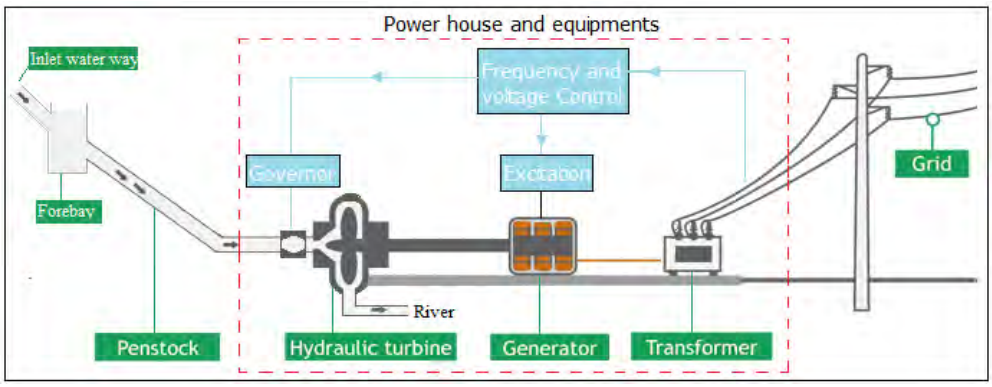

Figure 5.2: Layout of Run of River Hydropower Plant (Sharma & Singh, 2013)

The main elements of a hydropower plant include:

(a) Inlet water ways: Inlet water ways are the passages through which water is conveyed from the dam to the power house. It includes a canal, penstock (closed pipe), or tunnel, flume, fore way, and a surge tank (Paish, 2002).

(b) Forebay: Forebay is the tank at the head of penstock pipe that supplies water regularly at a constant head. The forebay serves as a miniature reservoir for the turbines. Its primary functions are to serve as a settling area for water-borne desires to provide storage for periods of low flow/increased power demand.

(c) Penstock: Water may be conveyed to turbines via open conduits/closed pressure pipes called penstocks made of reinforced concrete/steel. It is expected that the penstock should be sloping towards the power house, and its grade adjusted according to the topography. The thickness of the penstock increases as the working pressure or the head of the water increases.

(d) Power House and equipment: The power house is a building where the turbines, alternators, and the auxiliary plant are housed. Here, the conversion of the energy of water to electrical energy takes place. The following are some of the main equipment's provided in a power house:

1) Prime movers (turbines) coupled with governor
2) Generator
3) Generator Excitation
4) Transformers
5) Switch board equipment and instruments

5.2.1.1 Hydraulic Turbine

This research considers a non-linear hydraulic turbine without a surge tank and with a non-elastic water column. The nonlinear turbine models are required when speed and power changes are large during an islanding, load rejection, and system restoration conditions. The non-linearity of the model comes from the valve characteristic of the turbine. The block diagram of a hydraulic turbine is shown in Figure 5.3.

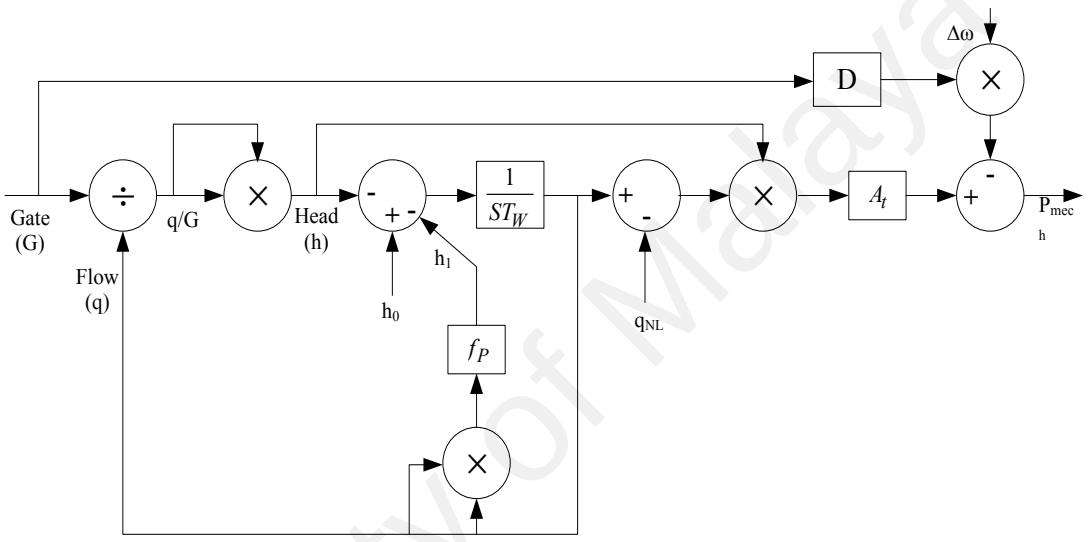

Figure 5.3: Block diagram of hydraulic turbine

In this model, the head losses h_1 are proportional to the flow squared and head loss coefficient f_P. Both the hydraulic characteristics and mechanical output power of the turbine must be modelled. The parameter values of hydraulic turbine used in this research are shown in Table 5.1.

Table 5.1: Value of hydro turbine parameters

Parameter	Value	Parameter	Value
TW	1.0	Initial output power	0.7
f_p	0.02	Initial operating head	1.0
D	0.5	Rated output power	1.0

5.2.1.2 Governor Model

The main function of the governing system is to regulate the turbine-generator speed in response to load variation. The speed control mechanism includes equipment such as relays, servomotors, power amplifying devices, and governor-controlled gates. The speed governor normally actuates the governor-controlled gates that regulate the water input to the turbine through the speed control mechanism. The general block diagram consists of the hydraulic turbine and governor, and is shown in Figure 5.4.

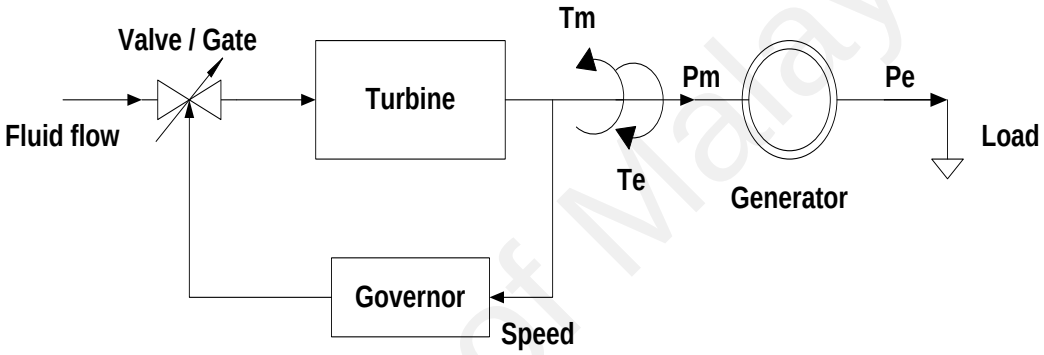

Figure 5.4: Block diagram of turbine speed control with governor

When the load demand in the system decreases, the generator speed will increase accordingly. In this situation, the turbine governor responds immediately and divert water flow by closing the gate to prevent the hydro turbine from over-speeding. However, in high load demand situations, the turbine governor opens the hydraulic valve to increase the generator's speed. In this research, an electro-hydraulic PID governor for speed control is used to regulate the generator speed. Figure 5.5 shows the block diagram of the electro-hydraulic PID governor.

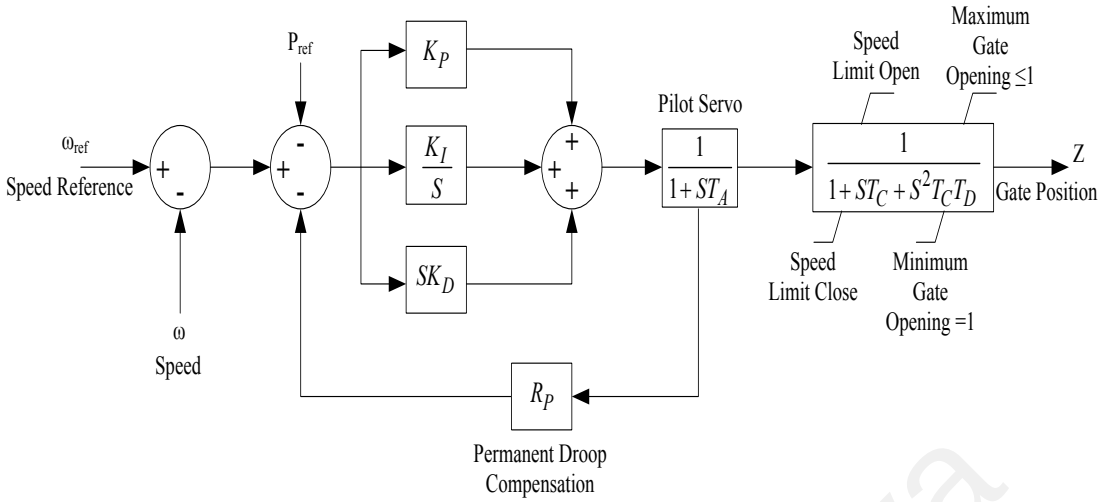

Figure 5.5: Block diagram of electro-hydraulic PID based governor

Where T_A is the time constant of pilot valve and servomotor, T_C is a gate servo gain, T_D is the gate servomotor time constant, and R_P is the permanent droop that determines the amount of change in output a unit produces in response to a change in unit speed. The parametric values used for governor are tabulated in Table 5.2. However, the values for K_P, K_I, and K_D are tuned using the trial-and-error method to provide satisfactory results.

Table 5.2: Parameters of the hydraulic governor

Parameter	Value	Parameter	Value
K_P	2.25	T_C	0.2 s
K_I	0.37	T_D	0.2 s
K_D	0.9	Max gate opening	0.16
T_A	0.05 s	Max gate closing	0.16
R_P	0.04	Dead band value	0
Max gate position	1.0	Min gate position	0

5.2.1.3 Synchronous Generator Model

Synchronous generators are the main sources used to provide energy in power systems. It is therefore very important to study the performance of synchronous machines. The synchronous machine is assumed to have a three-phase stator armature winding, a rotor field winding, and two rotors damper winding–one in the d-axis, and one in the q-axis. In this research, two synchronous generators of 2 MW capacity are driven by hydraulic

turbines and governor control mechanisms. The synchronous generator parameters for this test system are tabulated in Table 5.3. The specifications for both generators are similar.

Table 5.3: Synchronous generator parameters

Parameter	Value
Rated RMS line-to-line voltage	3.3 kV
Rated RMS line current	350 A
Inertia constant (*H*)	2.5 s
Iron loss resistance	300 p.u
Base angular frequency	314.159 rad/s
Armature resistance [*Ra*]	0.01 p.u
Potier reactance [*Xp*]	0.104 p.u
Unsaturated reactance [*Xd*]	0.838 p.u
Unsaturated transient reactance [*Xd'*]	0.239 p.u
Unsaturated transient time [*Tdo'*]	8.0 s
Unsaturated sub transient reactance	0.12 p.u
Unsaturated sub transient time [*Tdo''*]	0.05 s
Unsaturated reactance [*Xq*]	0.534 p.u
Unsaturated sub transient reactance	0.12 p.u
Unsaturated sub transient time [*Tqo''*]	0.1 p.u
Air gap factor	1.0

5.2.1.4 Exciter Model for Synchronous Generators

The main function of the excitation system is to maintain the terminal voltage of synchronous machine and control the reactive power flow. This operation was performed by adjusting the field current of the synchronous generator. The excitation systems have taken many forms over the years. In this research, the IEEE type AC1A standard model from the PSCAD/EMTDC library was used for interfacing with synchronous machines, as shown in Figure 5.6.

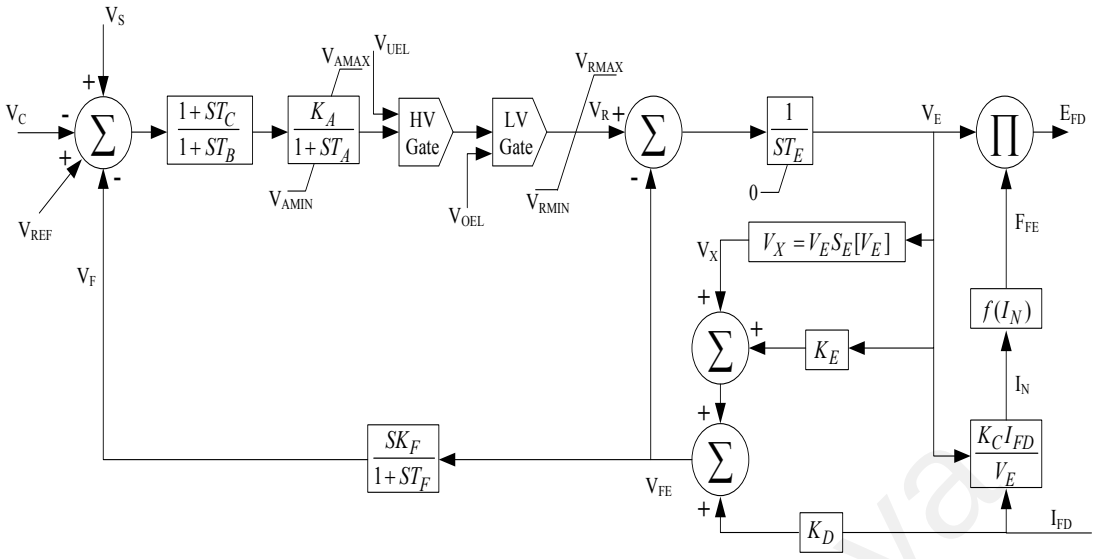

Figure 5.6: Block Diagram of IEEE type AC1A excitation system model

This model provides a field-controlled alternator excitation system with un-controlled rectifiers, and is applicable to brushless excitation systems. The typical parameters used in this research are presented in Table 5.4.

Table 5.4: Sample data of IEEE AC1A excitation model parameters

Parameter	Value	Parameter	Value
T_c	0	K_F	0.03
T_B	0	T_F	1
K_A	400	T_E	0.8
T_A	0.02	K_E	1
V_{AMAX}	14.5	K_C	0.2
V_{AMIN}	-14.5	K_D	0.38
V_{RMAX}	6.03	V_{RMIN}	-5.43
$SE(VE_1)$	0.1	$SE(VE_2)$	0.03
VE_1	4.18	VE_2	3.14

Figure 5.7 shows the synchronous generator with PID based governor, hydraulic turbine, and excitation control modelled in PSCAD.

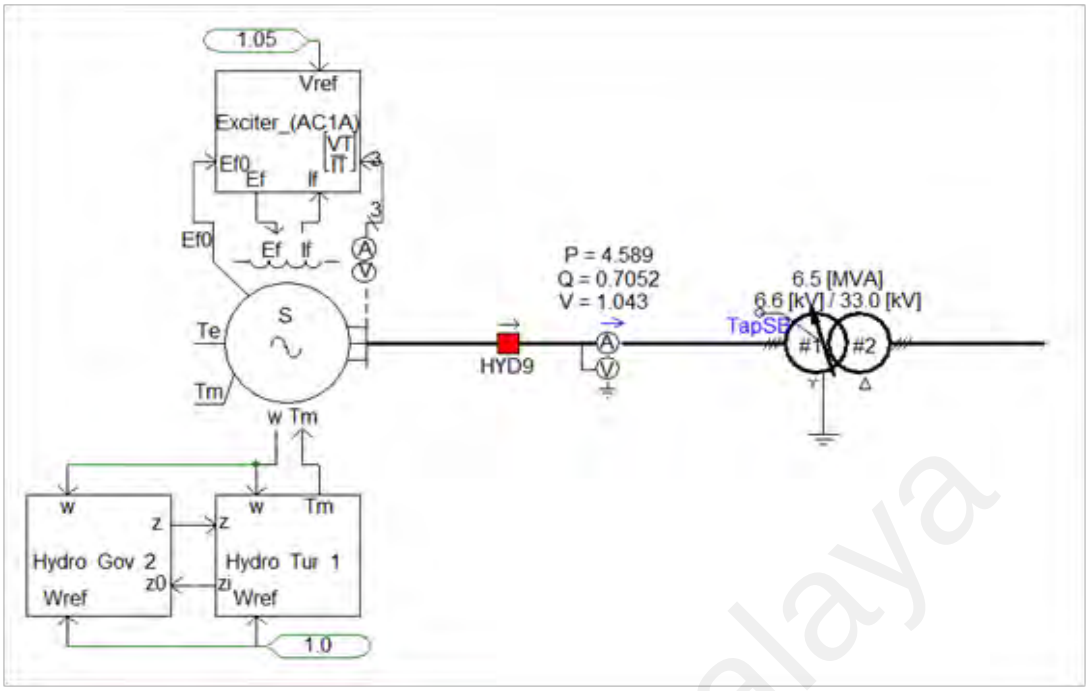

Figure 5.7: Mini-hydro power plant model in PSCAD/EMTDC software

5.2.2 Load Modelling of Distribution Network

The tested distribution network consists of 29 buses and 21 lumped loads. In this test system, static load type component was used to model the load, where the active and reactive power components were considered separately, as per (kundur et al., 1994).

$$P = P_0 \times \left(\frac{V}{V_0}\right)^a \times \left(1 + K_{pf} \times \Delta f\right) \tag{5.2}$$

$$Q = Q_0 \times \left(\frac{V}{V_0}\right)^b \times \left(1 + K_{qf} \times \Delta f\right) \tag{5.3}$$

where

P, Q = active and reactive power for corresponding voltage and frequency,

P_o, Q_o = active and reactive power at a base voltage and frequency,

K_{pf}, K_{qf} = coefficients of active and reactive load dependency on frequency, the range of K_{pf} usually between 0 and 3.0, while K_{qf} typically in between -2.0 to 3.0.

a, b = load model parameters, the range of a usually between 0.5 and 1.8, while exponent b typically in between 1.5 to 6.0.

Δf = the frequency deviation.

The value of K_{pf}, K_{qf}, a, and b are set to be 1.0, -1.0, 1.0, 2.0, respectively. The proposed load shedding technique was used on eleven loads from the distribution network. The loads, with their priority rankings, are tabulated in Table 5.5. Figure 5.8 shows the hourly load profile levels in pu.

Table 5.5: Load data of load buses that can be curtailed from the system and their Priority

Load Ranked	Bus Number	Active Power (MW)	Conventional Technique Priority	Adaptive Technique Priority	Proposed Technique Priority
1	1050	0.044	Fixed	Fixed	Random
2	1013	0.069	Fixed	Fixed	Random
3	1047,1026	0.15	Fixed	Fixed	Random
4	1012	0.314	Fixed	Fixed	Random
5	1151	0.435	Fixed	Fixed	Random
6	1029	0.520	Fixed	Fixed	Random
7	1010,1039	0.583	Fixed	Fixed	Random
8	1075	0.645	Fixed	Fixed	Random
9	1018,1020 ,1046	0.818	Fixed	Fixed	Random
10	1144	0.119	Fixed	Fixed	Random
11	1044	0.223	Fixed	Fixed	Random

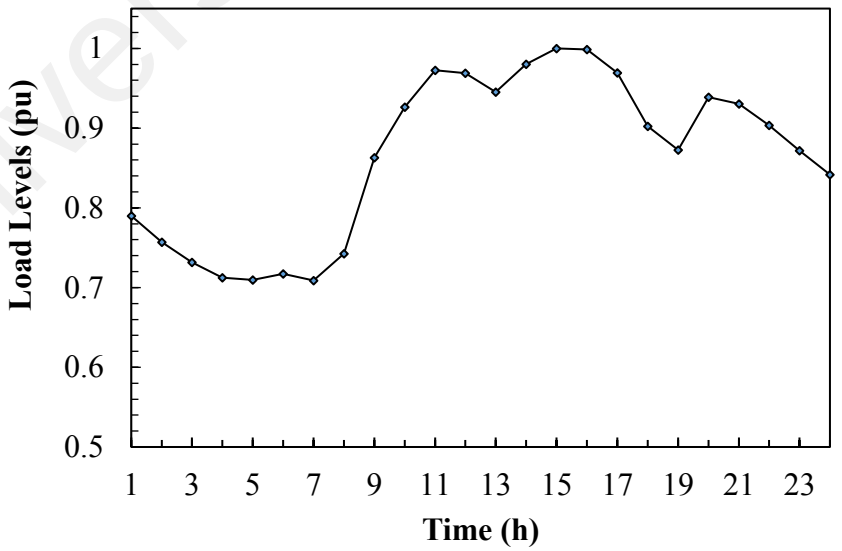

Figure 5.8: Hourly load profile for individual loads for test system

5.2.3 Modelling of Photovoltaic System

Figure 5.9 shows the PSCAD modeled of the solar PV unit. The main parts of solar PV unit are the DC-DC converter, PV array model, DC link capacitor, AC filter, three phase-inverter, and transformer. These parts are detailed in the next sections.

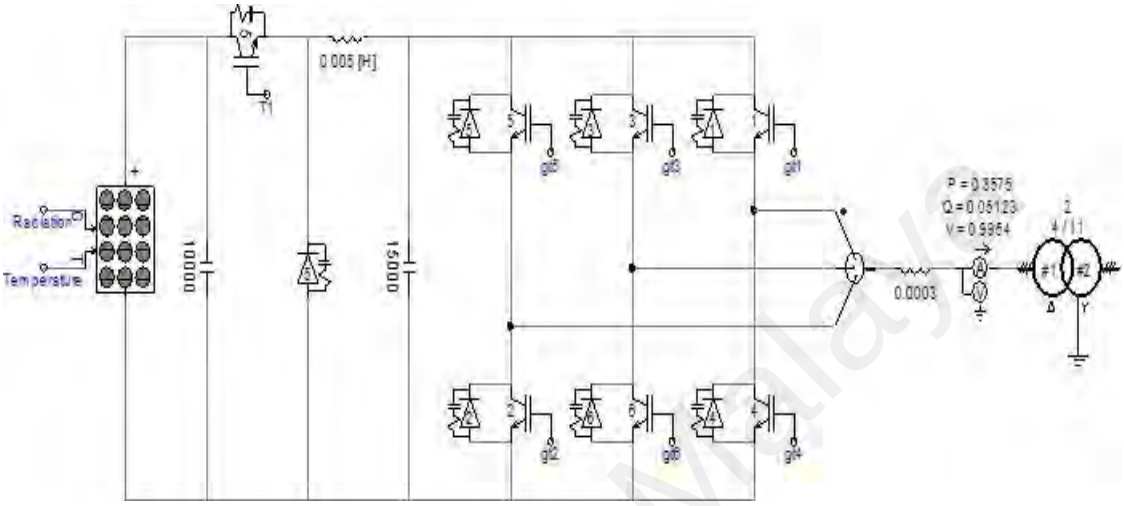

Figure 5.9: Solar PV generation unit using PSCAD software

5.2.3.1 PV Array unit

The PV solar was used to convert sunlight to electricity via the photoelectric effect. The PSCAD PV model was used to generate power from four solar PV units and inject their power into the distribution network.

The values tabulated in Table 5.6 were used to generate 380 W output power from the single module and 549 KW from a total of 1445 modules.

Table 5.6: Solar PV module SM380 Poly parameter at 1000 W/m^2, 25°C

Parameter	Symbol	Value
Open circuit voltage	V_{oc}	59.75 V
Max. power voltage	V_m	47.9 V
Short circuit current	I_{sc}	8.56 A
Max. power current	I_m	7.93 A
Peak power	P_{max}	380 W
Number of modules connected in series	NS	17
Number of modules connected in parallel	NP	85

To obtain the desired power level, the PV modules were connected in series and parallel. Figure 5.10 shows 85 strings connected in parallel, with each having 17 modules connected in series.

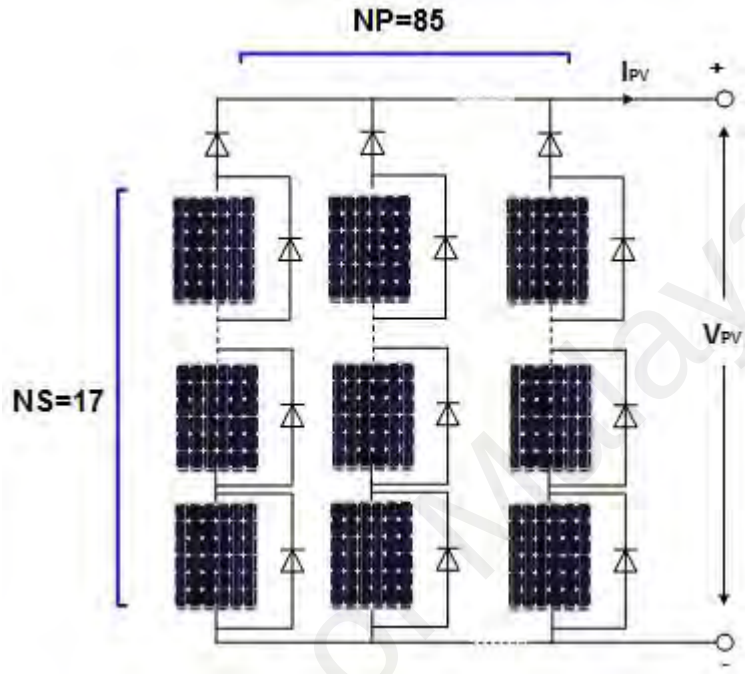

Figure 5.10: Connection of PV array

Figures 5.11 and 5.12 show the three main points in the I-V and P-V characteristics of the PV unit at standard test conditions (G=1000W/m^2, T= 25C°), respectively. The first point is the maximum power point (MPP), which describes the maximum power generated from the photovoltaic system at particular temperature and irradiance when the voltage is at MPP, V_{MPP}, and the current is at the MPP, I_{MPP}. The second point is the open circuit voltage, Voc, which is measured when the loads are disconnected. The third point is the short circuit current, Isc, which is measured when the voltage is zero.

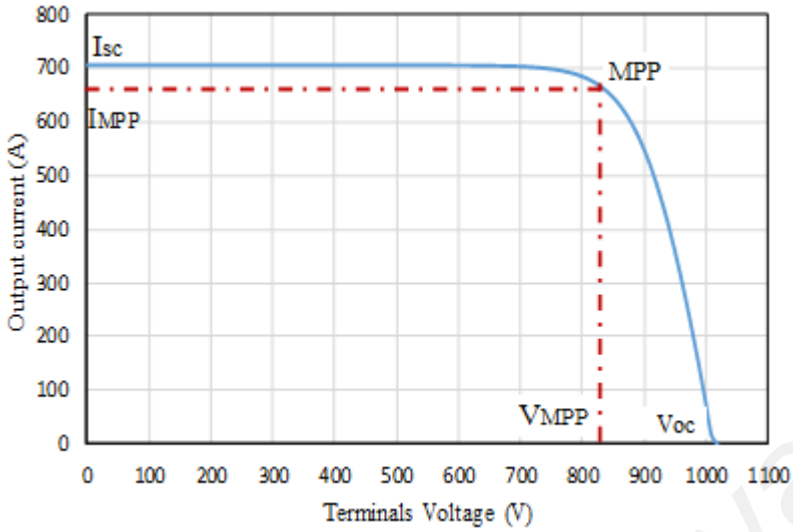

Figure 5.11: I-V curve of solar PV generation unit

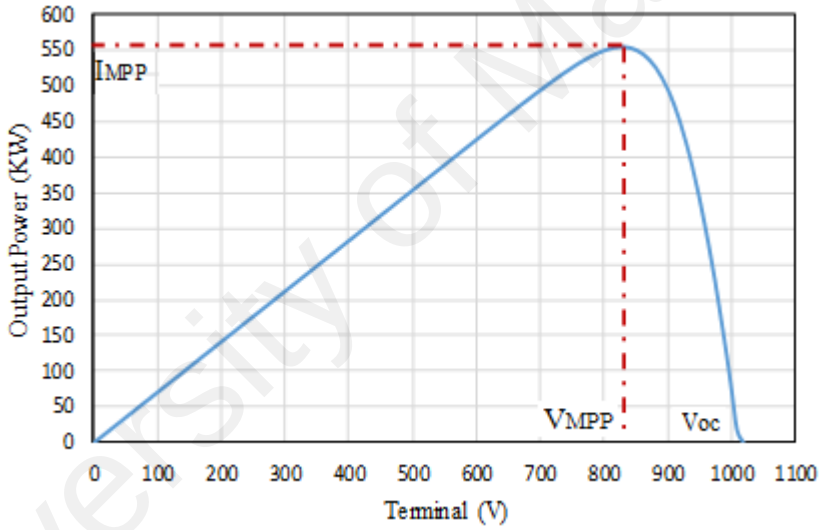

Figure 5.12: P-V curve of solar PV generation unit

5.2.3.2 Buck DC-DC Converter

The DC-DC converter is an electronic circuit that aims to control the DC output at a desired voltage level. There are several different kinds of DC-DC converters in use in the industry today, but most are based on two basic converter topologies: buck converter (step-down the input voltage) or boost converter (step-up the input voltage). In this study, the former was used to convert the input voltage that represents the renewable source of the solar PV system to a fixed output voltage at 700V DC.

Figure 5.13 illustrates the topology of buck convertor, which include Insulated Gate Bipolar Transistor (IGBT) switch, capacitor, inductor, and free-wheel diode. Table 5.7 shows the parameters of the buck converter device.

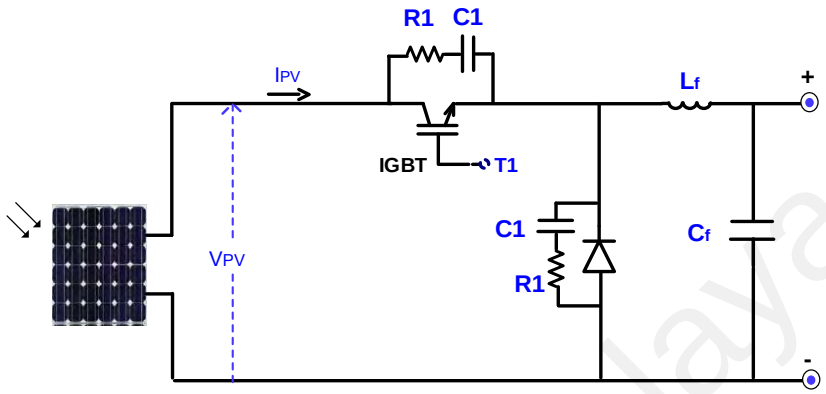

Figure 5.13: Buck DC-DC converter of solar PV unit

Table 5.7: Buck DC-DC converter parameters

Parameter Symbol Target	Parameter	Parameter value
Input Voltage	V_{IN}	830 V
Output Voltage	V_{OUT}	700 V
Switching Frequency	f_{SW}	1KHz
Inductor Current Ripple Ratio	LIR	0.3
Capacitor Voltage Ripple	CVR	0.04
Maximum Output Current	$I_{OUT, MAX}$	700 A
The minimum inductance	L_{min}	550 µH
The minimum capacitance	C_{min}	1000 µF

$$D = \frac{V_{out}}{V_{in}} = \frac{700}{830} = 0.84 \tag{5.4}$$

$$L_{MIN} = \frac{(V_{in}-V_{out})\times D}{L_I \times I_{out,MAX} \times f_{sw}} = \frac{(830-700)\times 0.84}{0.3\times 700\times 1000} = 520\ \mu H \tag{5.5}$$

$$C_{MIN} = \frac{LIR\times I_{out,MAX}}{8\times f_{SW}\times CVR\times V_{out}} = \frac{0.3\times 700}{8\times 1000\times 0.04\times 700} = 937\mu F \tag{5.6}$$

5.2.3.3 Three Phase Inverter

The inverter is an electronic circuit used to convert the DC output power of the DC-DC converter into a three phase AC power suitable for utility connection. In this PSCAD

model, the three-phase inverter consists of a simple active and reactive power controller, a firing pulse generator, and a three-phase inverter bridge.

(a) ***Active and Reactive Power Controllers***

The purpose of the active power controller is to maintain a constant DC bus voltage (dcvag) between the buck converter and the inverter at a value of 0.7 kV. Meanwhile, the reactive power controller aims to obtain a zero output of reactive power in order to force the inverter to operate at unity power factor, meaning that there is no phase shift between the voltage and current outputs. The active and reactive power controllers are shown in Figure 5.14.

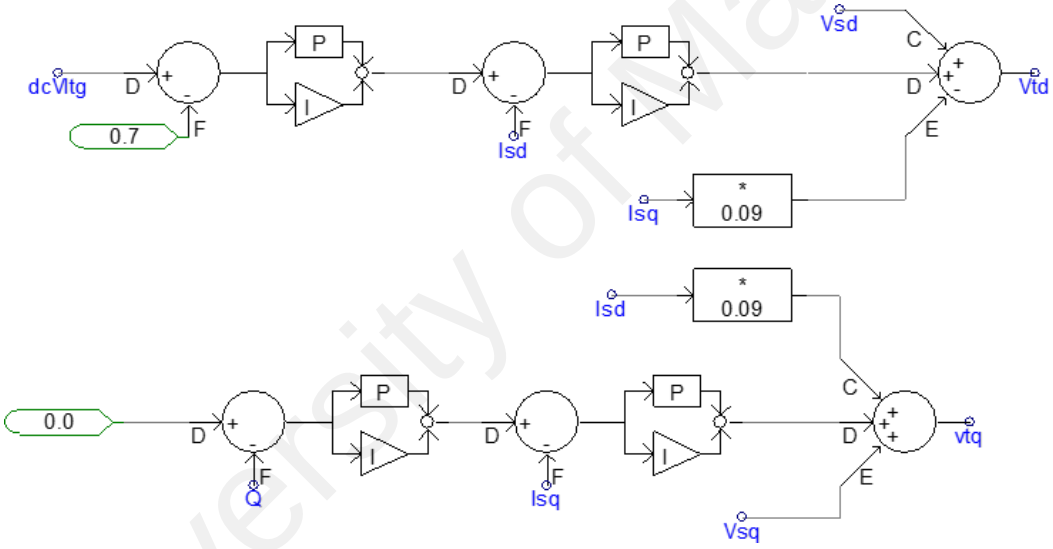

Figure 5.14: Active and reactive power controller of solar PV Inverter

(b) ***Firing Pulse Generation***

The switching signals of the six IGBT switches of the 3-legged inverter bridge is shown in Figure 5.15. It begins by creating three sinusoidal modulating waves with a frequency of 50 Hz and a phase shift equal to the output of the previous reactive controller (V_{tq}). The magnitude of the modulating waves is controlled by (V_{td}) from a previously active controller. Then, the three sinusoidal modulating waves were compared with a triangular carrier wave, with magnitudes between -1 and 1.

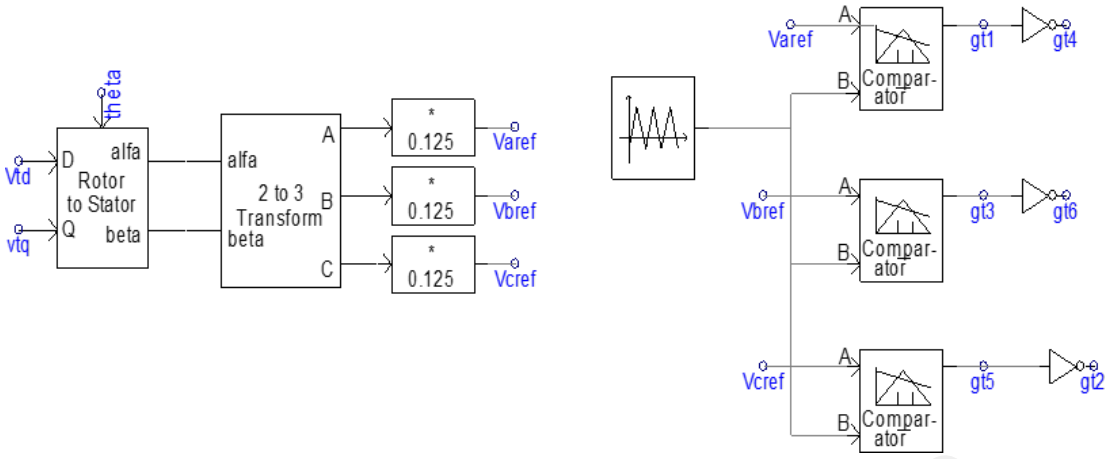

Figure 5.15: Firing pulse generation of solar PV inverter

(c) ***Three Phase Inverter Bridge***

Three phase inverter bridge was used to convert the DC bus voltage to AC voltage of 400 V/50 Hz. As shown in Figure 5.16, three phase bridge consists of six IGBT, where each IGBT switch is controlled by a firing signal. Due to the switching operation of IGBT, the output voltage of the inverter will be distorted. For this reason, an LC filter was implemented to improve the shape of the output voltage of the inverter.

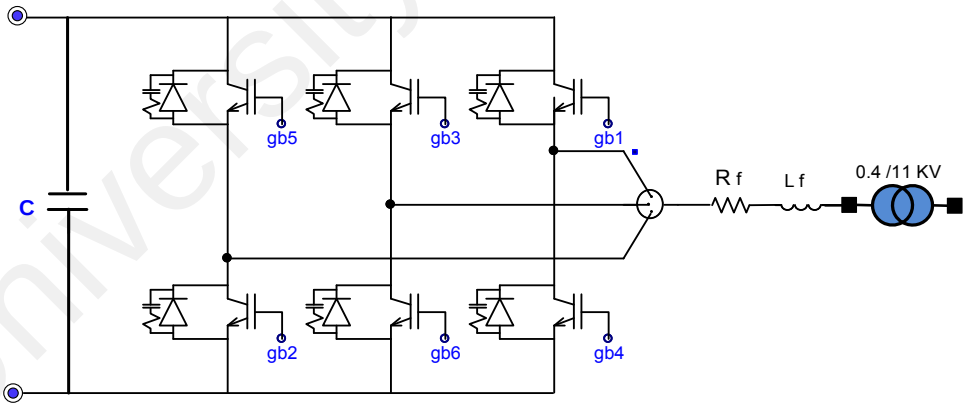

Figure 5.16: PSCAD model of solar PV inverter

5.2.4 Full Converter Wind Turbine Units Modelling with its Frequency Support Strategy

A full converter wind turbine (FCWT) is shown in Figure 5.17. The FCWT is used in this work to provide the primary frequency control. Without ancillary frequency control, FCWT operates based on the active power reference provided by MPPT control, while

the wind turbine generator cannot provide any response for the system frequency disturbance. The active power reserve by FCWT can be used to provide the ancillary frequency. In order to do so, a 10% de-loading power tracking is applied to the wind turbine, as shown in Figure 5.18.

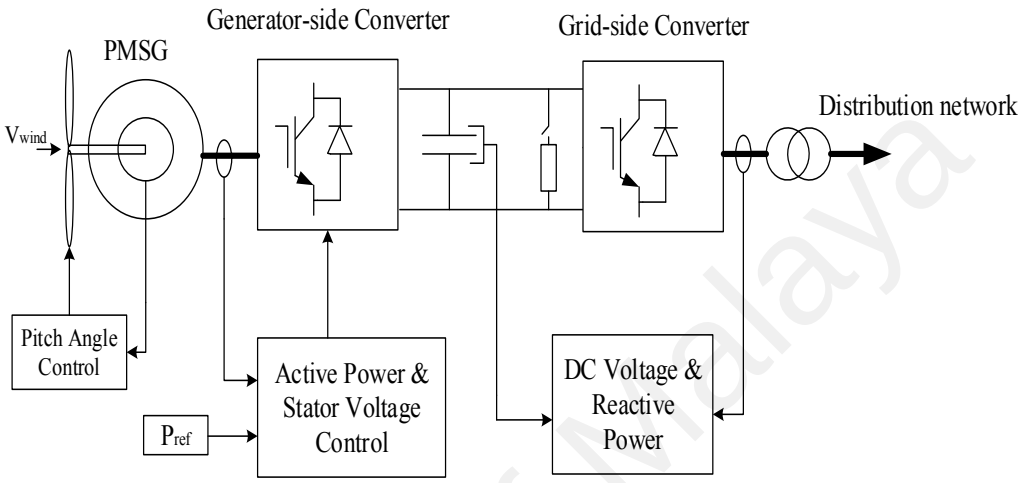

Figure 5.17: Main parts and control diagram of FCWT

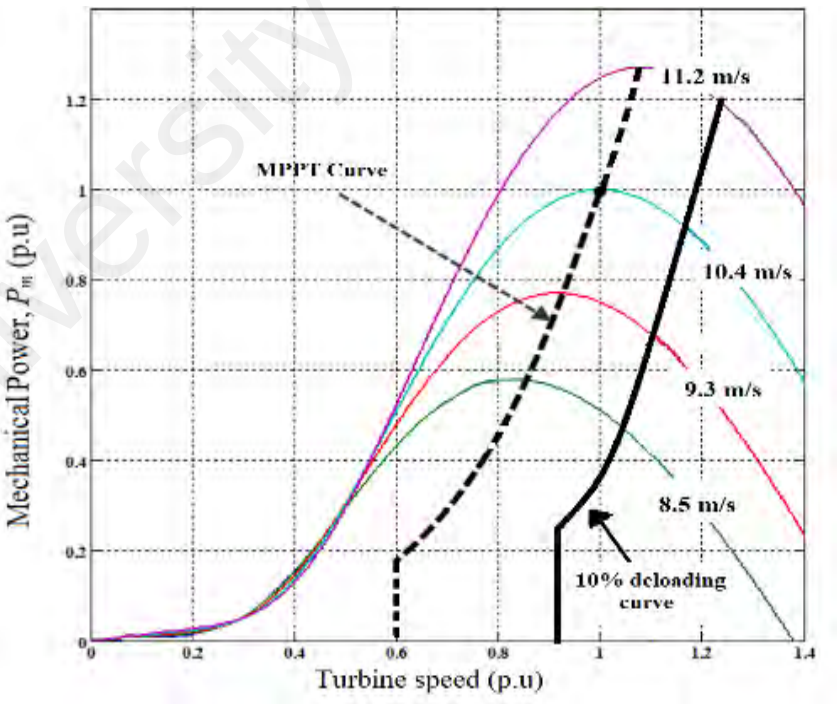

Figure 5.18: Operation curve of FCWT with 10% de-loading

5.2.4.1 Aerodynamic torque calculation

The aerodynamic torque developed by the rotor blades was calculated in this subsystem using the theory by (Manwell, McGowan, & Rogers, 2010). The kinetic energy *E* (in J) of an air mass m (in kg) moving at a speed *Vwind* (in m/s) is given by:

$$E = \frac{1}{2} m V_{wind}^2 \tag{5.7}$$

If the air density is ρ (kg/m^3), mass flow through an area *A* is given by:

$$\dot{m} = \rho A V_{wind} \tag{5.8}$$

Thus, an equation for the power (in W) through a cross-sectional area A normal to the wind is:,

$$P_{wind} = \frac{1}{2} \rho A {V_{wind}}^3 \tag{5.9}$$

In the case of a wind turbine, area *A* is the area swept by the rotor blades. Only a part of this power can be captured due to the non-ideal nature of the rotor, hence the need for the coefficient C_P. The result is shown in Equation 5.10:

$$P_{rotor} = \frac{1}{2} \rho C_p \pi {R_{rotor}}^2 {V_{wind}}^3 \tag{5.10}$$

5.2.4.2 Reference power calculation from wind speed

The reference power calculation is based on the user-defined wind speed, as shown in Figure 5.19. Wind speed is unitized based on rated wind speed, cubed, and multiplied by rated power (2 MW) to obtain output power. The output power will be 2 MW if the user defined wind speed exceeds the rated wind speed (13 m/s). A lookup table (wind speed -

output power) is used to drive the power output curve to be softened, especially when the power output has sharp changes. This lookup table will be presented as a curve in Appendix D.1

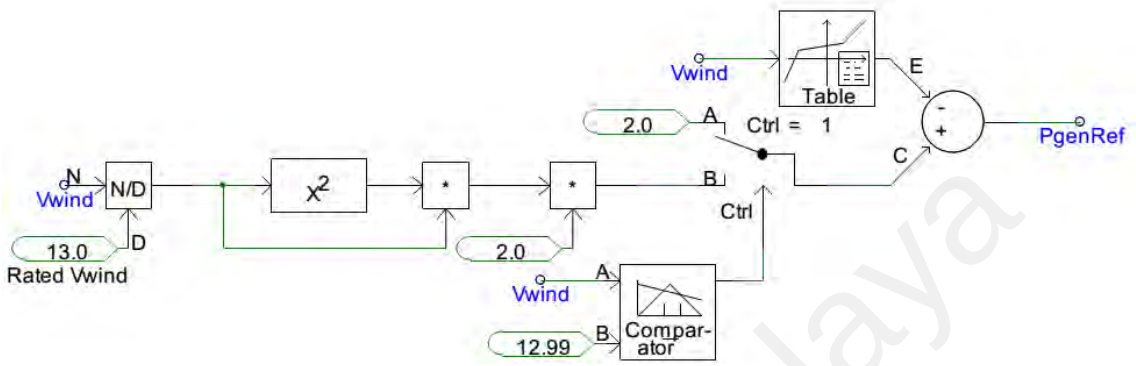

Figure 5.19: Reference power calculation

5.2.4.3 Pitch control block

The pitch angle controller in Figure 5.20 is used to regulate the blade pitch angle to keep the output power at a particular value even when the wind speed surpasses the rated wind speed. The reference power is converted to the reference speed in per unit based on a look-up table. The detail of this lookup table will be presented as a curve in Appendix D.2. Both actual and reference speeds were compared, and the resulting error was used to drive the upper PI controller. Both the actual and reference powers were compared, and the resulting error was used to drive the lower PI controller. Then, the outputs of the PI controllers were summed and hard-limited to generate the pitch angle signal.

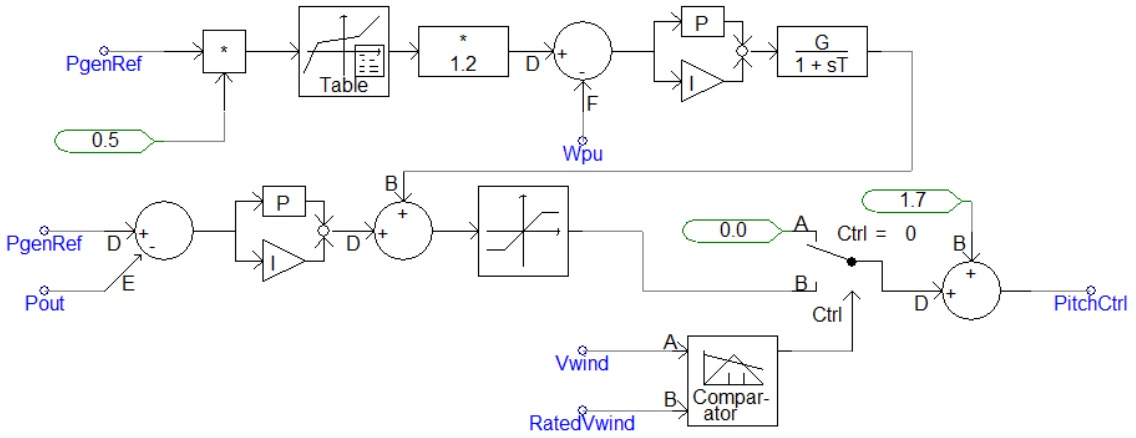

Figure 5.20: Pitch controller

A modified pitch angle controller was used to force the FCWT in de-loading mode by adding an angle increment (delta B =1.7^{o}).

5.2.4.4 Permanent magnet alternator

The permanent magnet alternator was modeled using a built-in PSCAD/EMTDC PMA block. The terminals of the block are shown in Figure 5.21.

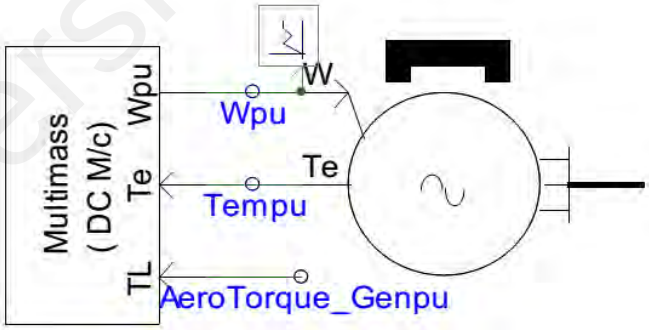

Figure 5.21: Permanent magnet alternator in PSCAD/EMTDC

5.2.4.5 Rectifier and buck/boost converter for DC-link voltage control

The AC output of the PMSG was converted to a fixed DC voltage using a rectifier and buck/boost converter models, as shown in Figure 5.22. An example of the use of buck/boost converters for DC link control for PMA wind turbines is provided in (Tafticht, Agbossou, & Cheriti, 2006). The PMA output was converted to a variable DC voltage

based on a 3-phase diode bridge, while the buck-boost converter preserves the DC link at a constant 3.6 kV. Based on the ground reference issues of the PSCAD/EMTDC software, the DC link capacitor was modeled as two similar capacitors with one ground between them. Figure 5.23 shows the controller of the buck/boost converter. This controller is based on an error between the desired voltage set-point (3.6 kV here); the PI control and PI controller drive the actual voltage and together, generate a duty signal output. This signal is compared to a triangle signal in order to generate firing signals for the IGBT in the buck/boost converter. In Figure 5.22, the values of C1, C2, and L are 10,000 uF, 10,000 uF, and 0.01 H, respectively.

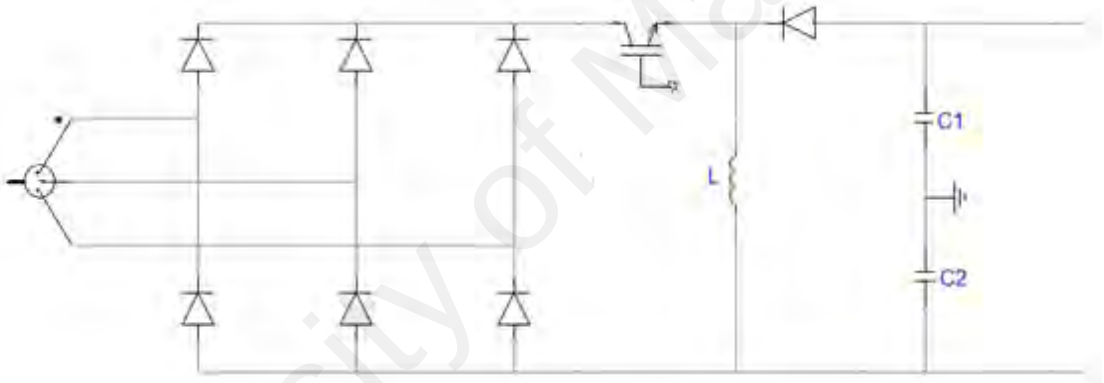

Figure 5.22: Rectifier and buck/boost converter circuit

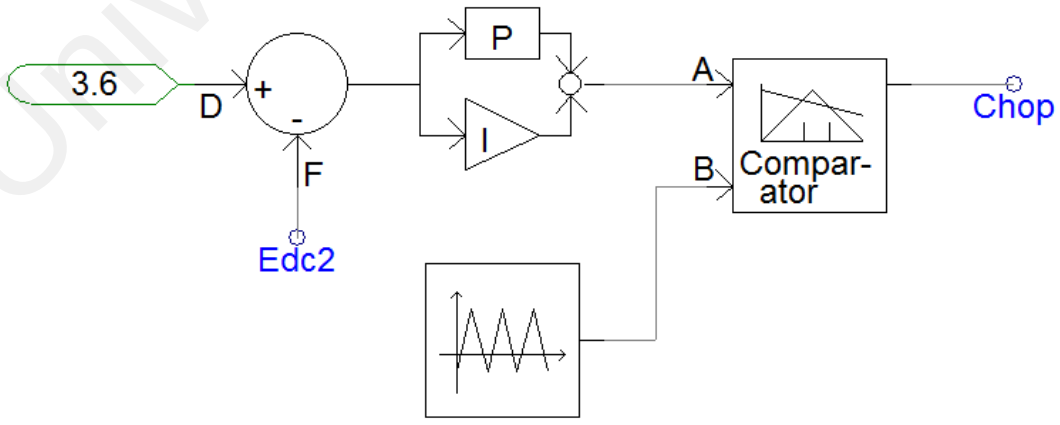

Figure 5.23: Buck/boost converter controller

5.2.4.6 Inverter

The inverter implemented in Figure 5.24 shows a current controlled voltage-source inverter. In this inverter, the control strategy uses the currents represented in the dq synchronous rotating reference frame and controlled by standard PI controllers. For that, the inverter is capable of decoupling active/reactive power controls. This control transforms the grid currents from the abc to their respective equivalents in the dq reference frame. It should also be pointed out that the abc variables are transformed to the dc components (dq components), and offers much simpler and feasible controllability. Power reference signals of both active and reactive powers are compared with the actual values, then the error is used to drive two independent PI controllers, as shown in Figure 5.25. The active power error generates the Iq signal, while reactive power error generates the Id signal. These dq0 domain values are converted to reference I_{abc} values, as shown in Figure 5.26. The reference active and reactive power achieved its desired value only when the reference currents are achieved. The value of component L in Figure 5.24 is 0.0001 H.

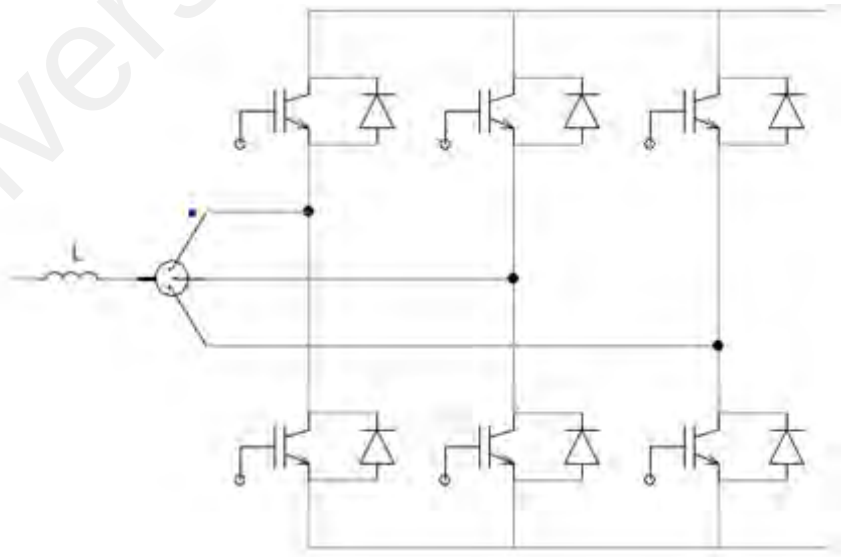

Figure 5.24: Inverter (current controlled VSI)

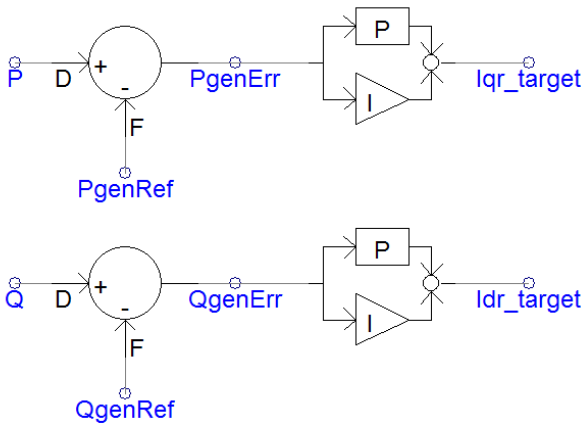

Figure 5.25: Active and reactive power errors drive q- and d-axis current controllers respectively

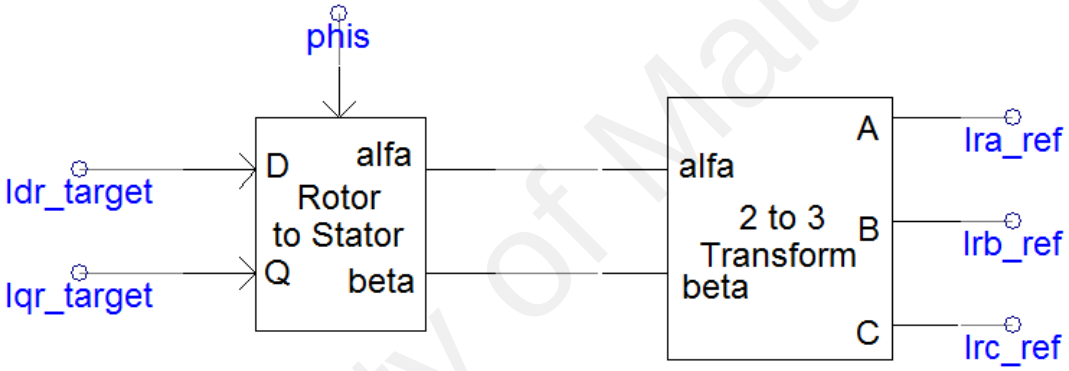

Figure 5.26: Currents are converted from dq0 domain to the abc domain

5.2.5 Model of Proposed UFLS in (Laghari et al., 2015)

In the UFLS method proposed in (Laghari et al., 2015), when the TLSA was determined, the proposed method generates all combinations of loads that can be shed from the system. In this study, 11 loads were selected to be shed from the distribution network. According to the number of loads that can be shed, all possible combinations of loads that can be shed is (2047), according to Equation (5.11).

Then, calculate the fitness value (TLSA - ∑Pi_Combination) for each combination. The loads combination with least fitness values will be selected for shedding from the microgrid.

$$Number\ of\ combination = 2^n - 1 \tag{5.11}$$

where n is the number of loads.

To illustrate the UFLS method proposed in (Laghari et al., 2015), let the TLSA be 1.2 MW and there are 11 loads in (MW). The length of each combination is 11. The value of each element in combination has two probabilities; zero, which represents the load remaining in network, and one, representing the load was removed from the networks. The best load combination that fulfils the minimum value of (TLSA - ∑Pi_Combination), namely when ∑Pi-Combination is close to TLSA, is the best load combination. As noted in Table 5.8, the best combination is combination (2046), because the value of (TLSA - ∑Pi_Combination) is the smallest value.

Table 5.8: Find the best combination of load removing when power deficit is 1.2 MW

Combination No.	**Load combination**	**∑Pi-Combination (MW)**	**TLSA - ∑Pi-Combination (MW)**
Combination (1)	10101101010	$P_{L2}+P_{L4}+P_{L6}+P_{L7}+P_{L9}+P_{L11}$ =0.95	0.25
Combination (2)	01000101011	$P_{L1}+P_{L2}+P_{L4}+P_{L6}+P_{L10}$ =1	0.2
Combination (3)	11110000001	$P_{L1}+P_{L8}+P_{L9}+P_{L10}+P_{L11}$ =1.1	0.1
.	.	.	.
.	.	.	.
Combination (2046)	.	PL1+PL2+PL3+PL7+PL8+PL9 =1.195	**0.005**
Combination (2047)	00111000111	$P_{L1}+P_{L2}+P_{L3}+P_{L7}+P_{L8}+P_{L11}$=1.15	0.05

5.2.6 Simulation results and discussion

The simulation results included in this thesis are divided into three case studies:

Case 1 represents the effect of a de-loading technique in RESs (wind turbine, PV system) in the distribution network when islanding formed without using an UFLS scheme.

Case 2 represents the comparative study between each of the proposed UFLS scheme, conventional UFLS scheme, adaptive UFLS scheme, and the method proposed in (Laghari et al., 2015) to show the importance of assuming the flexibility in load shedding priority and which method can be determined the optimal load shedding in terms of execution time.

Case 3 represents a comparative simulation study between the combined method of a de-loading technique in RESs and the proposed UFLS technique, with both the de-loading technique in RESs without the proposed UFLS technique and the proposed UFLS technique without the de-loading technique in RESs. It should also be pointed out that the maximum load level was used in all simulation case, as per Figure 5.8.

5.2.6.1 Case 1: aims to show the effect of using a de-loading technique in RES without using UFLS technique

Islanding occurs when the utility grid is disconnected from the distribution network. The islanding event was simulated at t = 10 s. The power imbalance at this point is (1.19 MW), since the distribution network was supplying the grid (1.19 MW) prior to islanding. An excess of power supplied by the DGs results in the system frequency increasing following islanding, since the generation power is larger than the total load. Losing the main grid forces, the DGs took over the generation from the grid to avoid over frequency. The active power dispatches are shown in Table 5.9. Note that all loads remain connected to the network without applying the load-shedding scheme.

Table 5.9: Active power of all indices for case 1

Active Power		Before Islanding (MW)	After Islanding at *t* = 10 s (MW)	After addition 1 MW at *t* = 40 s (MW)
P_{gen}	P_{grid}	-1.19	0.00	0.00
	P_{PV}	2.4	1.276	2.334
	P_{Wind}	1.305	1.305	1.453
	P_{hydro}×2	1.715×2	1.724×2	1.75×2
P_{shed}		0.00	0.0	0.0

It can be observed that the solar PV units have to change their operation by decreasing the amount of power dispatch after islanding. The solar PVs generation decreased to 1.2 MW through the de-loading technique in the solar PV system via the APC to prevent over frequency. Figure 5.27 shows the system frequency when the PV units do not use de-loading technique. It can be seen that the system frequency goes up to 52.5 Hz. However, the DGs protection devices was activated, then the distribution network experiences an immediate blackout. Figure 5.27 shows the system frequency to be within its range after islanding, because the PV units modified their power output to be suitable with the load demand in order to prevent overshooting frequency via de-loading technique, as seen in Figure 5.28.

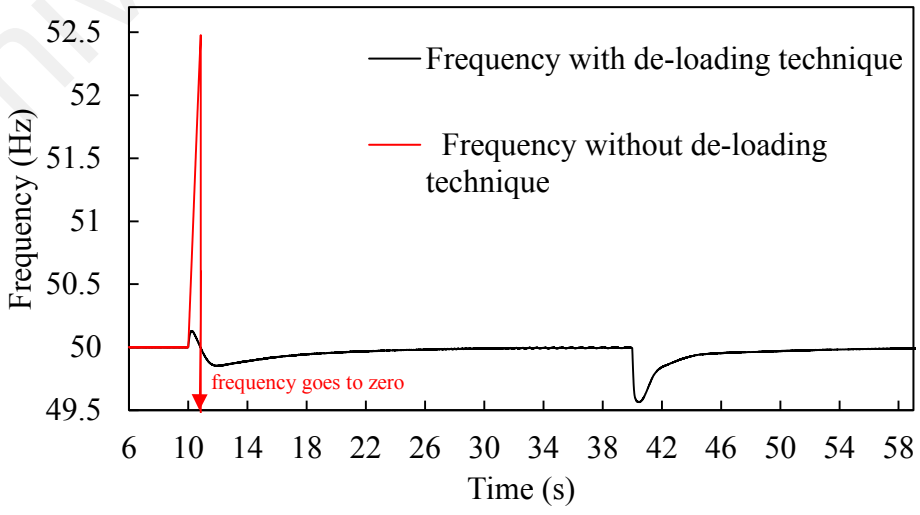

Figure 5.27: Frequency response with/without using de-loading technique for case 1

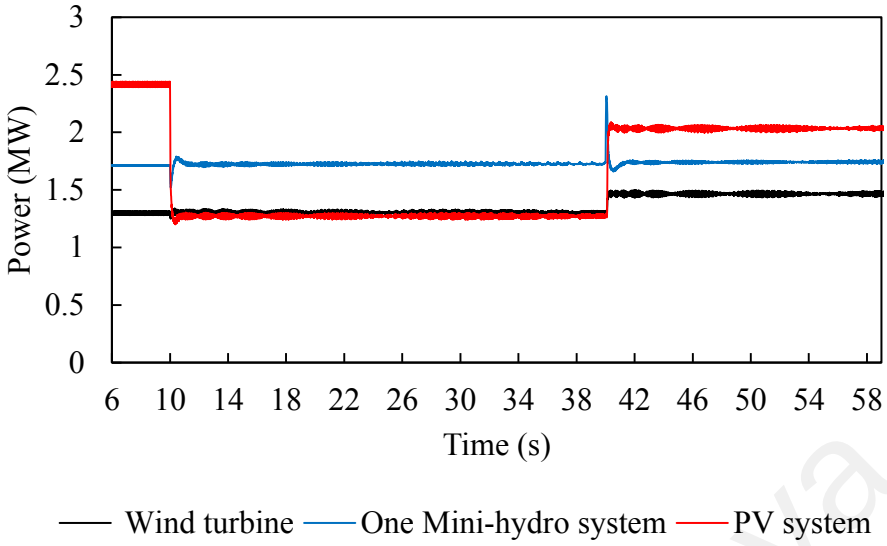

Figure 5.28: Output DG power when using a de-loading technique

Meanwhile, at a simulation time of 40s, a 1 MW extra load was suddenly added to the distribution network. In this case, the output of the solar PV units, two mini-hydro generation, and wind turbine increased to 2.334 MW, 3.5 MW, and 1.453 MW respectively, to compensate for the power deficit, as shown in Figure 5.28. In this scenario, the performance of the utilization of the de-loading technique was analyzed. For the two events, the output powers of all DGs are shown in Figure 5.28. It should also be pointed out that the UFLS scheme was not activated because the system's frequency did not fall under 49.5 Hz. For that, the distribution network holds all the loads, which will never be shed. Eventually, the system's frequency recovers and approaches its reference value.

5.2.6.2 Case 2: aims to show the importance of assuming the flexibility in load shedding priority

In this case, only two PV units were used to transmit electrical energy in one direction from the main grid to the distribution network. All the DGs were operated at its maximum generated power and the de-loading technique was not used in this case. The firefly algorithm was combined with the ANN technique to determine the best load combination

to be curtailed from the network. The BFA algorithm was executed in MATLAB on a PC with specs of 3.07 GHz CPU and 8-GB RAM. For the application of the algorithm, the population size was set to 100, while the iteration size was set to 300. For the distribution network, the minimum TLSA, maximum TLSA, and Δ TLSA were 0.01 MW, 4.0 MW and 0.01 MW, respectively. However, there are 400 values of TLSA that should determine the best combination of loads. For each value of TLSA, the BFA was repeated for 50 times to determine the best fitness (minimum error between the TLSA (MW) and the total of combination loads). Figure 5.29 shows the convergence characteristic for BFA for 1MW TLSA at run number 2. In this case, the loads that were selected to be shed were load 1, load 3, load 7 and load 11, with the sum equaling 1MW.

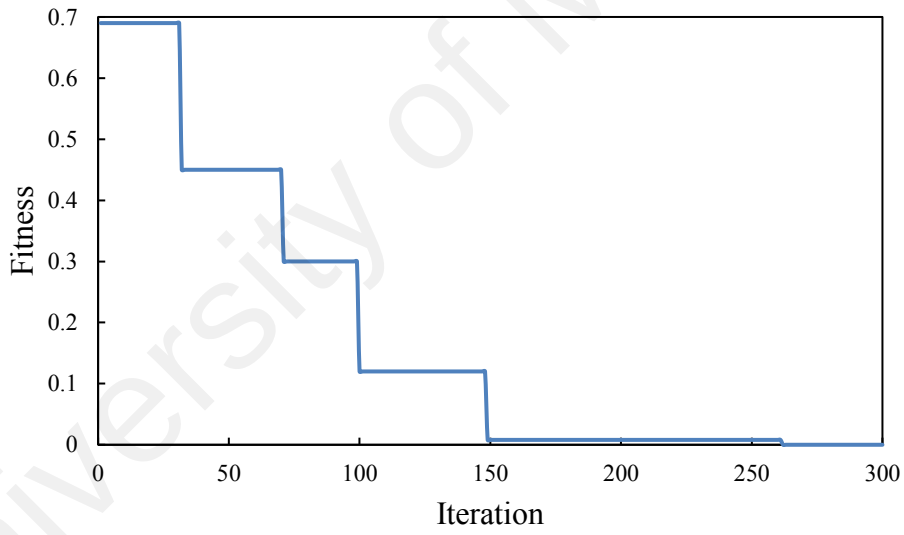

Figure 5.29: Convergence characteristic for BFA optimizations when TLSA equal 1MW at run number 2

This case is presented to show the preference of the proposed UFLS scheme based on the BFA_ANN method over the conventional UFLS, Adaptive UFLS, and the proposed method in (Laghari et al., 2015). There are two simulation times: at 10 s, when the islanding was formed, and 40 s, there are three events that will take place, which are: (1) add 1MW at bus number 1012 (referring to Figure 5.1), (2) the radiation changed from 500 W/m^2 to 200 W/m^2 and (3) outage of one of the mini-hydro generator. Table 5.10

presents the output power of the DG generators three times before islanding, after islanding at the simulation time 10 s, and after the simulation time 40s with the TLSA for each scenario. All of these scenarios will be discussed below:

Table 5.10: Active power of all indices for case 2 all scenarios

Active Power			Before Islanding (MW)	After Islanding at *t* = 10 s (MW)	After new imbalance at *t* = 40 s (MW)
P_{gen}	P_{grid}	A*	1.04	0.00	0.00
		B*			
		C*			
	P_{PV}	A*	0.98	0.98	0.877
		B*	0.98	0.98	0.451
		C*	0.98	0.98	0.98
	P_{Wind}	A*	0.48	0.48	0.48
		B*			
		C*			
	$P_{hydro}\times 2$	A*	1.712×2	1.80×2	1.80×2
		B*	1.712×2	1.80×2	1.80×2
		C*	1.712×2	1.80×2	1.80×1
TLSA	A*		0.00	0.864	0.864+1=1.864
	B*		0.00	0.864	0.864+0.53=1.394
	C*		0.00	0.864	0.864+1.8=2.664

*A, B, and C represent three scenarios in case 2, which are: add 1MW, change the radiation from 500W/m^2 to 200W/m^2, and outage of one mini-hydro generator, respectively.

(a) ***Intentional islanding at 1.04 MW imbalance power***

In this case, the intentional islanding occurred at t = 10 s in the three scenarios, when the solar radiation is 500 W/m^2 and wind speed is 10 m/s. Immediately after islanding, the frequency of the system starts to decline in response to excess loads (1.04 MW). Accordingly, the spinning reserve (0.18 MW) of the two mini-hydro generators were used, and it should be noted that this value does not affect the unbalance of power. In order to restore the system's frequency, all techniques of load shedding will be initiated. Table 5.10 shows the output power of all DGs in network and the total load shed amount

(TLSA) for three scenarios: before islanding, after islanding, and after a new imbalance power occurrence during the islanding mode. However, Tables 5.11, 5.12, and 5.13 show that the conventional UFLS sheds amount load more than TLSA, and more than the amount load shed in other UFLS techniques at a simulation time of 10s. For that, the system's frequency has overshoot, as shown in Figures 5.31, 5.32, and 5.33 at a simulation time of 10 s. On the other hand, the amount of load shed of UFLS method in (Laghari et al., 2015) is equal to the proposed UFLS, but the nadir frequency for the proposed UFLS method has higher value due to the time execution of the UFLS method in (Laghari et al., 2015) require more time to determine the best combination of loads.

(b) ***Scenario 1: Load increment of 1 MW occurred at 40 s after islanding***

In this scenario, the load increment occurred at t = 40 s, at a solar radiation value of 500 W/m^2 and a wind speed of 10m/s. Immediately after adding the load, the system's frequency begins to decline in response to the excess loads (1.0 MW). In this scenario, the two mini-hydro generators used their spinning reserve in the intentional islanding event at a simulation time of 10 s, and there is no spinning reserve in wind turbine and solar PV system, because it operates at its maximum power. For this reason, in order to restore the system's frequency, all load shedding techniques will be initiated. Table 5.11 shows the comparative performance for all of the load shedding techniques. It should be noted that the conventional UFLS has the maximum overshoot frequency due to the most loads being shed in the system. Contrarily, the proposed UFLS method and UFLS method in (Laghari et al., 2015) reported the minimum amount of load shedding, but the nadir frequency of the UFLS method in (Laghari et al., 2015) is less than the proposed UFLS method, as shown in Figure 5.30, due to the execution time for finding the best combination of loads being large.

Table 5.11: UFLS parameters for case 1 scenario 1

Parameter	Conventional UFLS		Adaptive UFLS		UFLS method in (Laghari et al., 2015)		Proposed UFLS	
	t =10s	t = 40s	t =10s	t = 40s	t =10s	t = 40s	t =10s	t = 40s
Total shed power (MW)	1.532	2.76	1.012	2.115	0.864	1.863	0.864	1.863
The loads that was shed	1,2,3,4,5,6	1,2,3,4,5,6,7,8	1,2,3,4,5	1,2,3,5,6,7	2,3,8	1,2,3,5,6,8	2,3,8	1,2,3,5,6,8
Nadir frequency (Hz)	48.80	48.48	48.98	49.18	49.03	48.53	49.17	49.30
Overshoot frequency (Hz)	51.79	51.17	-	50.51	-	-	-	-
Steady State Frequency (Hz)	50.012	50	50	50	-	50	50	50

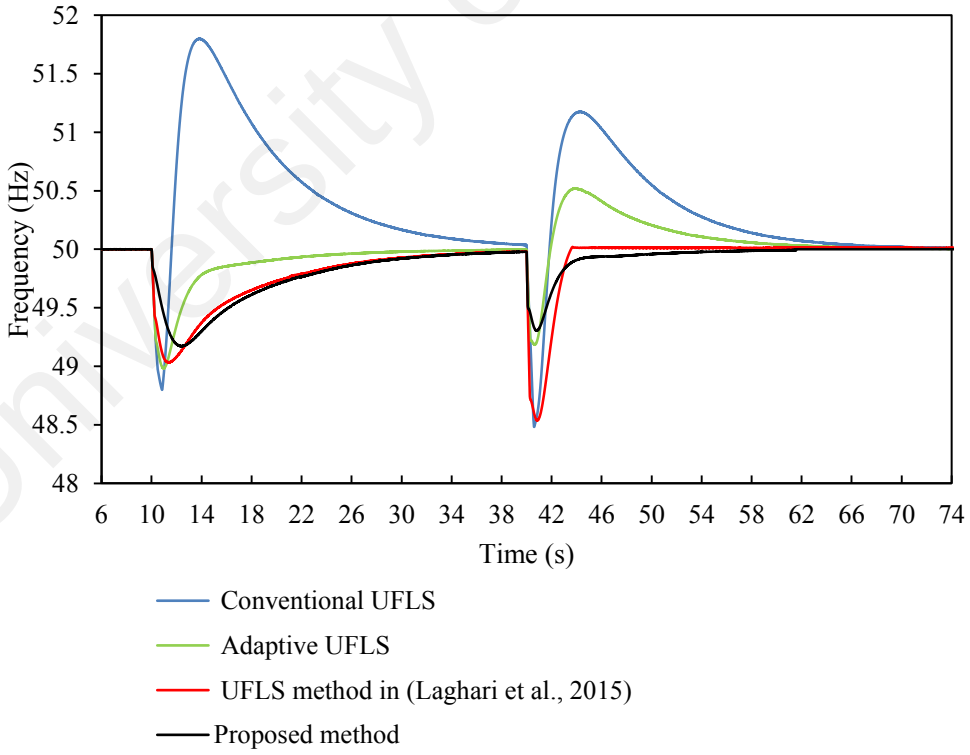

Figure 5.30: Frequency response for proposed, adaptive UFLS and conventional UFLS schemes in case 2 scenario1

(c) ***Scenario 2: Change the radiation from 500W/m^2 to 200W/m^2 at 40 s after islanding***

In this scenario, the radiation changes from 500 W/m^2 to 200 W/m^2 at t = 40 s, and the wind speed is 10 m/s. Immediately after the change in radiation, the system's frequency begins to decline in response to excess loads (0.53 MW). In this scenario, the two mini-hydro generators used their spinning reserve in intentional islanding event at a simulation time of 10 s, and there is no spinning reserve in the wind turbine and solar PV system, because it operated at its respective maximum power. For this reason, in order to restore the system's frequency, all of the load shedding techniques will be initiated. Table 5.12 shows the UFLS parameters for this scenario. However, Figure 5.31 shows that both of proposed UFLS method and the adaptive UFLS outperform on the UFLS method in (Laghari et al., 2015), in terms of the nadir frequency value. This is due to the execution time of proposed UFLS method being quicker compared to the UFLS method in (Laghari et al., 2015), and the large amount of total amount load shed for the adaptive UFLS compared to the UFLS method in (Laghari et al., 2015) as well. Moreover, the conventional UFLS shed most loads at its maximum overshoot frequency.

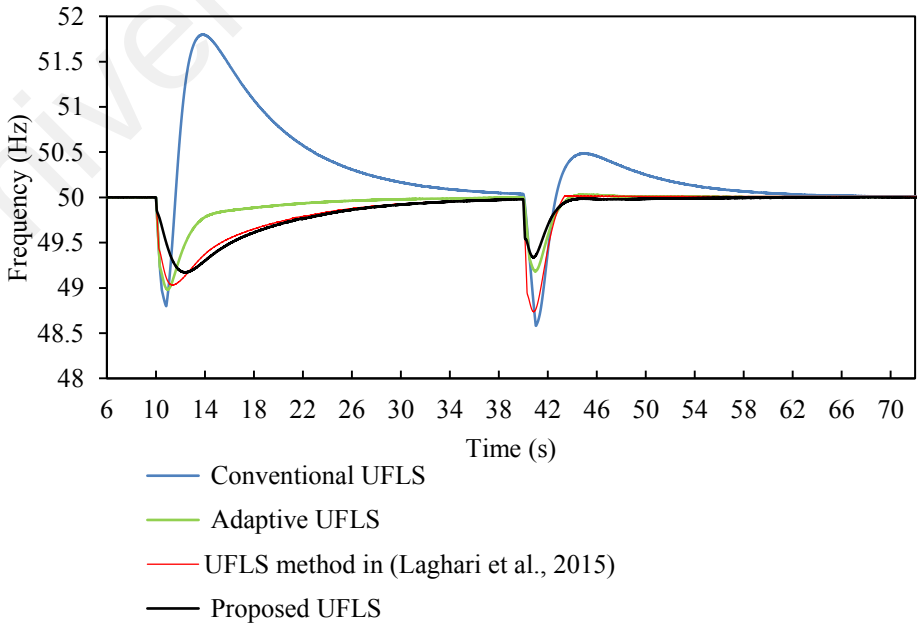

Figure 5.31: Frequency response for proposed, adaptive UFLS and conventional UFLS schemes in case 2 scenario 2

Table 5.12: UFLS parameters for case 2 scenario 2

Parameter	Conventional UFLS		Adaptive UFLS		UFLS method in (Laghari et al., 2015)		Proposed UFLS	
	t =10s	t = 40s	t =10s	t = 40s	t =10s	t = 40s	t =10s	t = 40s
Total shed power (MW)	1.532	2.115	1.012	1.532	0.864	1.349	0.864	1.349
The loads that was shed	1,2,3,4, 5,6	1,2,3,4, 5,6,7	1,2,3, 4,5	1,2,3,4, 5,6	2,3,8	4,5,8	2,3,8	4,5,8
Nadir frequency (Hz)	48.80	48.58	48.98	49.18	49.03	48.79	49.17	49.34
Overshoot frequency (Hz)	51.79	50.49	-	50.032	-	50.01	-	-
Steady State Frequency (Hz)	50.012	50	50	50	50	0	50	50

(d) ***Scenario 3: Mini-hydro DG tripping at 40 s after islanding***

In this scenario, the outage one of the mini-hydro DG occurred at t = 40 s when the solar radiation value is 500 W/m^2 and the wind speed is 10m/s. Immediately after adding the load, the system's frequency begins to decline in response to excess loads (1.8 MW). In this scenario, the mini-hydro generators used their spinning reserve in the intentional islanding event at a simulation time of 10 s, and there is no spinning reserve in the wind turbine and solar PV system, because it operates at their respective maximum power. In order to restore the system's frequency, all of the load shedding techniques will be initiated. Table 5.13 shows the UFLS parameters for this scenario. Figure 5.32 shows that the conventional and adaptive UFLS schemes failing to prevent the system frequency from shooting over 52.5 Hz after the mini-hydro DG tripping, which lead to all protection devices being activated and causing a total blackout. In fact, the large amount of load shedding is the main reason for frequency overshoot, and then protection failure. The UFLS method in (Laghari et al., 2015) has the minimum nadir frequency and the proposed UFLS has the best value of nadir frequency, as illustrated in Table 5.13.

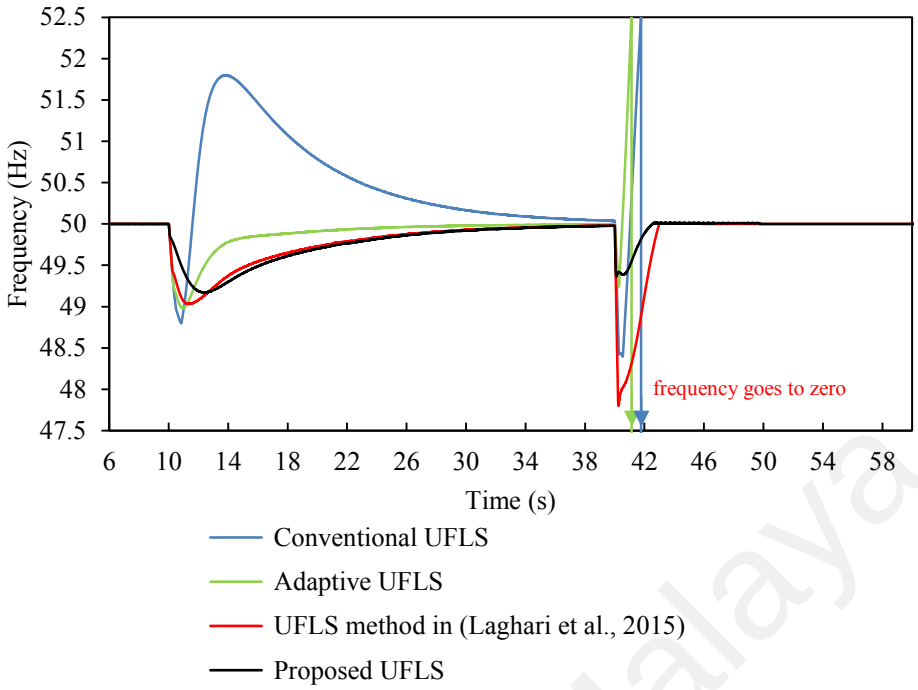

Figure 5.32: Frequency response for proposed, adaptive UFLS and conventional UFLS schemes in case 2 scenario 3

Table 5.13: UFLS parameters for case 2 scenario 3

Parameter	Conventional UFLS		Adaptive UFLS		UFLS method in (Laghari et al., 2015)		Proposed UFLS	
	t =10s	t = 40s	t =10s	t = 40s	t =10s	t = 40s	t =10s	t = 40s
Total shed power (MW)	1.532	3.578	1.012	3.578	0.868	2.667	0.868	2.667
The loads that was shed	1,2,3,4,5,6	1,2,3,4,5,6,7,8,9	1,2,3,4,5	1,2,3,4,5,6,7,8,9	2,3,8	1,2,4,5,8,9,10,11	2,3,8	1,2,4,5,8,9,10,11
Nadir frequency (Hz)	48.80	48.46	49.03	48.74	49.03	47.8	49.17	49.36
Overshoot frequency (Hz)	51.79	Up 52.5	-	Up 52.5	-	50.16	-	-
Steady State Frequency (Hz)	50.012	collapse	50	collapse	50	50	50	50

It is clear that the load shedding controller with fixed priority loads in both conventional and adaptive UFLS schemes cannot shed the optimal amount of loads, as discussed previously. On the other hand, the load shedding controller that uses random loads, similar to the UFLS proposed in (Laghari et al., 2015) and the proposed UFLS method have the ability to shed the optimal combination of loads. However, the UFLS proposed in (Laghari et al., 2015) still suffers from time delay, which effects the operation of the load shedding controller. This comparative study shows that the BFA-ANN technique shed the optimal combination of loads compared with the conventional and adaptive UFLS schemes, and is quicker compared with the proposed method in (Laghari et al., 2015). Accordingly, the BFA-ANN technique was selected to be used with the UFLS scheme in order to shed the optimal loads combination from the islanding distribution network.

5.2.6.3 Case 3: aims to show the effect of using a combined method of a de-loading technique in RESs and proposed UFLS technique

Islanding occurs when the utility grid is disconnected from the distribution network. The islanding event was simulated at t = 10 s. The power imbalance in this case is (-1.19 MW), since the distribution network was supplying the grid with 1.19 MW prior to islanding. An excess of power supplied by the DGs increased the system's frequency following islanding, since the generation power exceeds the total load. Losing the main grid forces the DGs to take over the generation from the grid to avoid over frequency. The active power dispatches are detailed in Table 5.14. Note that all the remaining loads are connected to the network without the application of the load-shedding scheme. In this case, the three solar PV unit was used to showcase the performance of the high penetration of power in the distribution network.

Table 5.14: Active power of all indices for case 3

Active Power	Before Islanding (MW)		After Islanding at t = 10 s (MW)	After addition 3 MW at t = 40 s (MW)
$\mathbf{P_{gen}}$	P_{grid}	-1.19	0.00	0.00
	P_{PV}	2.4	1.276	2.4
	P_{Wind}	1.305	1.305	1.453
	$P_{hydro}\times2$	1.715×2	1.724×2	1.80×2
TLSA	0.00		0.0	1.559

Meanwhile, at a simulation time of 40s, the 3 MW extra load was suddenly added to distribution network. In this case, the output of solar PV units, two mini-hydro generation, and wind turbine increased to 2.4 MW, 3.7 MW, and 1.453 MW, respectively, which represent their respective maximum output power to compensate for the power deficit, as shown in Figure 5.33. In this scenario, the performance of the utilization of the de-loading technique was analyzed. It should also be pointed out that the proposed UFLS scheme was activated because the system's frequency falls under 49.5 Hz. The distribution network curtailed loads number 1, 2, 5, 6, 10 and 11, based on the proposed UFLS scheme. Eventually, the system's frequency recovers and approaches its reference value. Figure 5.34 illustrates the system's frequency under different UFLS techniques. It can be noted from Table 5.15 that the proposed method has the best nadir frequency with optimum load shedding. Despite the adaptive UFLS having the least load shed, it did not report the best nadir frequency. The proposed method in (Laghari et al., 2015) has a similar load shedding such as that of the proposed method, but its execution time to find all combination probability and determine the best combination load that achieves a minimum error between the TLSA and the total load combination is longer relative to the proposed method.

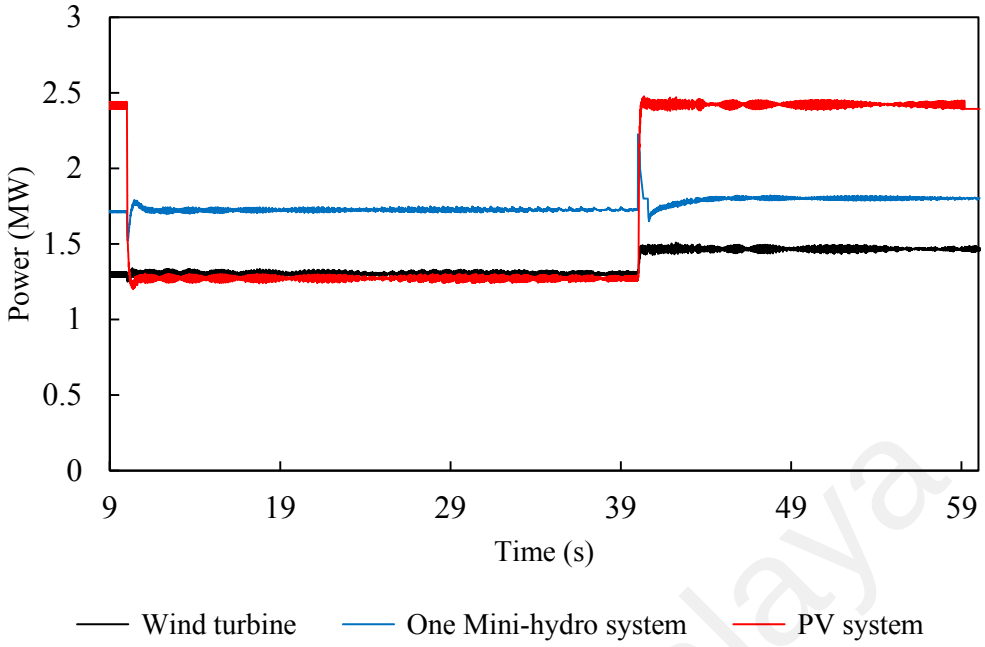

Figure 5.33: The output power of DGs when using a de-loading technique and proposed UFLS method in case 3

Figure 5.34 shows that the UFLS method in (Laghari et al., 2015) failed to prevent the system's frequency from dropping below 47.5 Hz after islanding, which leads to a total blackout. In fact, the large execution time of UFLS method in (Laghari et al., 2015) is the main reason for protection failure. Table 5.15 shows the performance of all the UFLS methods applied in this scenario. It can be noted that the proposed UFLS can fulfill the minimum amount of load shed with a small excitation time to calculate the best combination of loads to be shed from the system in order to restore the frequency to its reference value without overshooting.

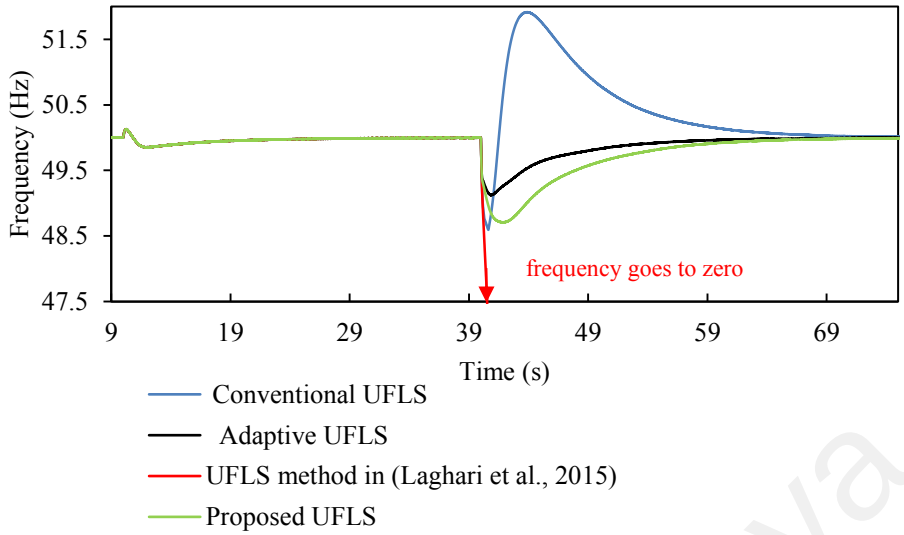

Figure 5.34: Using a de-loading technique and proposed UFLS method in case 3

Table 5.15: UFLS parameters for case 3

Parameter	Conventional UFLS		Adaptive UFLS		UFLS method in (Laghari et al., 2015)		Proposed UFLS	
	t=10s	t=40s	t=10s	t=40s	t=10s	t=40s	t=10s	t=40s
Total shed power (MW)	-	2.115	-	1.532	-	1.558	-	1.558
The loads that is shed	-	1,2,3,4,5,6,7	-	1,2,3,4,5,6	-	1,2,5,6,10,11	-	1,2,5,6,10,11
Nadir frequency (Hz)	49.85	48.59	49.85	48.93	49.85	collapse	49.85	49.09
Overshoot frequency (Hz)	50.12	51.91	50.12	-	50.12	-	50.12	-
Steady State Frequency (Hz)	50	50	50	50	50	0	50	50

5.3 Summary

This chapter discussed the modelling of the distribution network in the PSCAD/EMTDC software that was used to validate the proposed UFLS scheme-I. The effectiveness and robustness of this technique was investigated on a 29-Bus test system for islanding events, DG tripping event, and load increments. Through the simulation

results, it was proven that the proposed UFLS technique shed the optimal combination of loads relative to the conventional and adaptive techniques. This was achieved via the combined metaheuristic method (FA) and ANN technique, with flexibility towards load shedding priority. Accordingly, the proposed UFLS technique can restore the network frequency without overshooting. Also, the modified active power controller of PV system and pitch control angle in wind turbine were used to release the reserve power at under frequency events. Due to this, using the proposed UFLS scheme-I with a de-loading technique ensures high reliability in maintaining the stability of the frequency in the real distribution network.

CHAPTER 6: PERFORMANCE OF THE PROPOSED UFLS SCHEME-II IN OPERATION MODE

6.1 Introduction

The main difference between the proposed UFLS scheme-I and II and the load shedding in the proposed UFLS scheme-II is distributed in four steps, and can detect and estimate any power changes during the load shedding process.

This chapter validates the proposed UFLS scheme-II using various case studies, such as islanding, DG tripping, load increments, and changed wind speed during load shedding process. Furthermore, the proposed UFLS scheme-II will be compared with other UFLS methods in order to confirm its ability in shedding the optimal amount of loads from the distribution network.

6.2 Test system modeling for proposed UFLS scheme-II

The test system was a modified IEEE 33 bus radial distribution network with an additional three DG units, as shown in Figure 6.1. Table 6.1 detail the type of DGs, locations, and their corresponding active power rating. The network structure and DG location were selected based on (Rao, Ravindra, Satish, & Narasimham, 2013). The three DG are a two-mini-hydro power generator and a Full Converter Wind Turbine (FCWT). The rank of load priority percentage is shown in Table 6.2 by listing their respective percentages of load power that should be connected to the distribution network at each bus (Khamis et al., 2015). The loads that are connected to each bus were divided into two groups; one was connected to the loads that can be curtailed from a bus by a remote circuit breaker (RCB), while the other was connected to loads that cannot be curtailed from a bus, as shown in Figure 6.1. The load's remote circuit breaker (RCB) in the modelled system were linked to digital inputs of load shed controller via wireless communication,

and when the digital input was energized, the RCB opens and trips that load, and when the input was de-energized, the RCB stays closed.

Table 6.1: Rated power of DGs

DG no.	Bus no.	DG Type	Active power rating (MW)
1	31	FCWT	0.565
2	32	Mini-Hydro	0.532
3	33	Mini- Hydro	0.591

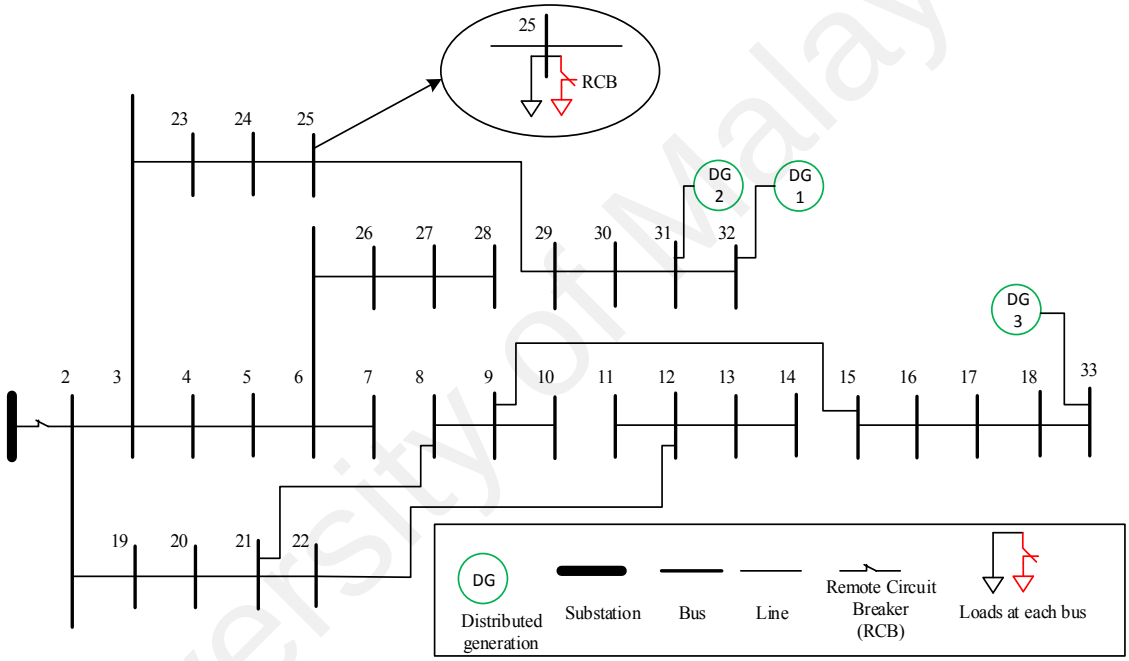

Figure 6.1: Modified IEEE 33 bus test system

An FCWT was used in this work for primary frequency control. Without the ancillary frequency control, FCWT operates based on the active power reference provided by the MPPT control. The active power reserve by FCWT was used to provide the ancillary frequency. To fulfil that need, a 10% de-loading power tracking was applied to the wind turbine.

A modified pitch angle controller was used to force the FCWT into the de-loading mode by adding an angle increment ($\Delta\beta$), as described in Chapter 3. Moreover, the control

frequency regulation was applied to the generator side converter. It can be divided into two controllers: inertia and droop. Both emulated the inertial response behavior and speed governor in synchronous generators. The output of the active power reference for both the inertia and droop controllers were proportional to the derivative of the system frequency and absolute difference between the system's frequencies with its respective reference values. Figure 6.2 shows the controller of the under frequency loop for FCWT.

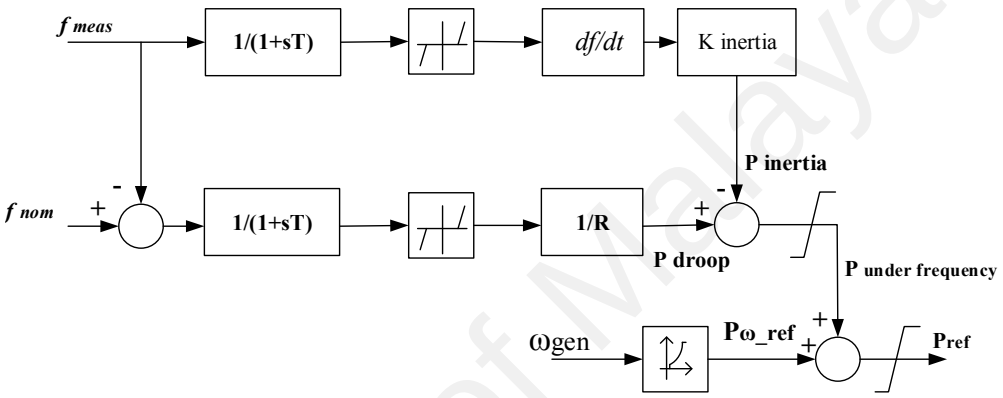

Figure 6.2: Ancillary under frequency control loop for FCWTs consists of inertia and droop controller (Liu & Chen, 2015)

Table 6.2: Priority bus and their load priority percentage at each bus for IEEE 33-bus radial distribution system limits and thresholds frequencies for conventional UFLS

Load Ranked	F_{TH} (Hz)	Bus Number	(%)	Load Ranked	F_{TH} (Hz)	Bus Number	(%)
1	49.5	2	34	**18**	49.0	19	60
2		3	4	**19**	48.9	20	53
3		4	64	**20**	48.8	21	20
4	49.4	5	15	**21**	48.7	22	50
5		6	43	**22**	48.6	23	4
6		7	35	**23**	48.5	24	15
7	49.3	8	21	**24**	48.4	25	10
8		9	5	**25**	48.3	26	59
9		10	21	**26**	48.2	27	2
10	49.2	11	0	**27**	48.1	28	28
11		12	52	**28**	48.0	29	15
12		13	11	**29**	47.9	30	55
13	49.1	14	47	**30**	47.8	31	25
14		15	57	**31**	47.7	32	30
15		16	61	**32**	47.6	33	3
16	49.0	17	37	-	-	-	-
17		18	34	-	-	-	-

6.3 Simulation Results

The proposed UFLS scheme-II was tested to verify its effectiveness by comparing it with (1) the proposed UFLS scheme-II without using the PSO algorithm, (2) conventional UFLS scheme, (3) adaptive UFLS scheme in (Karimi et al., 2017), (4) UFLS method in (Ketabi & Fini, 2015) with PSO algorithm, and (5) adaptive UFLS method in (Laghari et al., 2015). In UFLS method (3), load shedding is distributed in four steps at four frequency thresholds, as pointed out in the proposed technique methodology. The load shedding process in UFLS method (3) stops when the power deficit is equal to or less than 0.1 MW. Table 6.2 presents the amount of load to be shed at each frequency threshold in a conventional 21-step UFLS scheme. The proposed UFLS scheme-II should be able to cope with any sudden power deficit that might occur during the load shedding process and prevent any overshoot/undershoot frequencies. Four cases were considered: 1)

islanding operation of the distribution network; 2) applied disturbance on the system (overload); 3) the loss of one of the main generator in the system; 4) changes in wind speed. The last three cases occur during load shedding caused from the islanding case and at different times during load shedding.

6.3.1 Case 1: Islanding Operation of distribution network

This case involves simulating the islanding operation of the distribution network. The total load demand prior to islanding was 3.715 MW. The Grid and DGs supply the distribution network with 2.17 MW and 1.688 MW of active power, respectively. Due to islanding, the imbalance of power between generation and demand occurred, leading to a decrease in the system's frequency to a value lower than the allowed limits. In order to prevent this, the process starts shedding portions of loads to balance power generation and load demands. This event is simulated at time =10.0 s when it receives a 2.17 MW from the utility grid. The response of the proposed UFLS technique with/without PSO, adaptive UFLS, and conventional UFLS in the islanding mode are shown in Figure 6.3. It can be seen in Figure 6.3 that the proposed UFLS without PSO and adaptive UFLS in (Karimi et al., 2017) reported similar results, which is attributed to the proposed technique solving the power deficit after islanding and during load shedding. The proposed load shedding technique continuously check whether the distribution network has been islanded by checking the status of the incoming grid substation breaker, which is connected to the grid and distribution networks.

In the proposed load shedding technique, there are two strategies; (1) event based, and (2) response based to determine the amount of loads needed to be shed. The proposed method will have to decide on the right strategies based on the ROCOF and breaker status at the grids and generators. The response-based strategy was used to address the changes of frequency due to the sudden increment of load in an islanded system. The UFLS

method in (Ketabi & Fini, 2015) only used the ROCOF to determine the power deficit in the system. Due to this, the power deficit estimation was inaccurate. The UFLS method in (Laghari et al., 2015) also failed to shed the loads before the system frequency falls below 47.5 Hz, resulting in the activation of protection relays. Moreover, the lengthy time delay was due to the determination of all possible combinations of random priority loads, which might lead to power system blackouts. The results of this case are tabulated in Table 6.3.

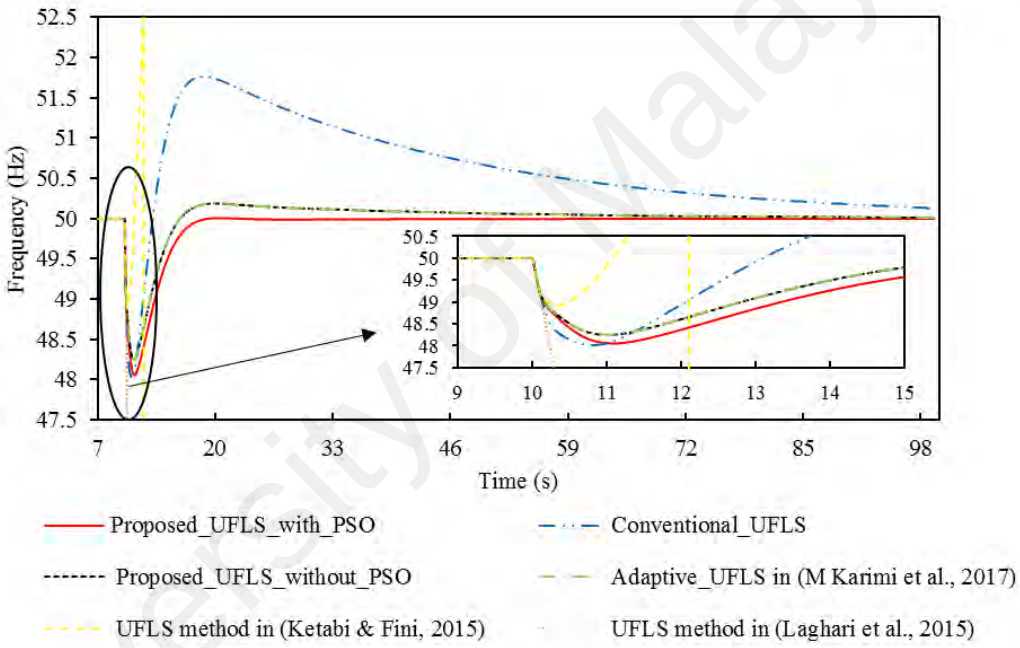

Figure 6.3: Frequency response for proposed UFLS with/without PSO, adaptive UFLS in (Karimi et al., 2017), conventional UFLS, UFLS method in (Ketabi & Fini, 2015) and UFLS method in (Laghari et al., 2015) schemes in case 1

Table 6.3: UFLS parameters for case 1

Parameter	Proposed UFLS with PSO	Proposed UFLS without PSO	Conventional UFLS	Adaptive UFLS in (Karimi et al., 2017)	UFLS method in (Ketabi & Fini, 2015)	UFLS method in (Laghari et al., 2015)
Reserve (MW)	0.178	0.178	0.178	0.178	0.178	0.178
Total shed Power (MW)	1.99	2.016	2.13	2.016	2.50	0
Load buses which still connected with system after load shedding	8,17,24,31	26,27,28,29 30,31,32,33	29,30,31,32,33	26,27,28,29 30,31,32,33	6,7	-
Nadir Frequency (Hz)	48.06	48.2	48.1	48.2	48.9	Under 47.5
Overshoot Frequency	-	50.19	51.764	50.19	Over 52.5	-
Steady State Frequency (Hz)	49.999	50.13	50.134	50.13	0	0

6.3.2 Case 2: Applying overload During Load Shedding Process

In this case, the performance of the proposed UFLS with/without the PSO algorithm, adaptive UFLS, and conventional UFLS schemes was analyzed for the overload scenario. The distribution network in the islanding mode was suddenly added with a load of 0.2 MW and 0.05 MVar at bus 27 after the first step shedding process at a simulation time of 10.09 s. Here, the adaptive shedding technique in (Karimi et al., 2017) can only detect and estimate the first power deficit (islanding action) occurring at a simulation time of 10s, but it is incapable of detecting the second power deficit caused by the addition of an extra load. The frequency system drops to 47.5 Hz, and the controller trips-off all of the

DGs. The conventional UFLS scheme can sense the declination of the frequency of the system. When the frequency of the system reaches a new threshold, the conventional UFLS controller shed more loads until it stops decreasing the frequency of the system.

It can be seen in Figure 6.4 that the frequency in the conventional UFLS scheme and UFLS method (Ketabi & Fini, 2015) overshot, which shows that the controllers have shed more load than required. The proposed technique can detect a new power imbalance in the system by monitoring the overshot signal of the second frequency derivative and estimate the second deficit power. It is clear from Figure 6.4 that the proposed UFLS perform well and prevents the frequency from decreasing to levels below the permissible limit, such as the adaptive UFLS, while its nadir frequency exceeds that of the conventional UFLS scheme. The usage of the PSO algorithm with the proposed UFLS resulted in better values than the proposed UFLS without the PSO algorithm. Table 6.4 shows the total load shed and other parameters pertaining to this case. To demonstrate the performance of the proposed UFLS method with PSO, the simulation was repeated with another extra load, which was suddenly added to bus 27 for testing. The value of the new extra load was 0.4 MW. It can be seen in Figure 6.5 that the proposed UFLS method with PSO can only maintain the system's frequency within allowable limits. Table 6.5 illustrates the total load shed and other parameters pertaining to this case.

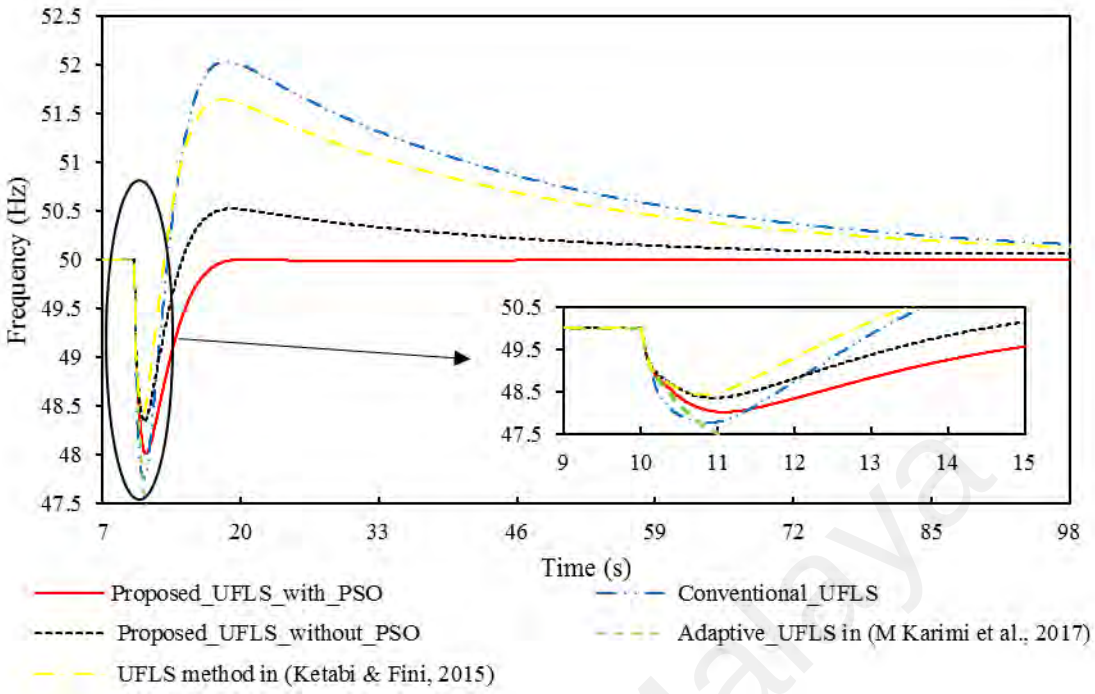

Figure 6.4: Frequency response for proposed UFLS with/without PSO, adaptive UFLS in (Karimi et al., 2017), conventional UFLS and UFLS method in (Ketabi & Fini, 2015) schemes in case 2 when adding 0.2 MW extra load

Table 6.4: UFLS parameters for case 2 when adding 0.2 MW after islanding event and during load shedding process

Parameter	Proposed UFLS with PSO	Proposed UFLS without PSO	Conventional UFLS	Adaptive UFLS in (Karimi et al., 2017)	UFLS method in (Ketabi & Fini, 2015)
Total shed Power (MW)	2.184	2.233	2.325	2.016	2.3
Load buses which still connected with system after load shedding	15,21,25	30,31,32,33	31,32,33	26,27,28,29 30,31,32,33	24
Nadir Frequency (Hz)	48.01	48.345	47.756	Under 47.5	48.43
Overshoot Frequency	-	50.52	52.03	-	51.64
Steady State Frequency (Hz)	49.995	50.07	50.15	0	50.1

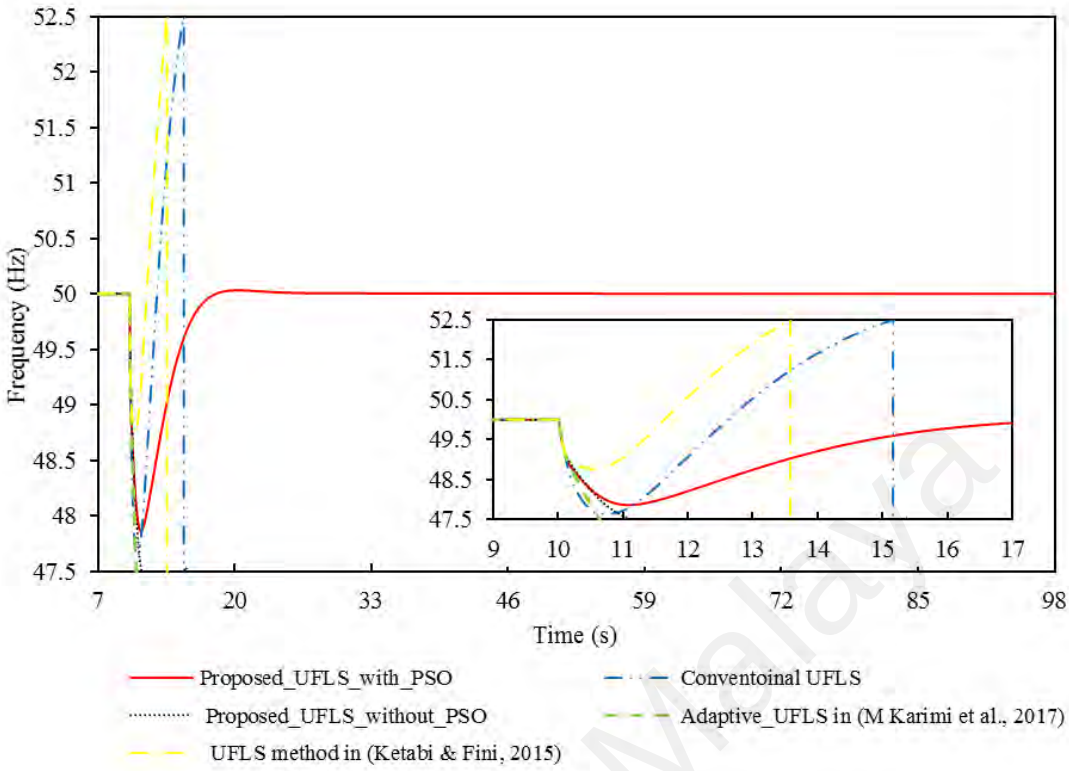

Figure 6.5: Frequency response for proposed UFLS with/without PSO, adaptive UFLS in (Karimi et al., 2017), conventional UFLS and UFLS method in (Ketabi & Fini, 2015) schemes in case 2 when adding 0.4 MW extra load

Table 6.5: UFLS parameters for case 2 when adding 0.4 MW after islanding event and during load shedding process

Parameter	Proposed UFLS with PSO	Proposed UFLS without PSO	Conventional UFLS	Adaptive UFLS in (Karimi et al., 2017)	UFLS Method in (Ketabi & Fini, 2015)
Total shed Power (MW)	2.42	2.23	2.6	2.016	2.61
Load buses which still connected with system after load shedding	16,17,23,26, 33	30,31,32,33	33	26,27,28,29 30,31,32,33	22
Nadir Frequency (Hz)	47.8	Under 47.5	47.67	Under 47.5	48.8
Overshoot Frequency	50.3	-	Over 52.5	-	Over 52.5
Steady State Frequency (Hz)	50.0	0	0	0	0

6.3.3 Case 3: Outage of One DG during load shedding

The loss of DG in the distribution network was due to disconnecting DG_1 in the simulation in order to test the effectiveness of the proposed UFLS scheme relative to other UFLS schemes. The UFLS process starts at t=10.0 s, followed by the tripping of DG_1 at t =10.11 s. DG_1 was supplying a power of 0.56 MW to the system. Figure 6.6 illustrates the ability of the proposed UFLS with the PSO algorithm to deal with the additional imbalance of power during load shedding by disconnecting a suitable amount of load. Due to the implementation of load shedding, the system frequency begins recovering. However, the frequency of the system needs some time to recover to its previously set values due to the slow response of the mini hydro generator. Contrarily, the adaptive

UFLS scheme was unable to recognize the additional power deficit and prevent the system from collapsing.

Furthermore, the proposed UFLS without the PSO algorithm was unable to shed all of the extra loads determined by the proposed UFLS after a new imbalance of power, because the choice of loads that would be shed depends on the fixed load priority, as shown in Table 6.6. Thus, the controller cannot shed the appropriate amounts of loads, and was unable to prevent the frequency system from decreasing to lower than 47.5 Hz. On the other hand, the conventional UFLS scheme prevents the system from blackout via shedding, but its nadir frequency value is less than that of the proposed UFLS scheme with the PSO algorithm. Furthermore, the amount of load shedding in the conventional algorithm exceeds that of the other UFLS schemes. The UFLS method in (Ketabi & Fini, 2015) was also unable to determine the accurate value of the new power deficit that is noticeable from the frequency overshoot in Figure 6.6. Table 6.6 shows the parameters of the UFLS schemes pertaining to this case. Table 6.6 also shows the proposed UFLS with PSO not shedding the lowest amount of loads when compared to the proposed UFLS without the PSO and adaptive UFLS in (Karimi et al., 2017). In that case, the distribution network goes towards blackout immediately when the system frequency is less than 47.5 Hz. This means that the amount of load shedding is inadequate to prevent a drop-in frequency. Thus, in order to realize the optimum load shedding, it is not necessary to remove the lesser load curtailment.

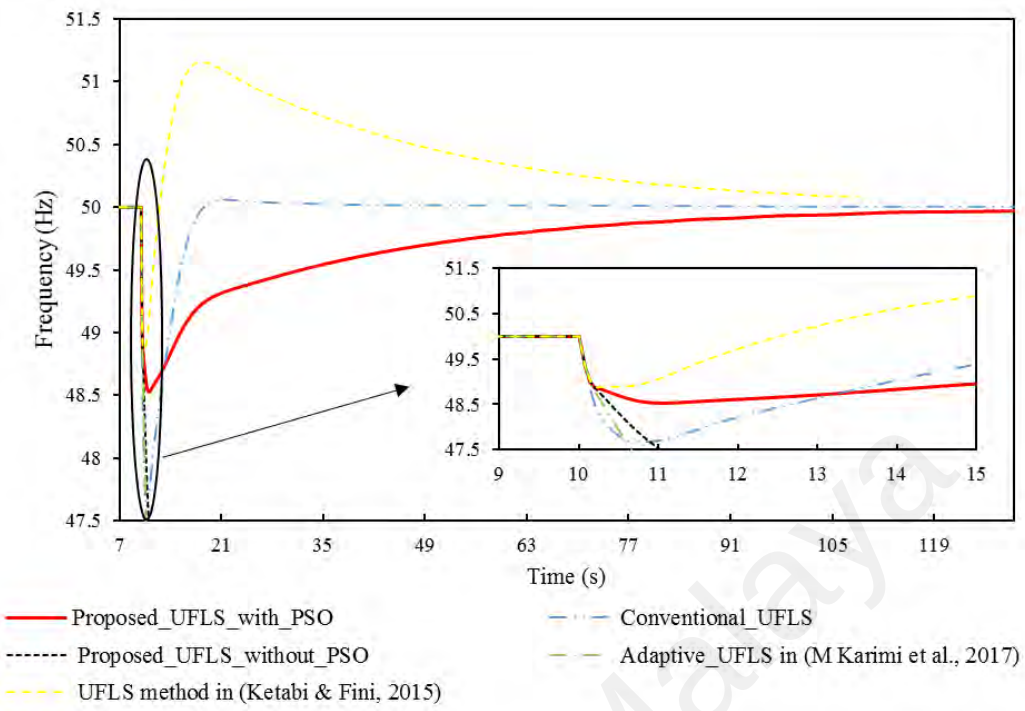

Figure 6.6: Frequency response for proposed UFLS with/without PSO, adaptive UFLS in (Karimi et al., 2017), conventional UFLS, UFLS method in (Ketabi & Fini, 2015) and UFLS method in (Laghari et al., 2015) schemes in case 3

Table 6.6: UFLS parameters for case 3

Parameter	Proposed UFLS with PSO	Proposed UFLS without PSO	Conventional UFLS	Adaptive UFLS in (Karimi et al., 2017)	UFLS Method in (Ketabi & Fini, 2015)
Total shed Power (MW)	2.543	2.444	2.60	2.016	2.66
Load buses which still connected with system after load shedding	31	30,31,32,33	33	26,27,28,29 30,31,32,33	-
Nadir Frequency (Hz)	48.527	Under 47.5	47.67	Under 47.5	48.87
Overshoot Frequency	-	-	50.059	-	51.15
Steady State Frequency (Hz)	49.998	0	50.06	0	50.07

6.3.4 Case 4: Change of wind speed During Load Shedding Process

The amount of power generated from the FCWT essentially depends on the wind speed. Therefore, a sudden change in the wind speed during load shedding affects the FCWT's output power. In this case, FCWT power was reduced to 0.28 MW due to an abrupt decrease in wind speed at 10.14s after the third step of the UFLS process. The proposed UFLS with the PSO algorithm was tested for this case, and its response was compared with the performance of the proposed UFLS without the PSO algorithm and the adaptive and conventional UFLS schemes. The UFLS process started at a 10 s consequence of the islanding mode. It can be seen in Figure 6.7 that the system frequency for all UFLS schemes decrease as a result of the decrease in power in FCWT.

It can also be noticed that the drop in the FCWT power cannot be realized by the adaptive UFLS scheme in (Karimi et al., 2017). Therefore, the frequency could not remain within the permissible limits, and fall under 47.5 Hz. The proposed UFLS scheme without the PSO algorithm is able to update the amount of load that needs to be shed due to a sudden decrease in wind speed, which will allow it to prevent the frequency from falling under a predetermined limit. Nevertheless, due to the absence of the PSO algorithm in selecting the loads to be shed, the controller unit disconnects all of the DGs in the distribution network. The higher amount of load shed occurred due to fixed load priority in the load shedding scheme. Consequently, it increased the system's frequency to over 52.5 Hz. The conventional UFLS scheme can keep the system's frequency within permissible limits, but its nadir frequency value is less than the proposed UFLS with the PSO algorithm. Moreover, Figure 6.7 shows that the system's frequency response of the UFLS with the PSO algorithm reaching the steady state value faster than the conventional UFLS scheme. The proposed UFLS method in (Ketabi & Fini, 2015) shed 2.66 MW of loads, which increased the system's frequency to over 52.5 Hz and activated the protection

relays, leading to blackouts. Table 6.7 shows the parameters of the UFLS schemes of this case.

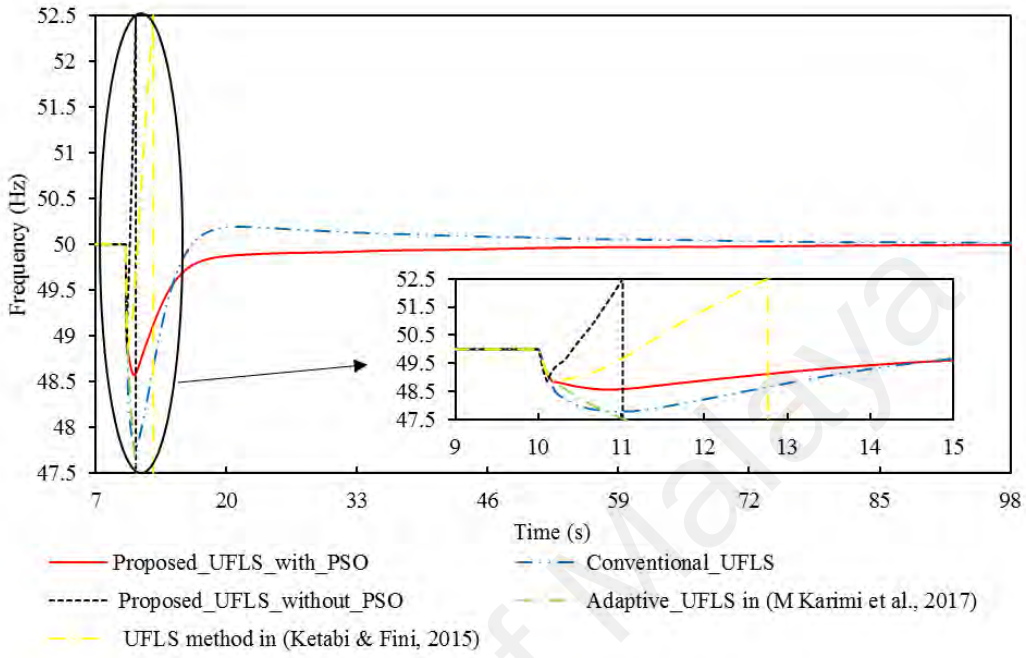

Figure 6.7: Frequency response for proposed UFLS with/without PSO, adaptive UFLS in (Karimi et al., 2017), conventional UFLS, UFLS method in (Ketabi & Fini, 2015) and UFLS method in (Laghari et al., 2015) schemes in case 4

Table 6.7: UFLS parameters for case 4

Parameter	Proposed UFLS with PSO	Proposed UFLS without PSO	Conventional UFLS	Adaptive UFLS in (Karimi et al., 2017)	UFLS Method in (Ketabi & Fini, 2015)
Total shed Power (MW)	2.33	2.662	2.325	2.016	2.60
Load buses which still connected with system after load shedding	8,23,30	-	31,32,33	26,27,28,29 30,31,32,33	6,16
Nadir Frequency (Hz)	48.573	0	47.788	Under 47.5	48.89
Overshoot Frequency	-	Over 52.5	50.188	-	Over 52.5
Steady State Frequency (Hz)	49.99	0	50.016	0	0

6.4 Summary

The UFLS scheme-II based on detecting and updating the estimated new power deficit during load shedding has been validated in this chapter. The proposed method can detect and estimate the power changes in the system. The PSO algorithm was used to determine the optimum loads at each shedding steps. The effectiveness of the proposed scheme has been investigated on an intentional islanding case, load increment case during load shedding, outage one DG during load shedding process, a decrease in wind speed during load shedding, and reduction in FCWT power at different times during load shedding. The system's frequency and amount of load shedding of the proposed UFLS with PSO algorithm were compared with the proposed UFLS without PSO algorithm, conventional UFLS, adaptive UFLS in (Karimi et al., 2017), UFLS method in (Laghari et al., 2015) and adaptive UFLS method in (Ketabi & Fini, 2015). The simulation results of the proposed method confirmed its capability of updating the estimation total imbalance of

power and the determination of the optimal load shed in each load shedding steps. Moreover, it can prevent the system's frequency from decreasing to levels below the allowable limit and overshooting.

CHAPTER 7: CONCLUSION & FUTURE WORK

7.1 Conclusion

The four main objectives of this research, as outlined in Chapter 1, have been met. The following describes the outcome for each objective:

A metaheuristic technique was used in the planning UFLS scheme after the intentional islanding mode in order to balance the active power between the demand and distributed generation in a distribution network. For that, the proposed optimal load shedding technique was based on the combination of the firefly algorithm and particle swarm optimization algorithm. The hybrid optimization of the algorithms aimed to maximize the amount of load remaining and simultaneously maximize voltage stability index in the distribution network. In this study, the Stability Index (SI) was used as an indicator to determine the load bus, which has the tendency to experience voltage collapse. To assess the capabilities of the proposed method, the IEEE 33-bus radial distribution system with different types of DGs was used. The effectiveness of the proposed method was tested with/without considering the load priority limit. The proposed method can retain the system's stability and prevent it from a complete blackout in two tested cases. The results of the proposed hybrid method were also compared with the FA, PSO, EP, and GSA optimization techniques. The comparison showed that the proposed method achieved the best maximum load remaining and simultaneously improved the voltage profile of the islanded system.

A coordination of de-loading technique for RESs (wind turbine, PV system) and optimal under frequency load shedding (UFLS) scheme-I in operation mode was used in order to solve the instability frequency in islanded distribution networks. This technique aimed to maintain the stability of the system's frequency by selecting the optimal amount of load curtailment. The de-loading technique comprises of two controllers: (i) Active

Power Controller (APC) for solar PV units, and (ii) Modified pitch angle controller for the wind turbine. Whenever the primary frequency controller is unable to handle power deficit, the proposed UFLS-I controller will be activated. The proposed UFLS scheme-I used a Binary Firefly Algorithm (BFA) and Artificial Neural Network (ANN). The former was used in two stages; one is to frame the optimization model and the other stage is to generate a data set for developing the ANN based intelligent load shedding model. The appropriate buses for load shedding were selected based on the minimum error between the sum of the best combination loads to be shed and the total amount of load shedding. The performance of the proposed techniques was validated using one of the Malaysian distribution network. The results of the proposed hybrid method were compared with the conventional, adaptive UFLS schemes, and UFLS method was used by (Laghari et al., 2015). The comparison confirmed that the proposed method achieved less load shedding with the ability to recover the network frequency to nominal value without any overshooting. In addition, the modified active power controller for the PV system and pitch control angle in the wind turbine was used to release the reserve power at under frequency events. Due to this, using the proposed UFLS scheme-I with a de-loading technique ensures high reliability in maintaining the stability of the frequency in real distribution networks.

This thesis discussed the variations in power generated by renewable energy systems that is integrated with distributed power system, adding sudden extra load to the system and disconnected generator during the load shedding process. This issue was solved by detecting and estimating a new power deficit resulting from previous changes. The proposed method was based on detecting the new power imbalance by monitoring the frequency second derivative of overshoot of center of inertia and estimating the new power deficit during the load shedding process. Since the inertia constant is the only parameter being considered in estimating the power imbalance, the inertia constant was

estimated when any disturbance might occur during the load shedding process. This technique was integrated in the UFLS scheme-II method in order to realize any power changes during the shedding process.

On the other hand, the total load shed amount (TLSA) in the UFLS scheme-II was distributed in four shedding steps according to the following threshold frequencies: 49.5, 49.2, 48.9, and 48.6 Hz. The load shed amount for these frequency thresholds were set to 35%, 30%, 20%, and 15% of the TLSA, respectively. The combination methods between detecting and estimating new power deficits during the shedding process with UFLS scheme-II aimed to determine the exact imbalance of power and select the optimal combination of loads to shed where the total amount of load combination is the closest to the amount of TLSA that was determined in the system. In order to achieve this, the proposed UFLS scheme-II used the PSO technique. The system's frequency and the amount of load shedding of the proposed UFLS scheme-II with the PSO algorithm were compared with the proposed UFLS-II without the PSO algorithm, conventional UFLS, the adaptive UFLS used by (Karimi et al., 2017), the UFLS method used by (Laghari et al., 2015), and the adaptive UFLS method used by (Ketabi & Fini, 2015) in different cases. The simulation results of the proposed method confirmed its capability of updating the estimated total imbalance of power and the determination of the optimal load shed in each load shedding steps. Moreover, it has the ability to prevent the system's frequency from decreasing to levels below the allowable limit and overshooting. Thus, the proposed UFLS scheme-II was more effective and robust in case of any changes in the power generated of the RES-DG and load increment event during load shedding process in islanding distribution network.

7.2 Future Work

This research proposes a frequency control scheme for the islanded distribution network with DG penetration. To improve the proposed research, the following are recommendations for future works:

1) It is recommended that the storage systems to provide frequency regulation services, such as Battery Storage System (BSS), hydro pumping, super-capacitor, and flywheel be studied as well.

2) The proposed load shedding controller can be combined with load restoration procedure to automatically perform the reconnection of disconnected loads.

3) The islanded distribution network is reconnected to the grid once the fault that caused the islanding has been identified and removed. This can be accomplished with the automatic grid reconnection scheme. To perform successful islanding operation of the distribution network connected with DG, the grid reconnection technique may be applied.

4) In this work, the UFLS schemes were applied for a modified IEEE 33bus distribution network and a 29-bus part of Malaysian distribution network. In future works, the researcher can use models with larger scale network. Thus, the efficiency and competency of the proposed schemes can be observed and compared.

REFERENCES

Abdullah, M. A., Yatim, A., & Tan, C. W. (2011). *A study of maximum power point tracking algorithms for wind energy system.* Paper presented at the IEEE Clean Energy and Technology (CET) Conference.

Ackermann, T. (2005). *Wind power in power systems*: John Wiley & Sons.

Ackermann, T., & Knyazkin, V. (2002). *Interaction between distributed generation and the distribution network: operation aspects.* Paper presented at the Transmission and Distribution Conference and Exhibition 2002: Asia Pacific. IEEE/PES.

Ahmad, S., Ab Kadir, M. Z. A., & Shafie, S. (2011). Current perspective of the renewable energy development in Malaysia. *Renewable and Sustainable Energy Reviews, 15*(2), 897-904.

Ahsan, M. Q., Chowdhury, A. H., Ahmed, S. S., Bhuyan, I. H., Haque, M. A., & Rahman, H. (2012). Technique to develop auto load shedding and islanding scheme to prevent power system blackout. *IEEE Transactions on Power Systems, 27*(1), 198-205.

Ahsanullah, K., Dutta, R., & Rahman, M. (2012). *Review of PM generator designs for direct-drive wind turbines.* Paper presented at the Power Engineering Conference (AUPEC), 22nd Australasian Universities.

Al-Hasawi, W. M., & El Naggar, K. M. (2002). *Optimum steady-state load-shedding scheme using genetic based algorithm.* Paper presented at the 11th Mediterranean Electrotechnical Conference, MELECON.

Ali, R., Daut, I., & Taib, S. (2012). A review on existing and future energy sources for electrical power generation in Malaysia. *Renewable and Sustainable Energy Reviews, 16*(6), 4047-4055.

Alsharafi, A. S., Besheer, A. H., & Emara, H. M. (2018). Primary Frequency Response Enhancement for Future Low Inertia Power Systems Using Hybrid Control Technique. *Energies, 11*(4), 699.

Amraee, T., Mozafari, B., & Ranjbar, A. (2006). *An improved model for optimal under voltage load shedding: particle swarm approach.* Paper presented at the IEEE Power India Conference.

Amraee, T., Ranjbar, A., & Feuillet, R. (2011). Adaptive under-voltage load shedding scheme using model predictive control. *Electric power systems research, 81*(7), 1507-1513.

Anderson, P., & Mirheydar, M. (1992). An adaptive method for setting underfrequency load shedding relays. *IEEE Transactions on Power Systems, 7*(2), 647-655.

Aponte, E. E., & Nelson, J. K. (2006). Time optimal load shedding for distributed power systems. *IEEE Transactions on Power Systems, 21*(1), 269-277.

Badran, O., Mokhlis, H., Mekhilef, S., & Dahalan, W. (2017). Multi-Objective Network Reconfiguration with Optimal DG Output Using Meta-Heuristic Search Algorithms. *Arabian Journal for Science and Engineering*, 1-14.

Baran, M. E., & Wu, F. F. (1989). Network reconfiguration in distribution systems for loss reduction and load balancing. *IEEE Transactions on Power Delivery, 4*(2), 1401-1407.

Barker, P. P., & De Mello, R. W. (2000). *Determining the impact of distributed generation on power systems. I. Radial distribution systems.* Paper presented at IEEE the Power Engineering Society Summer Meeting.

British_Petroleum. (2017). BP Statistical Review of World Energy.

Casazza, J., Casazza, J., & Delea, F. (2003). *Understanding electric power systems: an overview of the technology and the marketplace* (Vol. 13): John Wiley & Sons.

Castro, L. M., Fuerte-Esquivel, C. R., & Tovar-Hernández, J. H. (2012). Solution of power flow with automatic load-frequency control devices including wind farms. *IEEE Transactions on Power Systems, 27*(4), 2186-2195.

Chakravorty, M., & Das, D. (2001). Voltage stability analysis of radial distribution networks. *International Journal of Electrical Power & Energy Systems, 23*(2), 129-135.

Chang, L., & Wu, Z. (2011). Performance and reliability of electrical power grids under cascading failures. *International Journal of Electrical Power & Energy Systems, 33*(8), 1410-1419.

Chebbo, A., Irving, M., & Sterling, M. (1992). *Voltage collapse proximity indicator: behaviour and implications.* Paper presented at the IEE Proceedings C

(Generation, Transmission and Distribution) (Vol. 139, No. 3, pp. 241-252). IET Digital Library.

Das, D., Kothari, D., & Kalam, A. (1995). Simple and efficient method for load flow solution of radial distribution networks. *International Journal of Electrical Power & Energy Systems, 17*(5), 335-346.

De Almeida, R. G., & Lopes, J. P. (2007). Participation of doubly fed induction wind generators in system frequency regulation. *IEEE Transactions on Power Systems, 22*(3), 944-950.

De Brito, M. A. G., Galotto, L., Sampaio, L. P., e Melo, G. d. A., & Canesin, C. A. (2013). Evaluation of the main MPPT techniques for photovoltaic applications. *IEEE Transactions on Industrial Electronics, 60*(3), 1156-1167.

Delfino, B., Massucco, S., Morini, A., Scalera, P., & Silvestro, F. (2001). *Implementation and comparison of different under frequency load-shedding schemes.* Paper presented at the Power Engineering Society Summer Meeting.

Díaz-González, F., Hau, M., Sumper, A., & Gomis-Bellmunt, O. (2014). Participation of wind power plants in system frequency control: Review of grid code requirements and control methods. *Renewable and Sustainable Energy Reviews, 34*, 551-564.

Eberhart, R., & Kennedy, J. (1995). *A new optimizer using particle swarm theory.* Paper presented at Proceedings of the Sixth International Symposium on the Micro Machine and Human Science, MHS'95.

Eid, B. M., Rahim, N. A., Selvaraj, J., & El Khateb, A. H. (2016). Control methods and objectives for electronically coupled distributed energy resources in microgrids: A review. *IEEE Systems Journal, 10*(2), 446-458.

El-Sadek, M. (1998). Preventive measures for voltage collapses and voltage failures in the Egyptian power system. *Electric power systems research, 44*(3), 203-211.

Elmore, W. A. (2003). *Protective relaying: theory and applications* (Vol. 1): CRC press.

Energy. (2017). BP Statistical Review of World Energy.

Eurostat. (2013). Electricity generated from renewable sources.

Faranda, R., & Leva, S. (2008). Energy comparison of MPPT techniques for PV Systems. *WSEAS transactions on power systems, 3*(6), 446-455.

Gandomi, A. H., Yang, X.-S., & Alavi, A. H. (2011). Mixed variable structural optimization using firefly algorithm. *Computers & Structures, 89*(23-24), 2325-2336.

Garg, J., & Swami, P. (2014). Calculating voltage instability using index analysis in radial distribution system. *Int. J. Modern Eng. Res., 4*, 15-26.

Global_wind_energy_outlook. (2016). Publisher: Global Wind Energy Council.

Gonzalez-Longatt, F., Chikuni, E., & Rashayi, E. (2013). *Effects of the synthetic inertia from wind power on the total system inertia after a frequency disturbance.* Paper presented at IEEE International Conference on the Industrial Technology (ICIT).

Gonzalez-Longatt, F. M., & Alhejaj, S. M. (2016). *Enabling inertial response in utility-scale battery energy storage system.* Paper presented at IEEE the Innovative Smart Grid Technologies-Asia (ISGT-Asia).

Gonzalez-Longatt, F. M., Bonfiglio, A., Procopio, R., & Verduci, B. (2016). *Evaluation of inertial response controllers for full-rated power converter wind turbine (Type 4).* Paper presented at the Power and Energy Society General Meeting (PESGM).

Haidar, A. M., Mohamed, A., & Hussain, A. (2010). Vulnerability control of large scale interconnected power system using neuro-fuzzy load shedding approach. *Expert Systems with Applications, 37*(4), 3171-3176.

Hansen, A. D., Altin, M., Margaris, I. D., Iov, F., & Tarnowski, G. C. (2014). Analysis of the short-term overproduction capability of variable speed wind turbines. *Renewable Energy, 68*, 326-336.

Hashim, H., & Ho, W. S. (2011). Renewable energy policies and initiatives for a sustainable energy future in Malaysia. *Renewable and Sustainable Energy Reviews, 15*(9), 4780-4787.

Hooshmand, R., & Moazzami, M. (2012). Optimal design of adaptive under frequency load shedding using artificial neural networks in isolated power system. *International Journal of Electrical Power & Energy Systems, 42*(1), 220-228.

Hsu, C.-T., Chuang, H.-J., & Chen, C.-S. (2011). Adaptive load shedding for an industrial petroleum cogeneration system. *Expert Systems with Applications, 38*(11), 13967-13974.

Hsu, C.-T., Kang, M.-S., & Chen, C.-S. (2005). Design of adaptive load shedding by artificial neural networks. *IEE Proceedings-Generation, Transmission and Distribution, 152*(3), 415-421.

Hua, C., & Shen, C. (1998). *Study of maximum power tracking techniques and control of DC/DC converters for photovoltaic power system.* Paper presented at 29th Annual IEEE the Power Electronics Specialists Conference, PESC 98 Record.

Huang, H., Mao, C., Lu, J., & Wang, D. (2012). *Small-signal modeling and analysis of grid-connected photovoltaic generation systems.* Paper presented at the Zhongguo Dianji Gongcheng Xuebao(Proceedings of the Chinese Society of Electrical Engineering).

Hwas, A., & Katebi, R. (2012). Wind turbine control using PI pitch angle controller. *IFAC Proceedings Volumes, 45*(3), 241-246.

IEEE_Std_929-2000. IEEE Recommended Practice for Utility Interface of Photovoltaic (PV) Systems.

InternationalEnergyAgency. *Key world energy statistic* (2016 ed.).

Jenkins, N. (2010). *Distributed generation*: The Institution of Engineering and Technology.

Jiang, H., Yan, G., Ji, H., Liu, L., & Shan, D. (2010). *An improved under frequency load shedding scheme based on rate of change of frequency.* Paper presented at the International Conference on Electrical and Control Engineering (ICECE).

Johnson, K. E., Pao, L. Y., Balas, M. J., & Fingersh, L. J. (2006). Control of variable-speed wind turbines: standard and adaptive techniques for maximizing energy capture. *IEEE control systems, 26*(3), 70-81.

Josephine, R., & Suja, S. (2014). Estimating PMSG wind turbines by inertia and droop control schemes with intelligent fuzzy controller in Indian development. *Journal of Electrical Engineering and Technology, 9*(4), 1196-1201.

Kaffashan, I., MORTEZAEE, S. M. T. M., & Amraee, T. (2016). A robust undervoltage load shedding scheme against voltage instability. *Turkish Journal of Electrical Engineering & Computer Sciences, 24*(4), 3309-3320.

Kanimozhi, R., Selvi, K., & Balaji, K. (2014). Multi-objective approach for load shedding based on voltage stability index consideration. *Alexandria Engineering Journal, 53*(4), 817-825.

Karimi, M., Mohamad, H., Mokhlis, H., & Bakar, A. (2012). Under-frequency load shedding scheme for islanded distribution network connected with mini hydro. *International Journal of Electrical Power & Energy Systems, 42*(1), 127-138.

Karimi, M., Wall, P., Mokhlis, H., & Terzija, V. (2017). A new centralized adaptive underfrequency load shedding controller for microgrids based on a distribution state estimator. *IEEE Transactions on Power Delivery, 32*(1), 370-380.

Ketabi, A., & Fini, M. H. (2015). An underfrequency load shedding scheme for hybrid and multiarea power systems. *IEEE Transactions on Smart Grid, 6*(1), 82-91.

Ketabi, A., & Fini, M. H. (2017). Adaptive underfrequency load shedding using particle swarm optimization algorithm. *Journal of Applied Research and Technology, 15*(1), 54-60.

Khamis, A., Shareef, H., & Mohamed, A. (2015). Islanding detection and load shedding scheme for radial distribution systems integrated with dispersed generations. *IET Generation, Transmission & Distribution, 9*(15), 2261-2275.

Kundur, P., Balu, N. J., & Lauby, M. G. (1994). *Power system stability and control* (Vol. 7): McGraw-hill New York.

Kundur, P., Paserba, J., & Vitet, S. (2003). *Overview on definition and classification of power system stability.* Paper presented at the IEEE PES International Symposium on Quality and Security of Electric Power Delivery Systems.

Laghari, J., Mokhlis, H., Bakar, A. H. A., Karimi, M., & Shahriari, A. (2012). *An intelligent under frequency load shedding scheme for islanded distribution network.* Paper presented at the IEEE International Power Engineering and Optimization Conference (PEDCO) Melaka, Malaysia.

Laghari, J., Mokhlis, H., Karimi, M., Bakar, A. H. A., & Mohamad, H. (2015). A new under-frequency load shedding technique based on combination of fixed and

random priority of loads for smart grid applications. *IEEE Transactions on Power Systems, 30*(5), 2507-2515.

Lamchich, M. T., & Lachguer, N. (2012). Matlab Simulink as simulation tool for wind generation systems based on doubly fed induction machines *MATLAB-A Fundamental Tool for Scientific Computing and Engineering Applications-Volume 2*: InTech.

Langella, R., Testa, A., & Alii, E. (2011). IEEE Recommended Practice—Adoption of IEC 61000-4-15, Electromagnetic compatibility (EMC)—Testing and measurement techniques—Flickermeter—Functional and design specifications.

Liao, S., Xu, J., Sun, Y., Bao, Y., & Tang, B. (2017). Wide-area measurement system-based online calculation method of PV systems de-loaded margin for frequency regulation in isolated power systems. *IET Renewable Power Generation*, 12(*3*), 335 – 341

Liserre, M., Cardenas, R., Molinas, M., & Rodriguez, J. (2011). Overview of multi-MW wind turbines and wind parks. *IEEE Transactions on Industrial Electronics, 58*(4), 1081-1095.

Liu, H. (2014). *Grid Integration of Offshore Wind Farms via VSC-HVDC–Dynamic Stability Study.* Department of Energy Technology, Aalborg University.

Liu, H., & Chen, Z. (2015). Contribution of VSC-HVDC to frequency regulation of power systems with offshore wind generation. *IEEE Transactions on Energy Conversion, 30*(3), 918-926.

Lu, P., Ye, L., Sun, B., Zhang, C., Zhao, Y., & Teng, J. (2018). A New Hybrid Prediction Method of Ultra-Short-Term Wind Power Forecasting Based on EEMD-PE and LSSVM Optimized by the GSA. *Energies, 11*(4), 697.

Luan, W., Irving, M. R., & Daniel, J. S. (2002). Genetic algorithm for supply restoration and optimal load shedding in power system distribution networks. *IEE Proceedings-Generation, Transmission and Distribution, 149*(2), 145-151.

Lydia, M., Kumar, S. S., Selvakumar, A. I., & Kumar, G. E. P. (2014). A comprehensive review on wind turbine power curve modeling techniques. *Renewable and Sustainable Energy Reviews, 30*, 452-460.

Mahmud, A. (2016). Large Scale Renewable Power Generation: Springer, Singapore.

Malekpour, A. R., Seifi, A. R., Hesamzadeh, M. R., & Hosseinzadeh, N. (2008). *An optimal load shedding approach for distribution networks with DGs considering capacity deficiency modelling of bulked power supply.* Paper presented at the Power Engineering Conference, AUPEC'08. Australasian Universities.

Manwell, J. F., McGowan, J. G., & Rogers, A. L. (2010). *Wind energy explained: theory, design and application*: John Wiley & Sons.

Melício, R., Mendes, V., & Catalão, J. (2008). *Modeling and simulation of a wind energy system: matrix versus multilevel converters.* Paper presented at the 14th IEEE Mediterranean Electrotechnical Conference (MELECON).

Mishra, S., Zarina, P., & Sekhar, P. (2013). *A novel controller for frequency regulation in a hybrid system with high PV penetration.* Paper presented at the IEEE Power and Energy Society General Meeting (PES).

Mokhlis, H., Karimi, M., Shahriari, A., Bakar, A. H. A., & Laghari, J. A. (2013). *A new under-frequency load shedding scheme for islanded distribution network.* Paper presented at the IEEE PES Innovative Smart Grid Technologies (ISGT).

Mokhlis, H., Laghari, J., Bakar, A., & Karimi, M. (2012). A fuzzy based under-frequency load shedding scheme for islanded distribution network connected with DG. *Int Rev Electr Eng, 7*(4), 4992-5000.

Morren, J., De Haan, S. W., Kling, W. L., & Ferreira, J. (2006). Wind turbines emulating inertia and supporting primary frequency control. *IEEE Transactions on Power Systems, 21*(1), 433-434.

Niknam, T., Narimani, M. R., & Jabbari, M. (2013). Dynamic optimal power flow using hybrid particle swarm optimization and simulated annealing. *International Transactions on Electrical Energy Systems, 23*(7), 975-1001.

Okou, A., Akhrif, O., Beguenane, R., & Tarbouchi, M. (2012). *Nonlinear control strategy insuring contribution of PV generator to voltage and frequency regulation*. Paper presented at the 6th IET International Conference on Power Electronics, Machines and Drives (PEMD).

Paish, O. (2002). Small hydro power: technology and current status. *Renewable and Sustainable Energy Reviews, 6*(6), 537-556.

Pal, S. K., Rai, C., & Singh, A. P. (2012). Comparative study of firefly algorithm and particle swarm optimization for noisy non-linear optimization problems. *International Journal of intelligent systems and applications, 4*(10), 50.

Pappu, V. A. K., Chowdhury, B., & Bhatt, R. (2010). *Implementing frequency regulation capability in a solar photovoltaic power plant.* Paper presented at the North American Power Symposium (NAPS), 2010.

Pasand, M. S., & Seyedi, H. (2007). *New centralized adaptive under frequency load shedding algorithms.* Paper presented at the Large Engineering Systems Conference on Power Engineering.

Photovoltaics, D. G., & Storage, E. (2007). IEEE Guide for Monitoring, Information Exchange, and Control of Distributed Resources Interconnected with Electric Power Systems.

Poshtan, M., & Farinwata, S. (2006). *Intelligent Undervoltage Load Curtailment.* Paper presented at the IEEE International Conference on Fuzzy Systems.

Pourbeik, P., Kundur, P. S., & Taylor, C. W. (2006). The anatomy of a power grid blackout-Root causes and dynamics of recent major blackouts. *IEEE Power and Energy Magazine, 4*(5), 22-29.

Rad, B. F., & Abedi, M. (2008). *An optimal load-shedding scheme during contingency situations using meta-heuristics algorithms with application of AHP method.* Paper presented at the 11th International Conference on Optimization of Electrical and Electronic Equipment (OPTIM).

Rahmann, C., & Castillo, A. (2014). Fast frequency response capability of photovoltaic power plants: The necessity of new grid requirements and definitions. *Energies, 7*(10), 6306-6322.

Rao, R. S., Ravindra, K., Satish, K., & Narasimham, S. (2013). Power loss minimization in distribution system using network reconfiguration in the presence of distributed generation. *IEEE Transactions on Power Systems, 28*(1), 317-325.

Rashedi, E., Nezamabadi-Pour, H., & Saryazdi, S. (2009). GSA: a gravitational search algorithm. *INFORM SCIENCES, 179*(13), 2232-2248.

Report, I. E. A. (2002). Distributed Generation in Liberalized Electricity Market.

Report, T. E. U. C. (2005). The support of electricity from renewabke energy sources.

Rudez, U., & Mihalic, R. (2011). Monitoring the first frequency derivative to improve adaptive underfrequency load-shedding schemes. *IEEE Transactions on Power Systems, 26*(2), 839-846.

Sadati, N., Amraee, T., & Ranjbar, A. (2009). A global particle swarm-based-simulated annealing optimization technique for under-voltage load shedding problem. *Applied Soft Computing, 9*(2), 652-657.

Sallam, A., & Khafaga, A. (2002). *Fuzzy expert system using load shedding for voltage instability control.* Paper presented at the Large Engineering Systems Conference on Power Engineering (LESCOPE 02).

Schlueter, R. (1998). A voltage stability security assessment method. *IEEE Transactions on Power Systems, 13*(4), 1423-1438.

Seyedi, H., & Sanaye-Pasand, M. (2009). New centralised adaptive load-shedding algorithms to mitigate power system blackouts. *IET Generation, Transmission & Distribution, 3*(1), 99-114.

Sharma, H., & Singh, J. (2013). Run off river plant: Status and prospects. *International Journal of Innovative Technology and Exploring Engineering, 3*(2), 210-213.

Shi, Y., & Eberhart, R. C. (1999). *Empirical study of particle swarm optimization.* Paper presented at the Proceedings of the 1999 congress on Evolutionary computation, (CEC 99).

Shokooh, F., Dai, J., Shokooh, S., Taster, J., Castro, H., Khandelwal, T., & Donner, G. (2005). *An intelligent load shedding (ILS) system application in a large industrial facility.* Paper presented at the Fourtieth IAS Annual Meeting Industry Applications Conference.

SIEMENS. (2014). Siemens 6.0 MW Offshore Wind Turbine.

Strachan, N. P., & Jovcic, D. (2010). Stability of a variable-speed permanent magnet wind generator with weak AC grids. *IEEE Transactions on Power Delivery, 25*(4), 2779-2788.

Sugimoto, H., Goto, M., Wu, K., Yokomizu, Y., & Matsumura, T. (2002). *Comparative studies of subsynchronous resonance damping schemes.* Paper presented at the International Conference on Power System Technology.

Tafticht, T., Agbossou, K., & Cheriti, A. (2006). *DC bus control of variable speed wind turbine using a buck-boost converter.* Paper presented at the IEEE Power Engineering Society General Meeting.

Teng, F., Aunedi, M., Pudjianto, D., & Strbac, G. (2015). Benefits of demand-side response in providing frequency response service in the future GB power system. *Frontiers in Energy Research, 3*, 36.

Terzija, V., & Koglin, H.-J. (2002). Adaptive underfrequency load shedding integrated with a frequency estimation numerical algorithm. *IEE Proceedings-Generation, Transmission and Distribution, 149*(6), 713-718.

Terzija, V. V. (2006). Adaptive underfrequency load shedding based on the magnitude of the disturbance estimation. *IEEE Transactions on Power Systems, 21*(3), 1260-1266.

Tielens, P., De Rijcke, S., Srivastava, K., Reza, M., Marinopoulos, A., & Driesen, J. (2012). *Frequency support by wind power plants in isolated grids with varying generation mix.* Paper presented at the IEEE Power and Energy Society General Meeting.

Ulbig, A., Borsche, T. S., & Andersson, G. (2014). Impact of low rotational inertia on power system stability and operation. *IFAC Proceedings Volumes, 47*(3), 7290-7297.

Ullah, N. R., Thiringer, T., & Karlsson, D. (2008). Temporary primary frequency control support by variable speed wind turbines—Potential and applications. *IEEE Transactions on Power Systems, 23*(2), 601-612.

Vahedi, H., & Karrari, M. (2013). Adaptive fuzzy sandia frequency-shift method for islanding protection of inverter-based distributed generation. *IEEE Transactions on Power Delivery, 28*(1), 84-92.

Valujerdi, A. C., & Mohammadian, M. (2012). A novel load shedding method to improve transmission line performance and voltage stability margin. *Int. J. Tech. Phys. Probl. Eng, 4*(13), 110-118.

Verayiah, R., Mohamed, A., Shareef, H., & Abidin, I. Z. (2014). Review of under-voltage load shedding schemes in power system operation. *Przegląd Elektrotechniczny, 90*(7), 99-103.

Vu, K., Begovic, M. M., Novosel, D., & Saha, M. M. (1999). Use of local measurements to estimate voltage-stability margin. *IEEE Transactions on Power Systems, 14*(3), 1029-1035.

Wachtel, S., & Beekmann, A. (2009). *Contribution of wind energy converters with inertia emulation to frequency control and frequency stability in power systems.* Paper presented at the 8th international workshop on large-scale integration of wind power into power systems as well as on transmission networks for offshore wind farms, Bremen, Germany.

WADEReport. (2006). *World Survey of Decentralized Energy*: World Alliance for Decentralized Energy.

Wiszniewski, A. (2007). New criteria of voltage stability margin for the purpose of load shedding. *IEEE Transactions on Power Delivery, 22*(3), 1367-1371.

Wu, F., Zhang, X.-P., Godfrey, K., & Ju, P. (2006). *Modeling and control of wind turbine with doubly fed induction generator.* Paper presented at the IEEE PES Power Systems Conference and Exposition.

Wu, Z., Gao, W., Wang, J., & Gu, S. (2012). *A coordinated primary frequency regulation from permanent magnet synchronous wind turbine generation.* Paper presented at the IEEE Power Electronics and Machines in Wind Applications (PEMWA).

Xifan, W., Yonghua, S., & Malcolm, I. (2003). Modern power system analysis: Beijing: Science Press.

Xu, D., & Girgis, A. A. (2001). *Optimal load shedding strategy in power systems with distributed generation.* Paper presented at the IEEE Power Engineering Society Winter Meeting.

Yang, X.-S. (2010). *Nature-inspired metaheuristic algorithms*: Luniver press.

Yao, W., & Lee, K. Y. (2011). *A control configuration of wind farm for load-following and frequency support by considering the inertia issue.* Paper presented at the IEEE Power and Energy Society General Meeting.

Yu, M., Dyśko, A., Booth, C. D., Roscoe, A. J., & Zhu, J. (2014). *A review of control methods for providing frequency response in VSC-HVDC transmission systems.* Paper presented at the 49th International Universities Power Engineering Conference (UPEC).

Zarina, P., Mishra, S., & Sekhar, P. (2012a). *Deriving inertial response from a non-inertial PV system for frequency regulation.* Paper presented at the IEEE International Conference on Power Electronics, Drives and Energy Systems (PEDES).

Zarina, P., Mishra, S., & Sekhar, P. (2012b). *Photovoltaic system based transient mitigation and frequency regulation.* Paper presented at the Annual IEEE India Conference (INDICON).

Zhang, C.-j., Chai, X.-H., Wang, H., & Zang, X. (2012). *The islanding start and operation control of doubly fed wind generation system.* Paper presented at the IEEE 7th International Power Electronics and Motion Control Conference (IPEMC).

Zhang, Z.-S., Sun, Y.-Z., Lin, J., & Li, G.-J. (2012). Coordinated frequency regulation by doubly fed induction generator-based wind power plants. *IET Renewable Power Generation, 6*(1), 38-47.

Zhangjie, C., Xiaoru, W., & Jin, T. (2012). *Control strategy of large-scale DFIG-based wind farm for power grid frequency regulation.* Paper presented at the Control Conference Chinese (CCC).

Zhao, X., Zhang, X., & He, B. (2009). Study on self organized criticality of China power grid blackouts. *energy conversion and management, 50*(3), 658-661.

Zhou, S., Kang, L., Sun, J., Guo, G., Cheng, B., Cao, B., & Tang, Y. (2010). A novel maximum power point tracking algorithms for stand-alone photovoltaic system. *International journal of control, automation and systems, 8*(6), 1364-1371.

Zin, A. M., Hafiz, H. M., & Aziz, M. (2004). *A review of under-frequency load shedding scheme on TNB system.* Paper presented at the National Proceedings IEEE Power and Energy Conference (PECon).

LIST OF PUBLICATIONS AND PAPERS PRESENTED

Following papers have been published in journals from this research study.

1) Jallad, J., Mekhilef, S., & Mokhlis, H. (2017). Frequency Regulation Strategies in Grid Integrated Offshore Wind Turbines via VSC-HVDC Technology: A Review. *Energies*, *10*(9), 1244. (Published). (ISI-Cited Publication).
2) Jallad, J., Saad, M., Mokhlis, H., & Laghari, J. A. (2018). Improved UFLS with Consideration of Power Deficit during Shedding Process and Flexible Load Selection. *IET Renewable Power Generation*, *12*(5), 565-575. (Published). (ISI-Cited Publication).
3) Jallad, J., Mekhilef, S., Mokhlis, H., Laghari, J., & Badran, O. (2018). Application of Hybrid Meta-Heuristic Techniques for Optimal Load Shedding Planning and Operation in an Islanded Distribution Network Integrated with Distributed Generation. *Energies*, *11*(5), 1-25. (Published). (ISI-Cited Publication).

APPENDIX

APPENDIX A: Data for IEEE 33-test bus system

Line Number	From	To	R (p.u.)	X (p.u.)	Initial Bus voltage (p.u.)	P (p.u.)	Q (p.u.)
1	1	2	0.05753	0.02932	0.997078211	0.100	0.060
2	2	3	0.30760	0.15667	0.986991327	0.090	0.040
3	3	4	0.22836	0.11630	0.982472757	0.120	0.080
4	4	5	0.23778	0.12110	0.978158071	0.060	0.030
5	5	6	0.51099	0.44112	0.96731884	0.060	0.020
6	6	7	0.11680	0.38608	0.966677656	0.200	0.100
7	7	8	0.44386	0.14668	0.962615465	0.200	0.100
8	8	9	0.64264	0.46170	0.959247871	0.060	0.020
9	9	10	0.65138	0.46170	0.962697685	0.060	0.020
10	10	11	0.12266	0.04056	0.962782596	0.045	0.030
11	11	12	0.23360	0.07724	0.963077553	0.060	0.035
12	12	13	0.91592	0.72063	0.960496191	0.060	0.035
13	13	14	0.33792	0.44480	0.959702613	0.120	0.080
14	14	15	0.36874	0.32818	0.953193053	0.060	0.010
15	15	16	0.46557	0.34004	0.951436714	0.060	0.020
16	16	17	0.80418	1.07378	0.948518887	0.060	0.020
17	17	18	0.45671	0.35813	0.947493043	0.090	0.040
18	2	19	0.10232	0.09764	0.995076747	0.090	0.040
19	19	20	0.93851	0.84567	0.978245616	0.090	0.040
20	20	21	0.25550	0.29849	0.97361528	0.090	0.040
21	21	22	0.44230	0.58481	0.970155551	0.090	0.040
22	3	23	0.28152	0.19236	0.98342002	0.090	0.050
23	23	24	0.56028	0.44243	0.97677553	0.420	0.200
24	24	25	0.55897	0.44118	0.973455749	0.420	0.200
25	6	26	0.12666	0.06451	0.965539484	0.060	0.025
26	26	27	0.17732	0.09028	0.963183005	0.060	0.025
27	27	28	0.66074	0.58256	0.952663069	0.060	0.020
28	28	29	0.50176	0.43712	0.945131795	0.120	0.070
29	29	30	0.31664	0.16128	0.941923243	0.20	0.600
30	30	31	0.60795	0.60084	0.938500935	0.150	0.070
31	31	32	0.19373	0.2258	0.937826548	0.210	0.100

32	32	33	0.21276	0.33081	0.947163411	0.060	0.040
33	8	21	1.24785	1.24785			
34	9	15	1.24785	1.24785			
35	12	22	1.24785	1.24785			
36	18	33	0.31196	0.31196			
37	25	29	0.31196	0.31196			

Substation voltage = 12.66kV

APPENDIX B: Load profile and solar irradiance of a day

Hour	Load profiles (p.u.)	Solar Irradiance at Kuantan in 2008 (kW/m^2)
1	0.78995	0.00000
2	0.75703	0.00000
3	0.73171	0.00000
4	0.71230	0.00000
5	0.70950	0.00000
6	0.71735	0.00000
7	0.70890	0.00000
8	0.74242	0.06808
9	0.86315	0.30453
10	0.92631	0.55914
11	0.97244	0.79552
12	0.96897	0.94956
13	0.94524	1.04949
14	0.98010	0.97414
15	1.00000	0.90910
16	0.99878	0.63445
17	0.96951	0.52094
18	0.90252	0.30725
19	0.87264	0.09048
20	0.93885	0.00018
21	0.93039	0.00000
22	0.90368	0.00000
23	0.87167	0.00000
24	0.84179	0.00000

Ambient temperature at Kuantan in 2008 = 32°C

APPENDIX C: Testing the PV array

To show the performance of PV Array under different environmental cases, several PSCAD simulation scenarios were conducted. As shown in Figure C.1, the solar radiation significantly affects the output power from the PV array, whereas the temperature more affects the output voltage as shown in Figure C.2.

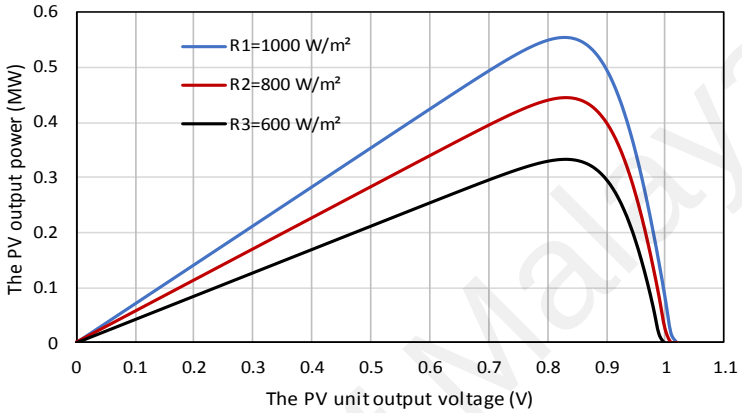

Figure C.1: Relation between voltage and power of PV for different radiation values

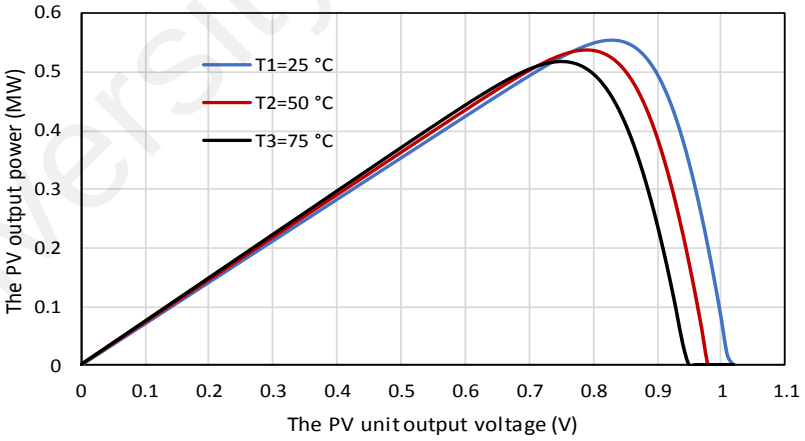

Figure C.2: PV voltage-power relation for different temperature values

APPENDIX D: Data for wind turbine model

To show the lookup tables data where were used in wind turbine model by PSCAD software. As shown in Figure D.1, Data for lookup table of power curve and wind speed, whereas the rotor speed lookup table as shown in Figure D.2.

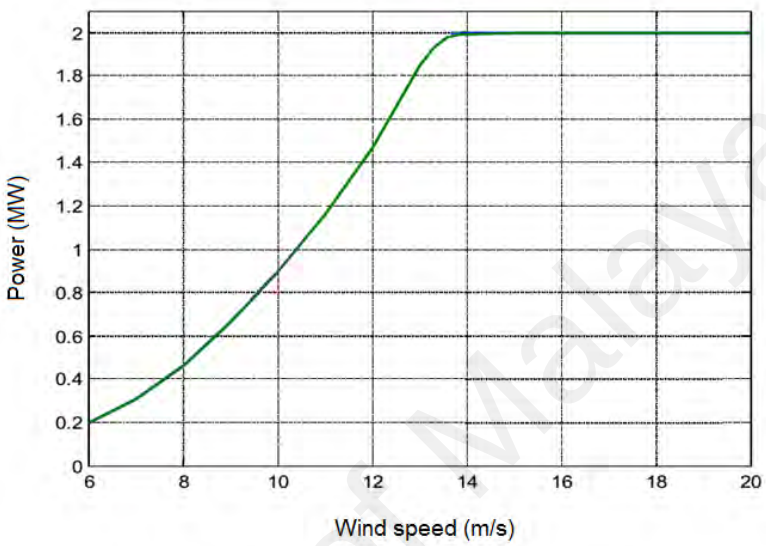

Figure D.1: Data for lookup table of power curve and wind speed

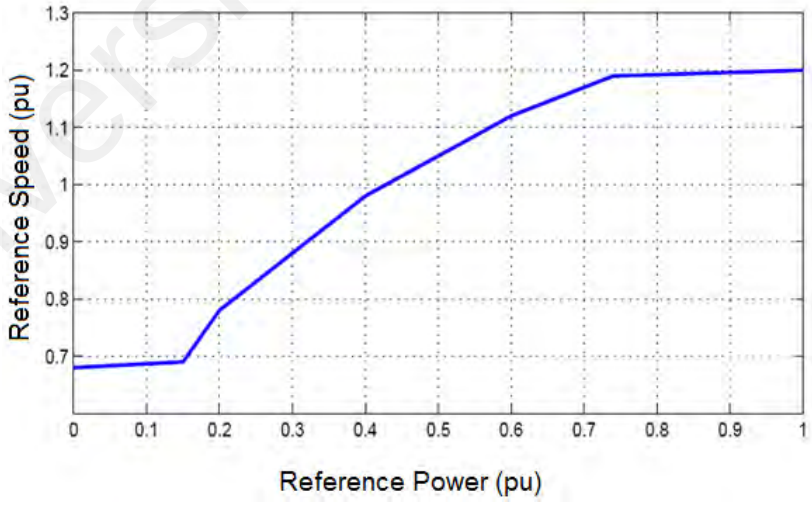

Figure D.2: Rotor speed lookup table